The effect of Co (cobalt) and In (indium) combinational doping on the structural and optical properties of ZnO nanoparticles

by

Mpho William Maswanganye

DISSERTATION

Submitted in (partial) fulfilment of the requirements for the degree of

Master of Science

in

Physics

in the

FACULTY OF SCIENCE AND AGRICULTURE

(School of Physical and Mineral Sciences)

at the

UNIVERSITY OF LIMPOPO

Supervisor : DR T.E Mosuang

Co- Supervisors : Prof K.E Rammutla

: DR B.W Mwakikunga

2017

Declaration

I declare that the dissertation hereby submitted to the University of Limpopo, for the degree of Master of Science in Physics has not previously been submitted by me for a degree at this or any other university, that it is my work in design and in execution, and that all material contained herein has been duly acknowledged.

Maswanganye M.W (Mr) **Date**

Acknowledgments

I would like to thank:

- My supervisors, Prof K.E Rammutla, Dr T.E Mosuang, Dr B.W Mwakikunga for their guidance and support during the execution of this research.
- The collaborators in this research project Prof M Maaza and Dr S.T Bertrand.
- My mother and sister for their support and encouragement on furthering my studies.
- My friends at the University of Limpopo and those who are no longer at the University.
- University of Limpopo, IBSA and the National Research Foundation for the financial assistance.

Dedications

This work is dedicated to:

My Sister

Ditaba Ephenia Maswanganye

My Mother

Mongi Martha Maswanganye

My late supervisor

Prof Koena Erasmus Rammutla

Abstract

The undoped ZnO nanoparticles, In or Co single doped ZnO nanoparticles and the In and Co combinational doped ZnO nanoparticles were synthesised through sol-gel technique. The samples were characterised using XRD, TEM, FTIR, Raman spectroscopy, UV-Vis, PL and also tested for the gas sensing applications. XRD patterns revealed that the synthesised samples were of ZnO hexagonal wurtzite structure. The lattice parameters and the bond length of all the undoped and doped ZnO samples were determined and found to be similar to that of the Bulk ZnO. The average particle size of the undoped and doped ZnO nanoparticles were calculated and found to reduce with an introduction of dopants while increasing with an increase in temperature. The strain of all the prepared samples were also determined and observed to be in an inverse relation to the particle size. TEM images showed that the synthesised samples were spherically shaped and that was in agreement with XRD results, while the EDS results showed that In and Co were successfully doped into the ZnO nanoparticles. Raman and FTIR spectroscopy indicated that the prepared samples were indeed ZnO nanoparticles which confirmed the XRD results. The UV-Vis results showed a red-shift in the energy band gap with an introduction of dopants and that was related to the reduction of the particle size, this results were consistent with the PL results. Gas sensing results showed that doping Co and In into the ZnO nanoparticles has an effect into ZnO properties. Combinational-doping of In and Co was found to increase the response to the gases CH_4, CO, NH_3 and H_2 as compared to the undoped and singly doped ZnO nanoparticle sensors. The response\recovery time was found to be affected with introduction of In and Co. Improvements were also observed in the operating temperature and the selectivity of the single doped and co-doped ZnO nanoparticles towards different gases used in this study.

List of Figures

Figure 2.2.1: A typical ZnO wurtzite structure [57]. 8

Figure 2.2.2: Schematic illustration of X-ray diffraction [60]. 10

Figure 2.3.1: Optical Absorption of ZnO [65]. 12

Figure 2.3.2: A typical Photoluminescence spectra of ZnO [61]. 13

Figure 3.2.1: X-ray diffraction equipment photograph [89]. 22

Figure 3.2.2: A photograph of a Raman spectroscopy machine [91]. 23

Figure 3.2.3: Schematic illustration of transitions experienced in Raman scattering [93]. 25

Figure 3.2.4: A photograph of a transmission electron microscope [98]. 27

Figure 3.2.5: An image of Nicolet iS10 FT-IR Spectrometer [103]. 30

Figure 3.2.6: A process of emission of the photoluminescence spectra [105]. 32

Figure 3.2.7: Kinesistec testing station used for gas sensing in this study 33

Figure 4.1.1: XRD patterns of undoped-ZnO at 400, 500 & 600 ℃. 35

Figure 4.1.2: XRD patterns of Co-doped-ZnO at 400, 500 & 600 °C. 35

Figure 4.1.3: XRD patterns of In-doped-ZnO at 400, 500 & 600 °C. 36

Figure 4.1.4: XRD patterns of In-Co-doped-ZnO at 400, 500 & 600 °C. 36

Figure 4.2.1: EDS and TEM of undoped ZnO 400 ℃. 40

Figure 4.2.2: EDS and TEM of Co-ZnO 400 ℃. 40

Figure 4.2.3: EDS and TEM of In-doped ZnO 400 ℃. 41

Figure 4.2.4: EDS and TEM of In-Co-doped ZnO 400 ℃. 41

Figure 4.2.5: EDS and TEM of Co-doped ZnO 500℃. 42

Figure 4.2.6: EDS and TEM of In-doped ZnO 500 ℃. 42

Figure 4.2.7: EDS and TEM of In-Co-doped ZnO 500 ℃. 43

Figure 4.2.8: EDS and TEM of Co-doped ZnO 600 ℃. 43

Figure 4.2.9: EDS and TEM of In-doped ZnO 600 ℃. 44
Figure 4.2.10: EDS and TEM of In-Co-doped ZnO 600 ℃..... 44
Figure 5.1.1: Absorbance spectra of undoped ZnO at 400, 500 and 600 °C. 48
Figure 5.1.2: Absorbance spectra of Co-doped ZnO at 400, 500 and 600 °C. 48
Figure 5.1.4: Absorbance spectra of In-Co co-doped ZnO at 400, 500 and 600 °C. 49
Figure 5.2.1: FTIR spectra of undoped doped ZnO nanoparticles annealed at 400 ℃, 500 ℃ and 600 ℃ 51
Figure 5.2.2: FTIR spectra of Co-doped ZnO nanoparticles annealed at 400 ℃, 500 ℃ and 600 ℃. 51
Figure 5.2.3: FTIR spectra of In-doped ZnO nanoparticles annealed at 400 ℃, 500 ℃ and 600 ℃ 52
Figure 5.2.4: FTIR spectra of In-Co co-doped ZnO nanoparticles annealed at 400 ℃, 500 ℃ and 600 ℃. 52
Figure 5.3.1: Raman spectroscopy of undoped doped ZnO nanoparticles annealed at 400 ℃, 500 ℃ and 600 ℃ 55
Figure 5.3.2: Raman spectroscopy of 5% Co-doped doped ZnO nanoparticles annealed at 400 ℃, 500 ℃ and 600 ℃..... 55
Figure 5.3.3: Raman spectroscopy of 5% Co-doped doped ZnO nanoparticles annealed at 400 ℃, 500 ℃ and 600 ℃..... 56
Figure 5.3.4: Raman spectroscopy of 5% In-Co co-doped doped ZnO nanoparticles annealed at 400 ℃, 500 ℃ and 600 ℃..... 56
Figure 5.4.1: Energy levels of different defect states of Zinc Oxide [138]..... 57
Figure 5.4.3: PL spectrum of Co-doped ZnO nanoparticles annealed at 400 ℃, 500 ℃ and 600 ℃. 59

Figure 5.4.4: PL spectrum of In-doped ZnO nanoparticles annealed at 400 ℃, 500 ℃ and 600 ℃. 60

Figure 6. 1: Response of the undoped ZnO, In doped, Co doped and In-Co co-doped ZnO nanoparticle sensors to Relative Humidity (RH). 63

Figure 6. 2: Responses of each sensor plotted against concentration of gases (a) CO (b) CH_4 (c) NH_3 and (d) H_2. 64

Figure 6. 3: Response of the undoped ZnO, In doped, Co doped, and In-Co co-doped ZnO samples plotted against temperature when exposed to 40 ppm of (a) CO (b) CH_4 (c) NH_3 and (d) H_2 gases. 66

List of Tables

Table 4.1.1: Lattice parameters a, b and c, bond length L, average particle size D and average strain ε. 38

Table 5.1.1 Energy band gap of undoped ZnO, Co doped ZnO, In doped ZnO, and In-Co co-doped ZnO in comparison with bulk ZnO of reference [26]. 46

Table 5.3.1: Raman vibration modes ($cm-1$) along with their assigned symmetry in undoped ZnO, 5% Co doped ZnO, 5% In doped ZnO, and 5% In-Co doped ZnO. .. 54

Table 6. 1: List of response and recovery times alongside the fitting parameters of Equation 6. 2 and 6. 3. 68

Table of Contents

Declaration i

Acknowledgments ii

Dedications iii

Abstract iv

List of Figures v

List of Tables viii

Chapter 1 1

General Introduction 1

1.1. Introduction 1

1.2 Aims and Objectives 4

1.2.1. Aim 4

1.2.2 Objectives 4

Chapter 2 5

Literature Review 5

2.1. Introduction 5

2.2. Structural Properties of ZnO 7

2.3. Optical Properties of ZnO 11

2.4. Gas Sensing Properties of ZnO 14

2.5. The effect of Particle size on ZnO 17

Chapter 3 19

Methodology 19

3.1. Sample Preparation 19
3.2. Characterisation Techniques 21
3.2.1 X-Ray Diffraction 21
3.2.2 Raman Spectroscopy 23
3.2.3 Transmission Electron Microscope 26
3.2.4 Ultraviolet-Visible Spectroscopy 28
3.2.5 Fourier Transform Infrared Spectroscopy 29
3.2.6 Photoluminescence (PL) Spectroscopy 31
3.2.7 Gas Sensing 33
Chapter 4 34
Structural Studies 34
4.1. XRD Results 34
4.2. TEM Results 39
4.3. Conclusion 45
Chapter 5 46
Optical Studies 46
5.1. UV-Vis Results 46
5.2. FTIR Results 50
5.3. Raman Results 53
5.4. Photoluminescence (PL) Results 57
5.5. Conclusion 61

Chapter 6 62

Gas Sensing Applications 62

6.1. Gas sensing Results 62

6.2. Conclusion 69

Chapter 7 70

Summary 70

8. References 72

9. Publications and Conference Presentations 93

9.1 Publications 93

9.2 Conference Presentations 93

Chapter 1

General Introduction

1.1. Introduction

Nanostructured materials have been found to be interesting and are currently investigated because of their unique properties compared to their bulk counterparts [1]. Bulk materials should have the same properties as nanomaterials regardless of their size, but at nanoscale (1 – 100 nm) different properties are often observed in materials. This informs us that properties of a material changes as its size approaches the nanoscale range. There are a variety of nanostructured materials such as nanoparticles, nanorods, nanospheres, nanowires, nanotubes and nanoflowers. Some of these nanomaterials can be used in applications like light emitting diodes (LEDs) [2], liquid crystal display (LCD), solar cells [3] and gas sensing [4]. Here in South Africa nanomaterials research has been identified for sustainable water purifications, energy source, drug delivery, as well as gas and biosensing [5].

At present transition metal (TM) oxide semiconductors such as TiO_2, SnO_2, ZrO_2, CdO, ZnO have become the main topic in numerous research at nanoscale investigations due to them having unique characteristics and an encouraging potential for applications such energy storage and gas sensing devices [6 - 10].

TiO_2 and SnO_2 are interesting and widely studied metal oxide materials having three different phases being rutile, anatase and brookite. Brookite phase is found to be stable at very low temperatures, anatase stability exits at comparatively low temperatures while rutile is the most stable phase which can be obtained at high

temperatures. Rutile phase has been dominating in electronic applications due to its high dielectric property [11] despite the fact that anatase phase has been found to be suitable for solar cells [12]. In these TiO_2 phases anatase has the energy band gap of 3.2 eV, with rutile and brookite having an energy band gap of 3.3 eV [13], while rutile phase of SnO_2 has an energy band gap of 3.6 eV [14].

These TiO_2 and SnO_2 materials can be used in several applications such as gas sensors, generation of hydrogen gas, dielectric materials, solar cells, etc. [15]. Other studies have considered TiO_2 as one of the best material in photocatalytic reactions due to its long-term thermodynamic stability, non-toxicity, strong oxidising power and low cost [16, 17], while SnO_2 is said to have potential applications such as catalysis [18], transparent conducting electrodes [19], optoelectronic devices [22], gas sensors [20] and lithium batteries [21] due to its unique electrical and catalytic properties.

Different methods such as sol-gel [22], microwave technique [23], carbothermal reduction [24] and laser-ablation [25] have been used to prepare both TiO_2 and SnO_2.

Furthermore Zinc oxide (ZnO) is an n-type semiconductor material having an energy band gap of 3.36 eV with a large exciton binding energy of 60 meV that ensures a stable exciton emission even at room temperature [26]. It possesses a hexagonal crystal structure with $a = b \neq c$. Lattice parameters were experimentally measured to be a = 0.32495 nm and c = 0.52069 nm [27]. It has ruggedness, chemically inertness, and abandons availability [28]. ZnO shows visible luminescence even when excitation is done at different UV-wavelengths because of different types of defects that are formed [29]. This material has a wide range of resistivity, greater electron hall mobility, high transparency at room temperature [30], excellent chemical and thermal stability under usual operating conditions [31]. Commercially, ZnO is cheap, nontoxic and bio-

safe for implantation as a biosensor [32]. When doped with a variety of transition metals, ZnO adopts a ferromagnetic property and they are called diluted magnetic semiconductors (DMSs) [33]. These DMSs enables the fabrication of optical devices such as spin LEDs [34] and spin-polarized solar cells [35].

Different types of ZnO nanostructures ranging from nanodots to tetrapods have been reported and found to be having interesting optical properties [8]. Independent studies by S.Y. Kim *et al*. [36], B.K. Woo *et al*. [37], and R.K. Dutta *et al*. [38] have shown that ZnO nanostructured materials are influenced by their size, shape and structural aspect and in turn those factors relay mostly on the technique used to synthesise the nanostructures. M. Poloju *et al*. [39] reported that doping ZnO with controlled amounts of impurities can have an effect on the structural, electrical and optical properties of ZnO nanostructures. Several techniques like chemical vapour deposition (CVD) [40], physical vapour deposition (PVD) [41], hydro thermal and sol-gel method [42] have previously been used to synthesise the pure and doped ZnO nanostructures. Among these techniques, sol-gel is the most favoured method due to its accurate arrangement control on the structure of the material, ability to dope homogeneously on the molecular level, easy to reproduce and low cost.

In this dissertation, effects of single doped Co and In as well as Co and In as combinational dopants on the structural, optical and gas sensing properties of ZnO nanoparticles are discussed. Structural property study is ensured using XRD, TEM and the optical properties are carried out using Raman spectroscopy, UV-Vis, PL and FTIR. Gas sensing property is explored by measuring the gas response of ZnO nanoparticles samples annealed at different gas concentrations of CO, CH_4, NH_3 and H_2 whilst varying temperature in range of 250 – 400 °C using a Kinesistec testing

station. The undoped and doped ZnO nanoparticle samples utilised in this project were synthesised using sol-gel approach as it has been found to be cost effective.

1.2 Aims and Objectives

1.2.1. Aim

The aim of this study is to determine the effect of Co and In as combinational dopants on the structural and optical properties of ZnO nanoparticle powder samples synthesised using a sol-gel method.

1.2.2 Objectives

The objectives of the study are to:

i. synthesise ZnO nanoparticles doped simultaneously with two metals (Co and In),
ii. investigate the structural and optical properties of combinational-doped ZnO,
iii. investigate the efficiency of nano-sized undoped, “single doped” and “double doped” ZnO as gas sensors.

Chapter 2

Literature Review

2.1. Introduction

Metal oxide nanostructured materials have become a hot topic of research in recent years because of their observed unique properties. Properties of these metal oxides are continuously investigated in order to improve their applications in vast areas like solar cells, fuel cells, gas sensing of which are mainly concerned with opto-electronics.

Gas detection is one of the most important aspects for monitoring the environment, industries and the households. Gas sensing devices have been developed to detect gases such as CO, NO_2, CO_2, H_2 and SO_2 because of their toxicity [43]. CO, NO_2 and CO_2 are among the gases that affect our day to day life's since they are emitted daily from the combustion processes of cars, farm and industrial machineries. These gases are toxic even at very low concentrations but are usually found with high concentrations in our homestead, parking garages and in the mines. High concentrations of these pollutants are harmful to humans as well as other animals as a result these gases should be continuously monitored and controlled at all times. However the gas sensing devices that are currently used to detect these gases are not ideal. Therefore there is a need to improve them since frequently are found to be having a high operating temperatures and low sensitivity [44]. J. Xu *et al*. [45] have reported that sensitivity of metal oxides sensors depend on the particle size while the particle size is said to have an inversely proportional relation to the energy band gap so reducing the particle size is one way of improving the sensitivity of a metal oxide sensors.

ZnO has been reported to have good properties for gas sensing at nanoscale levels due to high surface areas [45]. Studies have shown that doping this material can improve its optical properties and at the same time reduce the particle size of a material [44] and hence much effort has been devoted in doping this material in order to improve it for different applications. Previous work has demonstrated the effect of elements such as Al, In, Cu, Fe on ZnO nanostructures as single dopants for different applications [39], [46 – 49].

In this dissertation focus will be on the effect of In^{3+} and Co^{2+} as single and combinational-dopants on the properties of ZnO nanoparticles. In^{3+} has ionic radius of 0.810 Å, also considered to be one of the best dopants in ZnO nanostructures and has been reported to increase the gas sensitivity of ZnO nanoparticles [50]. Co^{2+} having an ionic radius of 0.745 Å which is comparable to that of Zn^{2+} (0.740 Å) has been reported to reduce the particle size of ZnO nanoparticles and also enhances its optical properties [47]. Only few papers [51 – 55], have reported that doping ZnO nanoparticles with a combination of two or more elements can affect the properties of ZnO.

2.2. Structural Properties of ZnO

ZnO is mostly found as a white or slightly yellow powder which is insoluble in water and ethanol while soluble in dilute mineral acids. It can experimentally be obtained in three different polymorphs being the hexagonal wurtzite, cubic rock salt cubic and zinc blende structures. Theoretical studies have shown that there exists a fourth phase being of a cubic cesium chloride structure at high temperatures but this phase has never been experimentally observed [56].

The ZnO zinc blende structure is only found to be stable when grown on the cubic substrates while the rock salt structure can be obtainable at comparatively high pressures. The wurtzite structure is the most stable and also the most common known structure of ZnO. An example of a ZnO wurtzite structure is shown in Figure 2.2.1. The figure illustrates that the ZnO wurtzite structure consists of interchanging zinc (Zn) and oxygen (O) atoms with lattice positions [57]. The illustration displays two surfaces being the polar surface (0001), they may be occupied by the Zn or O atom and non-polar surfaces (1120) and (1010) having equivalent number of atoms for both Zn and O [57]. This polar surface in wurtzite ZnO structure is found to be metastable in nature and may also be responsible for properties such as piezoelectric [57]. Hexagonal ZnO has a space group C_{6v}^{4} in the Schoenflies notation and p_6mc in the Hermann–Mauguin notation.

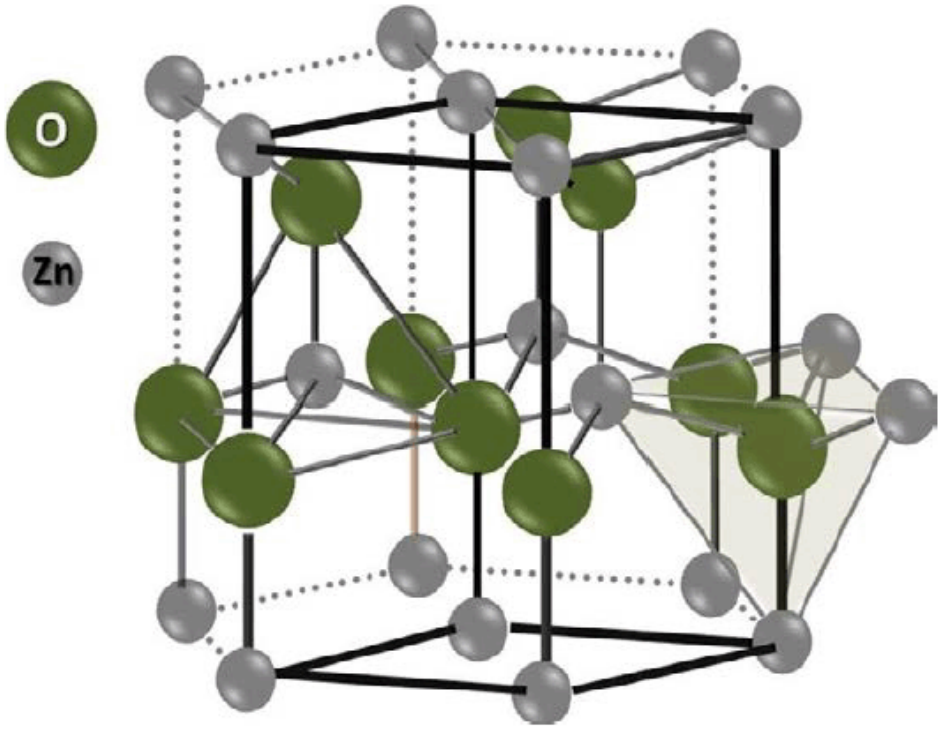

Figure 2.2.1: A typical ZnO wurtzite structure [57].

The interlayer spacing *d* of this material can be determined using Bragg's law:

$$\lambda = 2d\,sin\,\theta, \qquad (2.2.1)$$

which is derived from figure 2.2.2. In equation 2.2.1, λ denotes the incident radiation wavelength, θ denotes the angle between layers of the crystal and the incident radiation. The lattice parameters of ZnO wurtzite hexagonal structure can be determined using the equation:

$$\frac{1}{d^2_{(hkl)}} = \frac{h^2}{a^2} + \frac{k^2}{b^2} + \frac{l^2}{c^2}, \qquad (2.2.2)$$

where $a = b \neq c$ with the ratio of $^c/_a$ = 1.633 and (hkl) are the Miller indices. The volume of the unit cell can be determined from the equation:

$$v = 0.866a^2c\,. \qquad (2.2.3)$$

The bond length (L) between the Zn and O ions can be determined using the equation [58]:

$$L = [\frac{a^2}{3} + \left(\frac{1}{2} - u\right)^2 c^2], \qquad (2.2.4)$$

where u for the wurtzite ZnO structure may be defined by [58]:

$$u = \frac{a^2}{3c^2} + \frac{1}{4}. \qquad (2.2.5)$$

In every material there are three types of strains (ε) that are present, namely; the tensile, the compressive and the shear strain and all of these strains are responsible for the deformations in a material. These strains can be determined using different equations, where the strain due to the crystal imperfection and the distortion is given by:

$$\varepsilon = \frac{\beta_{(hkl)} \cos\theta}{4 \sin\theta} \ , \qquad (2.2.6)$$

where $\beta_{(hkl)}$ is the full width at half maximum from the XRD peaks and θ is the angle of diffraction from the XRD pattern. The strain along the c-axis of the hexagonal ZnO material can be given by [59]:

$$\varepsilon\ \% = \frac{c - c_0}{c_0} \times 100. \qquad (2.2.7)$$

The dislocation density (τ) can be calculated using the equation:

$$\tau = \frac{1}{D^2}, \qquad (2.2.8)$$

where *D* is the particle size of the material.

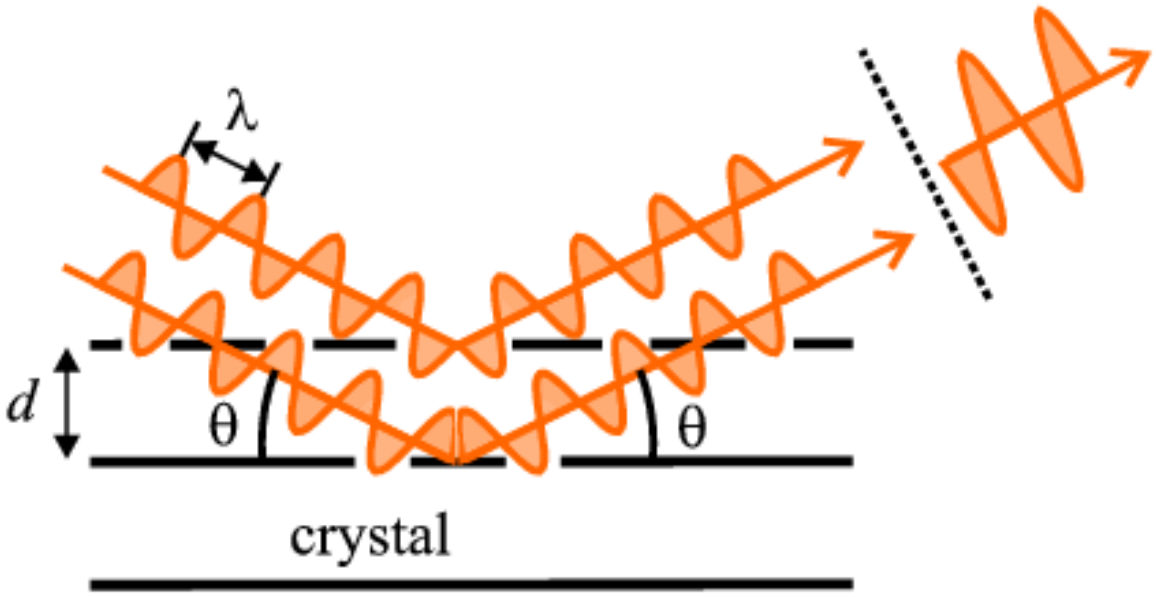

Figure 2.2.2: Schematic illustration of X-ray diffraction *[60]*.

2.3. Optical Properties of ZnO

Optical properties of semiconductors are mostly attributed to the intrinsic and the extrinsic effects [61]. The intrinsic effect transpires in the region between the conduction band and the valence band, where we have electrons and holes respectively [61]. This includes the excitonic influence because of the Coulomb interaction [61]. These exciton creations occur so that there is balance between the group velocity of electrons and holes. The excitons can be grouped into two excitons being free and bound excitons; where for materials with greater quality and less amount of contamination, the free exciton may also show excited states, in additional to their ground-state transitions [61]. Extrinsic properties are mostly due to impurities added into the material or defects in a material. These mostly produce separate electronic states in the band gap, which tend to affect both the emission processes and the optical absorption [61].

The optical transitions of ZnO materials have been extensively studied using different types of experimental methods like reflection, transmission, optical absorption, and photoluminescence (PL). Optical absorption, transmission and reflection can entirely be used to estimate the band energy gap using different relations, where the Tauc relation given by the equation [62]:

$$(\propto hv)^n = A(hv - E_g) \qquad (2.3.1)$$

is applied to determine the energy band gap E_g, where $\propto$ denotes the absorption coefficient, hv is the photon energy, A is a constant and $n = 2$ for direct band gap semiconductors. Extrapolating a linear region from a Tauc plot of $(\propto hv)^2$ against hv, if $(\propto hv)^2 = 0$, then the x-intercept results as energy band gap (E_g). The E_g can also be determined using the equation

$$E_g = \frac{hc}{\lambda_{cut\ off}} \quad , \qquad (2.3.2)$$

where h denotes Planck's constant, c the speed of light and $\lambda_{cut\ off}$ denotes the cut off wavelength. The standard value of the energy band gap for bulk ZnO is reported to be 3.36 eV [26], but due to the difference between the bulk and the nanostructured material properties the energy band gap of ZnO nanostructures are usually found to be different from that of the bulk ZnO [32, 63, 47]. Previous work has shown that the band gap of ZnO reduces with increase in annealing temperature and which likewise tends to shift the maximum absorption to higher wavelengths [64]. The behaviour of optical absorption relative to wavelength in ZnO according to D. Sridevi *et al*. [65] is presented in Figure 2.3.1.

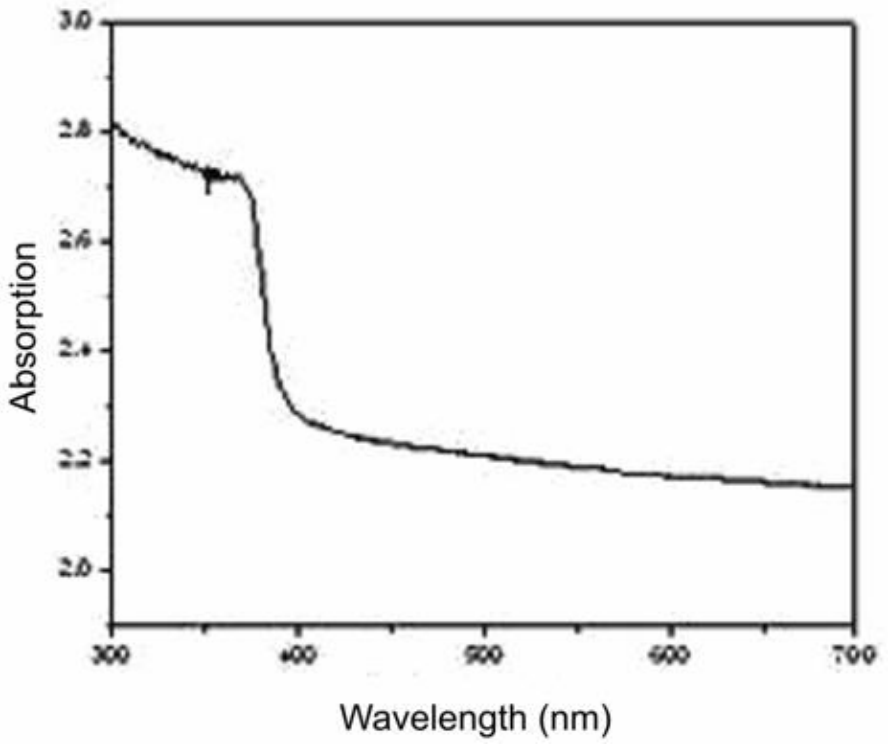

Figure 2.3.1: Optical Absorption of ZnO *[65]*.

Bulk ZnO materials are usually transparent to visible light but yet are found to absorb ultra-violet (UV) light below 369 nm, but Behera *et al*. [66] reported that ZnO nanoparticles are believed to have greater UV blocking properties as compared to the bulk ZnO, this is due to the fact that nanoparticles have different energy band gaps as compared to the bulk materials.

It has been realized that at room temperature the PL spectrum of ZnO naturally exhibit a UV emission band and a broad emission band at longer wavelengths [61]. The UV emission band is mostly conquered by the free exciton (FE) emission and the broad emission band can be found around 420 - 700 nm, this broad emission is named the deep level emission band (DLE) [61]. An example of a photoluminescence spectrum of a ZnO sample according to L. Yang *et al*. [61] is depicted in Figure 2.3.2.

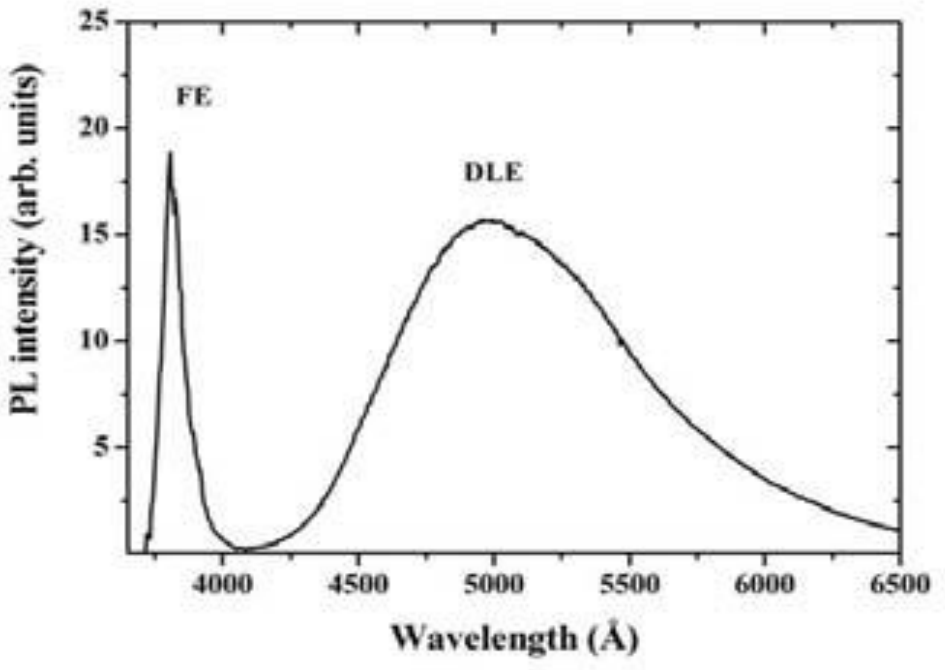

Figure 2.3.2: A typical Photoluminescence spectra of ZnO [61].

The UV emission band is associated to the near band-edge transition of ZnO, being the recombination of the free excitons. The DLE band has in some papers been linked

to varies defects like O-vacancy (V_O) [67 -69], Zn-vacancy (V_{Zn}) [70 – 72], O-interstitial (O_i) [73], Zn-interstitial (Zn_i) [74], and extrinsic impurities such as substitution of Zn^{+2} by other metals. According to Q. X. Zhao *et al*. [75], the DLE band has been identified and it had been attributed to the V_O and V_{Zn} defects with different optical properties contributing to this DLE band [76, 77]. Some studies may suggest that the growth technique is the explanation of the impurities and the intrinsic and extrinsic defects implying the dominant defect for the visible emission might be different for different growth techniques. So when comparing the defects you have to use the ones of the same growth technique. Gong *et al*. [78] reported that the green band emission is mostly due to the oxygen vacancies located in the surface of ZnO nanoparticles and by changing the surface states, the green luminescence can effectively be improved.

2.4. Gas Sensing Properties of ZnO

A gas sensor is a machine that can be used to measure the concentration of a specific gas. These gas sensors are classified in different ways where there can be physical sensors, chemical sensors, and biochemical sensors. Every gas sensing material has its different properties i.e., operation temperature, sensitivity, selectivity, reversibility and the response-recovery time. This implies that every sensor has different characteristics and each specific sensor has its best efficiency at a particular temperature. The operating temperature is basically the temperature where the sensitivity of a sensor is at its maximum. The operating temperature of individual sensors can be measured experimentally by exposing the sensor to a specific amount of gas, at various temperatures.

One of the main properties of a gas sensor is said to be the sensitivity, where the sensitivity of a material is found to depend on the particle size, surface area, gas adsorption quantity on the surface of the material, activation energy of the gas

adsorption and lattice defects [45]. Xu *et al*. [45] reported that when a material has a particle size greater than 40 nm, its gas sensitivity reduces rapidly because its surface area goes down quickly. P. Qi *et al*. [79] also reported that nanostructured materials have advantages for sensing materials such as sensitivity, operation at room-temperatures and large surface area required for reduction and construction of bigger sensor arrays. Where the greater active sites the surface has, the more sensitive the sensor becomes. The sensitivity of a material can be explained as $\frac{R_a}{R_g}$ for reducing gases and $\frac{R_g}{R_a}$ for oxidizing gases, where R_a represents the resistance of air and R_g represents the resistance of the targeted gas.

Another property playing an important role in gas sensing is the selectivity of the sensor. The selectivity of a sensor can be defined as how good can a sensor be able to recognize one gas amongst other gases. The selectivity of a sensor can be obtained by the ratio of the sensitivity of one particular gas relative to another gas being treated in the same conditions [80], equation (2.4.1) describes the selectivity of the sensor.

$$\text{selectivity} = \left|\frac{X_{gas\,(a)} - X_{gas\,(b)}}{X_{gas\,(a)}}\right| \qquad (2.4.1)$$

The response and recovery time are another properties that play an important role in designing gas sensors. The response time is defined as the time taken by the sensor to respond to 90 % of a particular gas concentration while the recovery time is the time taken by the sensor signal to return to 10 % of its initial value.

The mechanism of gas sensors (in these case ZnO sensors) involves an adsorption and desorption of oxygen atoms from the atmosphere on the oxide surface of the material. These oxides then extract electrons from the material resulting to carrier change and electrical conductivity changes [81]. The change in conductivity of the gas sensing device can be described as a measure of gas concentration on the surface.

In the case of oxidizing gases; conductivity decreases for n-type materials and increases for p-type materials. For the reducing gases; conductivity is the reverse the oxidizing gases. Due to the fact that the mechanism of the gas sensor is based on surface of the material, it implies that nanostructured materials will improve the gas sensing properties as compared to the bulk materials as nanostructured materials have bigger surface areas.

In general semiconductors are usually large band gap metal oxides were the semiconducting performance of the material occurs from variation of stoichiometry. These metal oxides semiconductor materials may be separated into n-type and p-type were we have electrons and holes as major carrier respectively. In an n-type we have materials such as In_2O_3, TiO_2, SnO_2, CdO and ZnO and in an p-type we have materials such as NiO, CuO and TeO_2. Metal oxide semiconductors materials are broadly being investigated as gas sensors due to their low cost and relative simplicity.

It is in this regard that ZnO is considered as one of the greatest materials of high efficiency sensing. The material has high chemical stability and sensitivity to gases like NH_3, O_3, NO_2, CO, H_2 and many more [43, 82]. The ZnO gas sensors behave differently to different gases and it has been reported that gas sensors depend on their processing methods, morphology in the surface of the material, sensor construction orientation and the operating temperature [43, 82]. Previous work has showed that the sensitivity of ZnO nanostructures rises due to an increase in the targeted gas concentration [83] but the sensitivity of ZnO nanostructures towards gases such as H_2, NO_2, CO and O_2 is relatively low in the absence of dopants on the ZnO nanostructures [83]. On the other side these nanostructures are noticed to respond badly to gases such as O_2, CO, and CH_4 at lower temperatures [84] but demonstrate a good response toward oxidizing gas such as NO_2 [83]. The performance of gas

sensors is said to also depend critically on the shape, orientation and the operating temperature of ZnO nanostructures being used. Zhu *et al*. [85] demonstrated that the sensitivity depends on the temperature and the maximum sensitivity for thick films is between 300 – 400 ˚C which is less than the one of the bulk ZnO being 450 ˚C and this reduction is due to the surface area effect of the nanoparticles. In another paper Liu *et al*. [86] gave details on the sensing properties of ZnO nanostructured (nanowires and nanorods) and found the grain size reduction to be increasing the sensing properties of ZnO nanostructures. Gupta *et al*. [81] reported that the number of oxygen vacancies in a lattice can also improve the gas sensing response of ZnO material.

2.5. The effect of Particle size on ZnO

When a material has a smaller particle size it implies that the material will have a bigger surface area to volume ratio. This suggests that the smaller the particle size the greater the surface area. Hence this informs us that particles size plays an important role in a material because nanostructured materials do not have the same properties as the bulk materials and therefore the properties of bulk materials can be improved by producing their nanomaterials. The particle size $D_{(hkl)}$ of a material can be determined using Debye-Scherrer's equation:

$$D_{(hkl)} = \frac{k\lambda}{\beta_{(hkl)} \cos\theta}, \qquad (2.5.1)$$

where λ denotes the incident waves wavelength, k the shape factor (0.89 for spherical particles) and $\beta_{(hkl)}$ is the full width at half maximum. C. Wang *et al*. [44] and Z.L.S. Seow *et al*. [87] published that nanoparticles with particle size smaller than 20 nm are excellent candidates for applications such as gas sensing, catalysts and solar cells. The large surface area can also be advantageous in applications such as sensor devices since a metal oxide semiconductor sensor having a large surface area allows

more of the targeted analyte to be absorbed in the surface of the semiconductor giving a stronger and more measurable response. On the other hand, caution must be heeded as having a larger surface area can also be problematic for other applications such as optoelectronic devices like LEDs and solar-cells [61].

Factors such as growth technique, annealing temperature and dopants have been found to be playing an important role in the particle size of the ZnO nanoparticles. Yang *et al*. [88] reported that the particle size of ZnO increase as the annealing temperature increases due to the fact that at high temperatures the grain boundaries increase causing the particles to grow. Li *et al*. [47] observed that doping can significantly reduce the particles size of the ZnO nanoparticles. Likewise, Xu *et al*. [45] reported that the gas sensitivity depends upon the particle size of ZnO so reducing the particle size would improve the gas sensitivity of ZnO and one way of reducing the particle size was by introducing dopants in the ZnO nanostructures.

Chapter 3

Methodology

3.1. Sample Preparation

All the samples were synthesised through the sol-gel synthesis route. Sol-gel method can be used to synthesise powders and thin films of any compounds. In this instance ZnO nanoparticles having different morphology can be produced. It has many advantages such as its quality to be homogeneous, the ability to introduce dopants in larger quantities, control over the structure being prepared, and its capability to coat huge and difficult areas compared to other synthesising methods. In a usual sol-gel procedure, from the precursors being used a solution is created from the hydrolysis and polymerisation. The whole polymerization and loss of solvent results into a solid gelation form. Sol-gel technique can generally be divided into two ways, being the non-alkoxide and the alkoxide. Where the non-alkoxide process uses inorganic salts that requires additional eliminations of inorganic anion and the alkoxide process (the most employed) uses metal alkoxides.

The undoped, single doped and double doped ZnO nanoparticle samples were synthesised using the following chemicals: zinc acetate dihydrate ($C_4H_6O_4Zn{\cdot}2H_2O$), ethanol (C_2H_6O), ethanolamine (C_2H_7NO), cobalt (II) nitrate hexahydrate ($CoN_2O_6{\cdot}6H_2O$) and indium (III) nitrate hydrate ($InN_3O_9{\cdot}xH_2O$) where the water soluble salts, i.e. cobalt (II) nitrate hexahydrate and indium (III) nitrate hydrate were used as sources of Co and In metal dopants. All chemicals utilised were standard chemicals purchased from Sigma-Aldrich. Single doped ZnO nanoparticles with Co and In where prepared at a doping levels of 5 % whereas in the double doping samples, were prepared at 2.5 % of each dopant.

When preparing the undoped ZnO nanoparticles 0.2 M zinc acetate dihydrate solution was mixed with 0.2 M ethanol in order to obtain homogeneity. This was done at a continuous stirring, 0.2 M ethanolamine was added as a stabilizer and then the solution was stirred for 2 hours at 70 ˚C. When preparing the doped ZnO nanoparticles, cobalt (II) nitrate hexahydrate or indium (III) nitrate hydrate were added into 0.2 M zinc acetate dihydrate solution for the single doped ZnO nanoparticles and cobalt (II) nitrate hexahydrate and indium (III) nitrate hydrate were added simultaneously into 0.2 M zinc acetate dihydrate solution for the combinational doping then mixed with 0.2 M of ethanol in order to obtain homogeneity. Again this was done at a continuous stirring, 0.2 M ethanolamine was added as a stabilizer and then the solution was stirred for 2 hours at 70 ℃. The precipitate formed was collected using a filter paper, and dried at 100 ℃ for 1 hour in a hot air oven. All the ZnO nanoparticles powder samples were thus annealed at various temperatures (400 ℃, 500 ℃ and 600 ℃) for 1 hour. After annealing all the samples were taken for characterisation.

3.2. Characterisation Techniques

In order to study the structural properties of the undoped and doped ZnO nanoparticles, the samples were characterised using X-ray diffraction (XRD), Raman spectroscopy (RS), Transmission electron microscope (TEM) while the optical properties were studied using the Ultraviolet-visible (UV-vis), Fourier transformation infrared (FTIR) and the Photoluminescence (PL) spectroscopy.

3.2.1 X-Ray Diffraction

X-ray diffraction (XRD) is a well-known method that can be used in various investigations such as determining the lattice parameters, microstrains and grains or particle sizes of crystals. In this study XRD results were obtained using Philips Analytical X-Ray B.V diffractometer using CuKα ($\lambda = 0.15405$ nm).

The XRD method is mostly known for its use as a phase characterisation tool because it can differentiate between phases having the same chemical composition but different crystal structures. An x-ray diffractometer photograph is represented in Figure 3.2.1. [89]. A specimen sample is irradiated with monochromatic x-rays of wavelength λ and the diffracted x-rays get detected by the x-ray detector. A diffraction pattern representing the x-rays in the detector is registered from the x-rays in the detector.

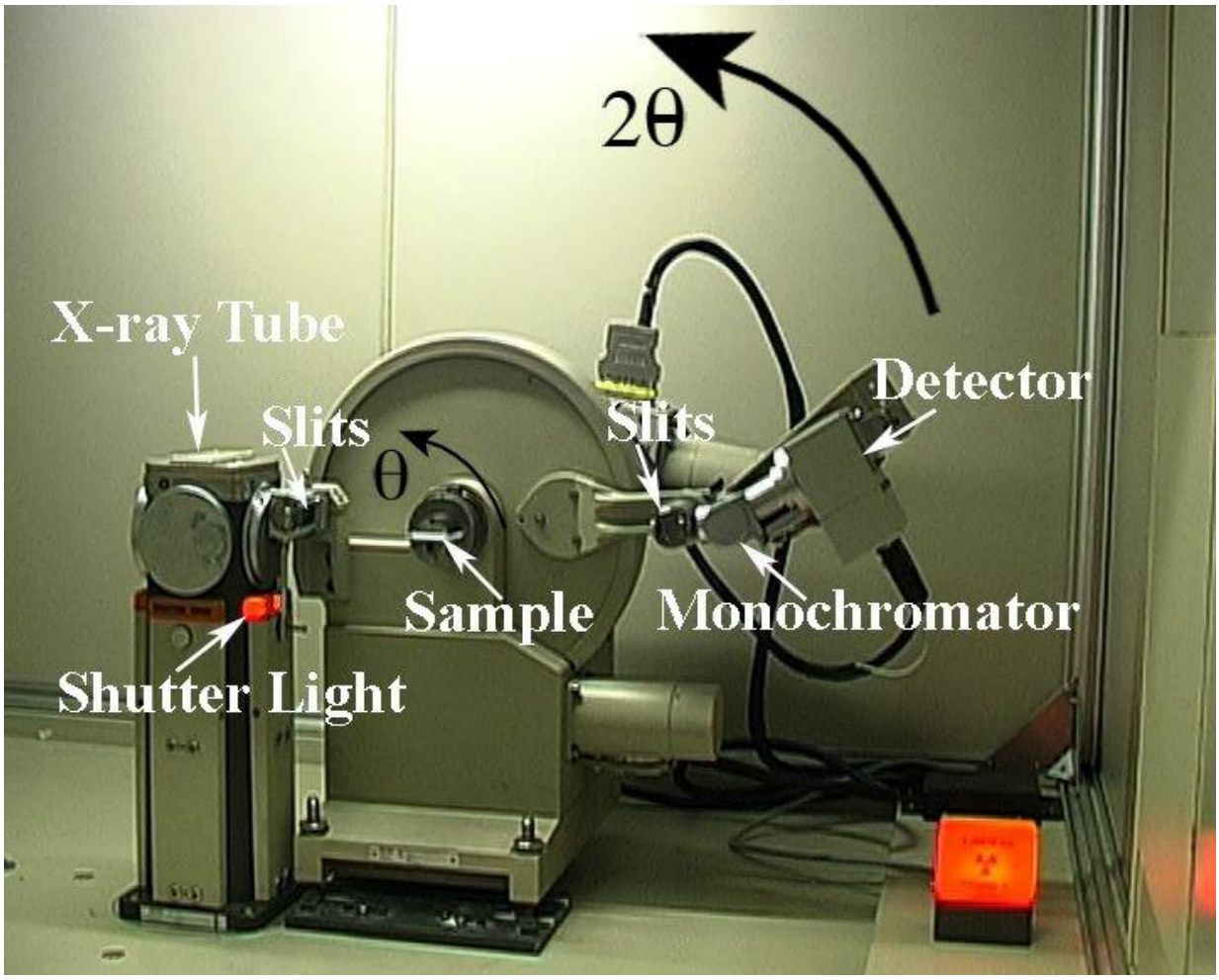

Figure 3.2.1: X-ray diffraction equipment photograph [89].

3.2.2 Raman Spectroscopy

Raman spectroscopy (RS) is an analytical technique that uses inelastic scattering of monochromatic light to obtain the properties of a material. During the Raman scattering technique, a photon from a particular light source interacts with molecules from the sample and is then scattered into the surroundings in all directions. After this process the photons loses or gains energy that is later detected and analysed by the instrument [90]. A photograph of a typical Raman spectrometer Jobin Yvon LabRAM HR 800 UV-VIS-NIR that was employed in the current study is shown in Figure 3.2.2. [91].

Figure 3.2.2: A photograph of a Raman spectroscopy machine [91].

In the Raman spectroscopy there are three types of scattering happening; the Rayleigh, Stokes and anti-Stokes scattering [92]. In the Rayleigh scattering a light source hits a molecule which results in an electron in the ground vibrational state absorbing a photon with a frequency, v_0 and moves to a higher vibrational state [90], [92]. After relaxation the excited electron will then return to their original ground vibrational state an a radiation with the same frequency, v_0 as an excitation source is emitted [90]. In the Stokes an electron in the ground vibrational state absorbs a photon with a frequency, v_0 and moves to a higher vibrational state. Thereafter, the electron relaxes to a lower vibrational state with the energy higher than that of the ground vibration state of frequency v_m [90]. As a consequence, the electron emits a photon with frequency, $v_0 - v_m$. For the anti-Stokes scattering an electron in the vibrational state higher than the ground vibrational state of frequency v_m absorbs a photon with a frequency, v_0 [90]. Subsequent relaxation the electron moves to the ground vibrational state emitting a photon with frequency $v_0 + v_m$ [90]. A diagrammatic representation of the Raman spectroscopy scatterings described over is shown in Figure 3.2.3. [93]. Rayleigh scattering is considered to be elastic while Stokes and anti-Stokes are inelastic. Stokes scattering is the scattering that is mostly used in the Raman spectroscopy since the electrons in most of the molecules are found at ground vibrational state [90]. Raman spectroscopy can provide information about vibrational spectra of numerous molecules and crystals.

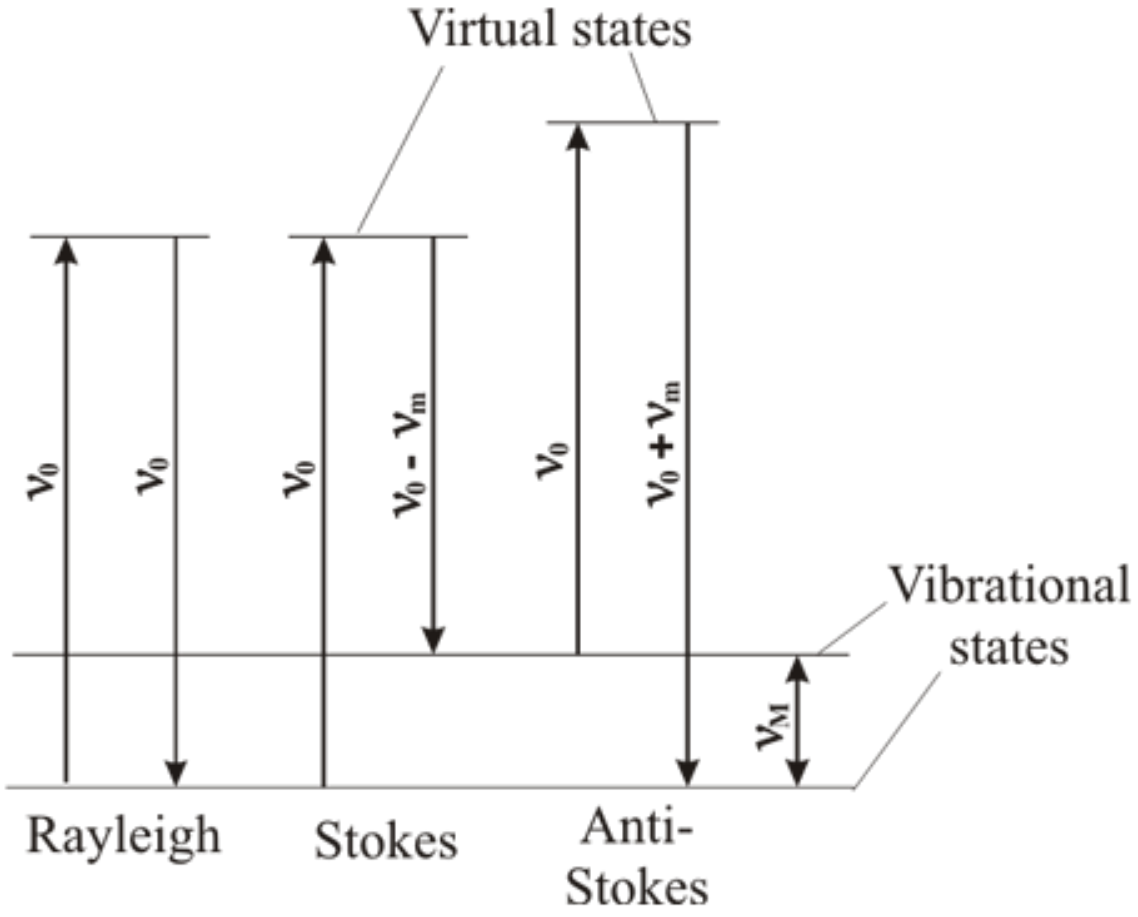

Figure 3.2.3: Schematic illustration of transitions experienced in Raman scattering *[93]*.

3.2.3 Transmission Electron Microscope

TEM is an imaging method where a ray of electrons are transmitted over a sample, and then those transmitted electrons are projected on the screen in a form of an image about that sample [90, 94]. The image is then enlarged and focused to be seen on either the fluorescent screen or it can be detected by a CCD camera [94 – 96]. TEM can study the size, shape and orientation of particles which make up a particular material as and well as how they relate to each other at an atomic level [94]. Materials that can be analysed using this method need to have sizes insignificantly sufficient to allow electron to pass through and must be to be produced by the coating a dilute sample containing the sample on the support grids.

Its possibility of high magnifications has made it an important instrument in different field such as medicine, biology and material sciences research [97]. In these entire fields, the sample must be very thin and be able to withstand the high vacuum that occurs in the instrument while operating [97]. In this study the TEM used is the Tecani G2 transmission electron microscope, an image of the TEM used is presented in Figure 3.2.4. [98].

Figure 3.2.4: A photograph of a transmission electron microscope [98].

3.2.4 Ultraviolet-Visible Spectroscopy

Ultraviolet-visible spectroscopy (UV-Vis) is the spectroscopy that probes using photons in the ultraviolet and visible region from the electromagnetic spectrum [99]. In the UV-Vis region of the electromagnetic spectrum, atoms and molecules undergo electronic transitions where this allows an examination of electronic and optical properties of materials. When a light of a wavelength or radiation interacts with atoms or molecules, a number of processes can occur during the interaction, including reflection, transmission, scattering, absorption and emission [99, 100]. The UV-Vis spectroscopy is generally used to determine the absorbance of a material. The UV-vis spectroscopy is governed by the Lambert's Law which tells us that each layer of equivalent width of an absorbing material absorbs an equivalent amount of energy that pass through it [99, 100] and if the intensity of the initial light is given by I_0 and the light that passes through is denoted by I, then the fraction transmitted defined as:

$$\frac{I}{I_0} = T \qquad (3.2.4.1)$$

where the transmitted percentage is given as:

$$\%T = \frac{I}{I_0} \times 100. \qquad (3.2.4.2)$$

The absorbance:

$$A = \log_{10}\left({}^{I_0}/_{I}\right)$$

$$= log_{10}\left({}^{100}/_{T}\right)$$

$$= \varepsilon cL$$

where L denotes the length of the radiation path through the material, c defined as the concentration of absorbing molecules in the particular path and ε is the coefficient of the molar extinction.

3.2.5 Fourier Transform Infrared Spectroscopy

Fourier transform-infrared spectroscopy (FTIR) is an instrument used to identify organic and inorganic materials [101]. The spectroscopy mainly gives the information about the specific molecular structures present in a material, this occurs when an IR energy is directed through a sample where part of the infrared radiations get to be absorbed and some is gets to be transmitted through the sample. The results obtained from the absorption and transmittance of the sample then gives the molecular type of bond in the material [102]. This radiation absorption occurs under two conditions; firstly when an infrared radiation interacts with the molecule undergoing a change in dipole and secondly when the incoming infrared photons have sufficient energy to move to the next vibration energy state [101].

Each infrared spectrum is said to represent a unique fingerprint of a material with absorption peaks corresponding to the frequencies of the vibrations between the bonds of the atoms making up that particular material [101]. This tell us that each and every material has a different combination of atom, hence not more than one compound or combination of atoms can have the same infrared spectrum. In this study the FITR model used is the Nicolet iS10 FT-IR Spectrometer; an image of the FTIR used is presented in Figure 3.2.5. [103].

Figure 3.2.5: An image of Nicolet iS10 FT-IR Spectrometer [103].

3.2.6 Photoluminescence (PL) Spectroscopy

PL can be defined as the emission of light from a material under optical excitation from a particular light source. This excitation occurs when a light having a particular energy is incident on a material and the material absorbs photons with some of the electrons from the material getting excited and move to higher energy states, eventually these electrons emit photons and return to the ground state [104]. These emitted photons or light are called the photoluminescence and the energy of the photons is the direct measure of the energy band gap. A process of emission of the photoluminescence is represented in Figure 3.2.6. [105]. Since different materials can absorb and emit energy of different wavelength, these photons can be used to get information or identify a particular material [106].

The PL spectra can be obtained by either varying the intensity of the emitted radiation as a function of excitation wavelength or as a function of emission wavelength where in an excitation spectrum the excitation wavelength is varied while keeping the emission wavelength fixed [104]. In an emission process a monochromatic light source is selected in order to excite a particular material where the intensity of the emitted radiation is varied as a function of wavelength [104]. PL spectrum gives transition energies that may be used to identify electronic energy states of a material. The intensity of the PL spectrum measures the relative rates of radiative and non-radiative recombination [104]. Photoluminescence is usually used to [106, 107]:

- study and understand the processes of the recombination,
- identify the surface, interface, and impurity levels,
- detect the defect in the material and
- determine the energy band gap of a material.

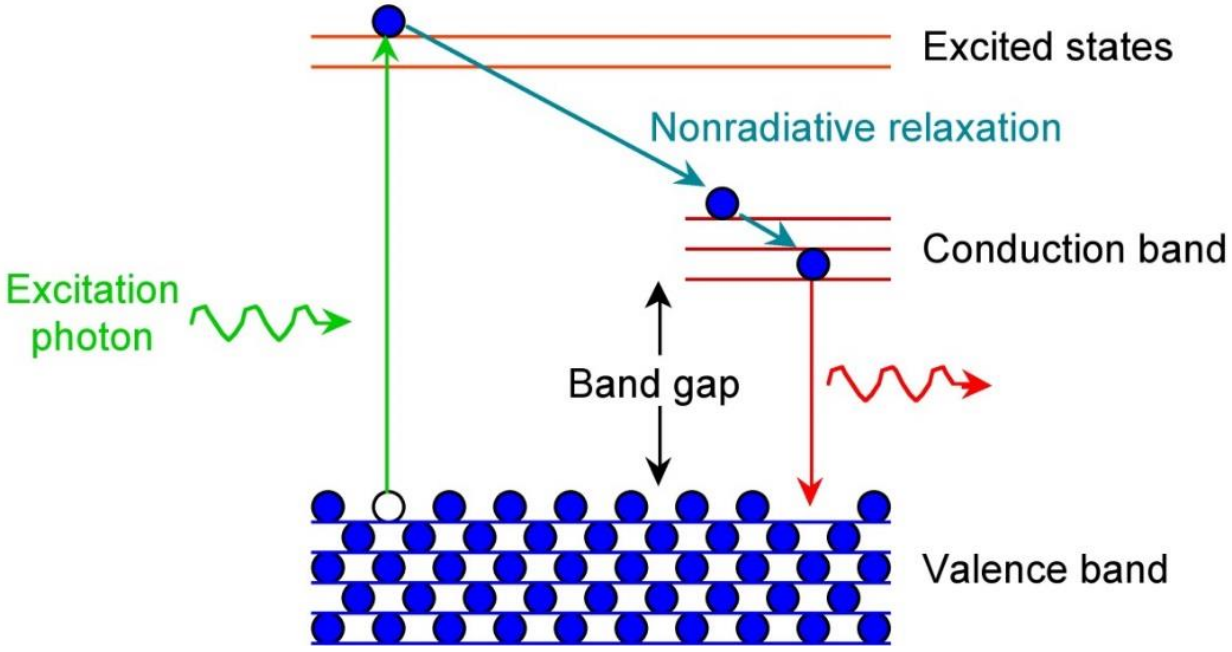

Figure 3.2.6: A process of emission of the photoluminescence spectra [105].

3.2.7 Gas Sensing

When preparing the samples for gas sensing, the synthesised ZnO nanoparticle samples were mixed with ethanol then drop-coated on the surface of the aluminium substrate having to Pt electrodes one side and a heater on the other side. Four samples were prepared for the undoped, In and Co single doped and Co and In combinational doped ZnO nanoparticles. The substrates were then inserted into a chamber inside the machine shown in Figure 3.2.7. The samples were exposed to concentrations: 5, 10, 20, 40, 60, 80, and 100 ppm of CH_4, CO, NH_3 and H_2 gases. The humidity measurement were carried out for the set RH % as 10, 20, 30 40, 50, 60, 70, 80, 90 and 100%. The samples were analysed for different temperatures (250, 300, 350 and 400 $°C$) in order to find the better operating temperature. These electrical characterisations were done at a constant biasing voltage of 0.5 V and the resistance was measured using the kinesistec testing station as shown in Figure 3.2.7. The gas in and out time periods were set at 5 minutes each respectively.

Figure 3.2.7: Kinesistec testing station used for gas sensing in this study

Chapter 4

Structural Studies

4.1. XRD Results

In this study the XRD characterisations were done in order to investigate the structural properties of the Co and In single doped and Co and In co-doped ZnO nanoparticles. The results are shown in figures 4.1.1 to 4.1.4. It can be seen that the prepared undoped and doped ZnO nanoparticles are of a hexagonal wurtzite structure. The ZnO peaks were observed at 2θ = 31.770, 34.432, 36.265, 47.562 and 56.631º which belongs to the (100), (002), (101), (102) and (110) planes respectively. These peaks are consistent with those on the reported standard card values (JCPDS No. 36-1451). The peaks are found to be sharp indicating that the prepared samples are crystallised. No peaks related to Co or In were detected in the samples indicating that Co and In ions have substituted for the Zn ions and that In and Co were successfully incorporated into the ZnO nanostructure. Similar contention results were obtained by M. Thambidurai *et al*. [108], H. Gu *et al*. [54], R. Bhargava *et al*. [46], S. Kumar *et al*. [109], and D. Fang *et al*. [110]. Only Al peaks were detected in the XRD patterns belonging to the XRD sample holder (peaks indicated by asterisk (*)), the peaks were indexed as (111) and (200) COD entry No 96-431-3207.

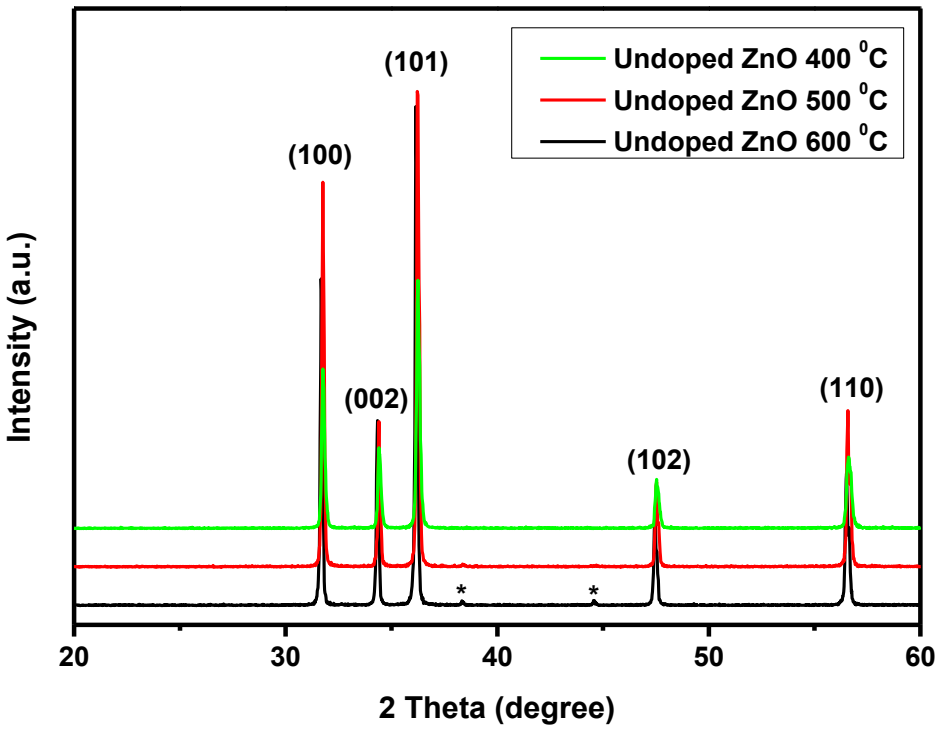

Figure 4.1.1: XRD patterns of undoped-ZnO at 400, 500 & 600 °C.

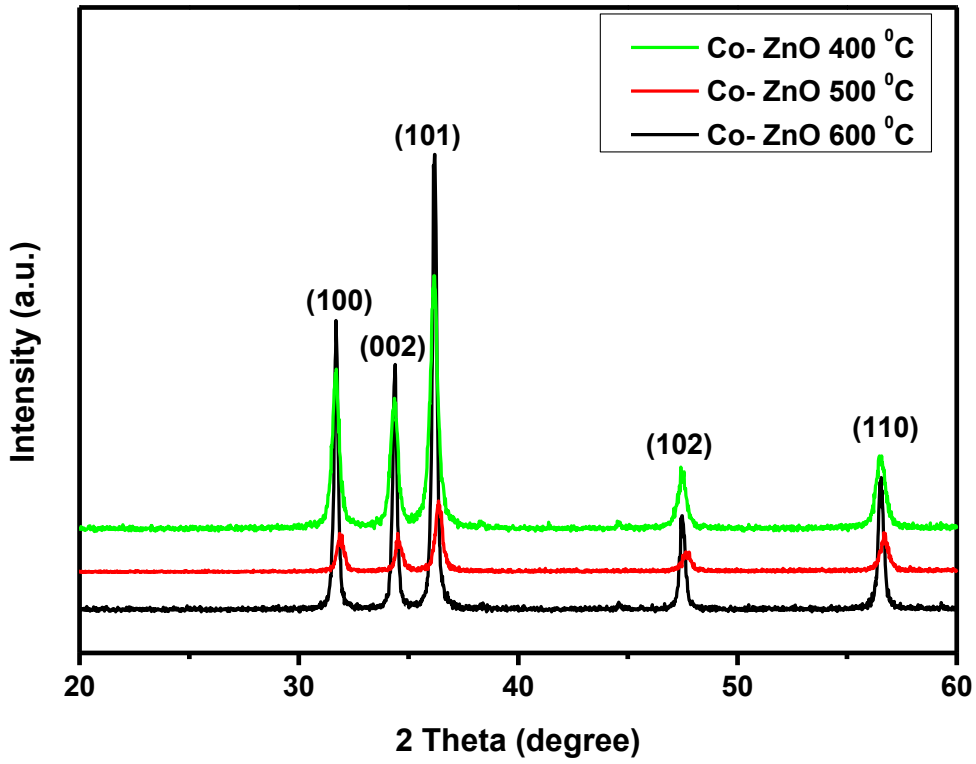

Figure 4.1.2: XRD patterns of Co-doped-ZnO at 400, 500 & 600 °C.

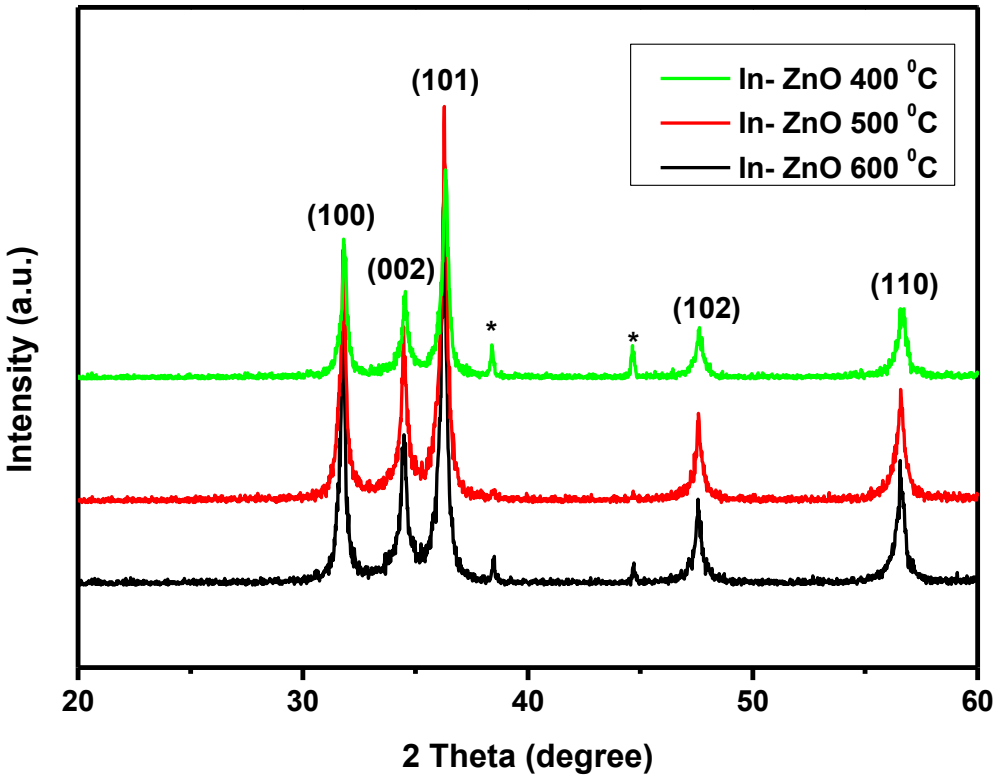

Figure 4.1.3: XRD patterns of In-doped-ZnO at 400, 500 & 600 °C.

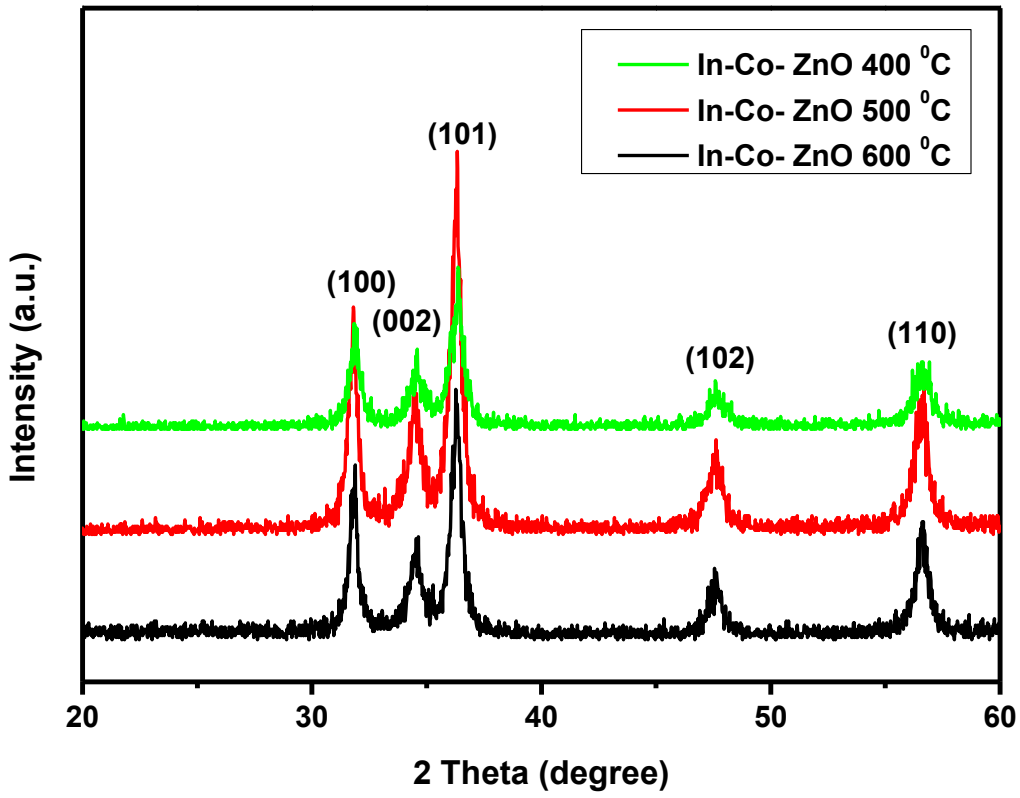

Figure 4.1.4: XRD patterns of In-Co-doped-ZnO at 400, 500 & 600 °C.

The lattice parameters were calculated from the XRD result using the (100) and the (002) planes. The values of the lattice parameters are represented in table 4.1.1. For the undoped ZnO nanoparticles the lattice parameters are observed to increase with an increase in annealing temperature. For the Co-doped ZnO nanoparticles the lattice parameters increased as compared to the undoped ZnO nanoparticles (S. Kumar *et al*. [109] and A. Mesaros *et al*. [111] reported similar results) and are found to be slightly increasing with an increase in temperature. For the In doped ZnO nanoparticles the lattice parameters decrease compared to the undoped ZnO nanoparticles (Thambidurai *et al*. [108] reported similar results) and increase with an increase in temperature. For the In-Co co-doped the lattice parameters are small in comparison with the undoped ZnO nanoparticles and increase with increasing temperature.

The bond length of the undoped and doped ZnO nanoparticle samples were determined and a difference was observed between the bond length of the undoped and doped ZnO nanoparticles, that was due to the introduction of the In and Co dopants into the ZnO structure.

The particle size of all the samples were determined from the XRD results and presented in table 4.1.1. The particle size of the Co-doped, In-doped and In-Co co-doped ZnO particles are found to be 19.054, 22.136, 11.498 nm respectively. This indicates that the introduction of Co and In dopants reduced the particle size from 42.419 nm of the undoped ZnO nanoparticles and this reduction significantly happened to the In-Co co-doped ZnO nanoparticles. The particle sizes of all the prepared samples were found to increase with temperature and this is due to the fact that annealing at high temperature is found to enhance the mobility of atoms and also

decreasing the diffusion rate, where enhanced mobility at high temperatures reduces the grain boundary tension letting the grain size or particle size to grow [112 – 114]. Results comparable to these were reported by D. Fang *et al*. [110] and A.K. Zak *et al*. [115] .

The strain on the nanoparticles for all the prepared ZnO nanoparticles has also been determined, an inverse relationship has been observed between the strain and the particle size. The strain is also found to decrease with an increase in temperature which implies that the peak broadening is due to the particle size.

Table 4.1.1: Lattice parameters a, b and c, bond length L, average particle size D and average strain ε.

Sample Name	**Temperature (°C)**	**a = b (nm)**	**c (nm)**	**L (Å)**	**D (nm)**	**ε ($\times 10^{-3}$)**
Undoped-ZnO	400	0.32491	0.52048	3.9096	42.41895	2.4014
	500	0.32500	0.52070	3.9122	52.26525	1.9509
	600	0.32575	0.52177	3.9296	53.51675	1.9108
Co-doped ZnO	400	0.32582	0.52170	3.9289	19.05428	5.3637
	500	0.32370	0.51861	3.8809	20.13383	5.0575
	600	0.32566	0.52131	3.9260	32.38677	3.1506
In-doped ZnO	400	0.32428	0.51892	3.8919	22.13600	4.6034
	500	0.32480	0.51953	3.9034	21.72721	4.7072
	600	0.32533	0.51969	3.9128	22.61027	4.5066
In-Co doped ZnO	400	0.32394	0.51830	3.8833	11.49835	8.9786
	500	0.32474	0.51939	3.9016	13.16581	7.8151
	600	0.32672	0.52164	3.9450	16.30980	6.3561

4.2. TEM Results

The TEM measurements were performed for the undoped ZnO nanoparticles at 400 ℃, the In and Co single doped ZnO nanoparticles and the In-Co co-doped ZnO nanoparticles annealed at 400 ℃, 500 ℃ and 600 ℃. The results of the energy-dispersive x-ray spectroscopy (EDS) and the transmission electron microscope (TEM) images are represented in figures 4.2.1 - 4.2.10. In the case of the undoped ZnO nanoparticles annealed at 400 ℃ spherical partciles can be seen in figure 4.2.2 and alongside the spherical nanoparticles there are big rods which are basically created when spherical nanoparticles come together and hence smaller particles can be seen inside the rods. Similar results were reported by Liguo Xu *et al*. [116]. From figure 4.2.2, EDS results confirmed that Co has been doped into ZnO nanoparticles and the spherical nanoparticles can be observed on the TEM image. Similar results can be observed in figure 4.2.5 and figure 4.2.8. Looking at figure 4.2.1; the EDS results confirmed the presence of In in the medium and showed that the nanoparticles are spherical. In a similar manner figures 4.2.6 and 4.2.9 confirm the results. From figure 4.2.4, EDS results confimed the precence of both In and Co, impliying that both In and Co were sucessfully doped into the ZnO nanoparticles. Comparable effects have been observed in figure 4.2.2 and 4.2.10. In all the doped samples it can be seen that as the temperature increases, the nanoparticles became more agglomated and hence the particle size increases, and this consequence is coherent with the XRD results.

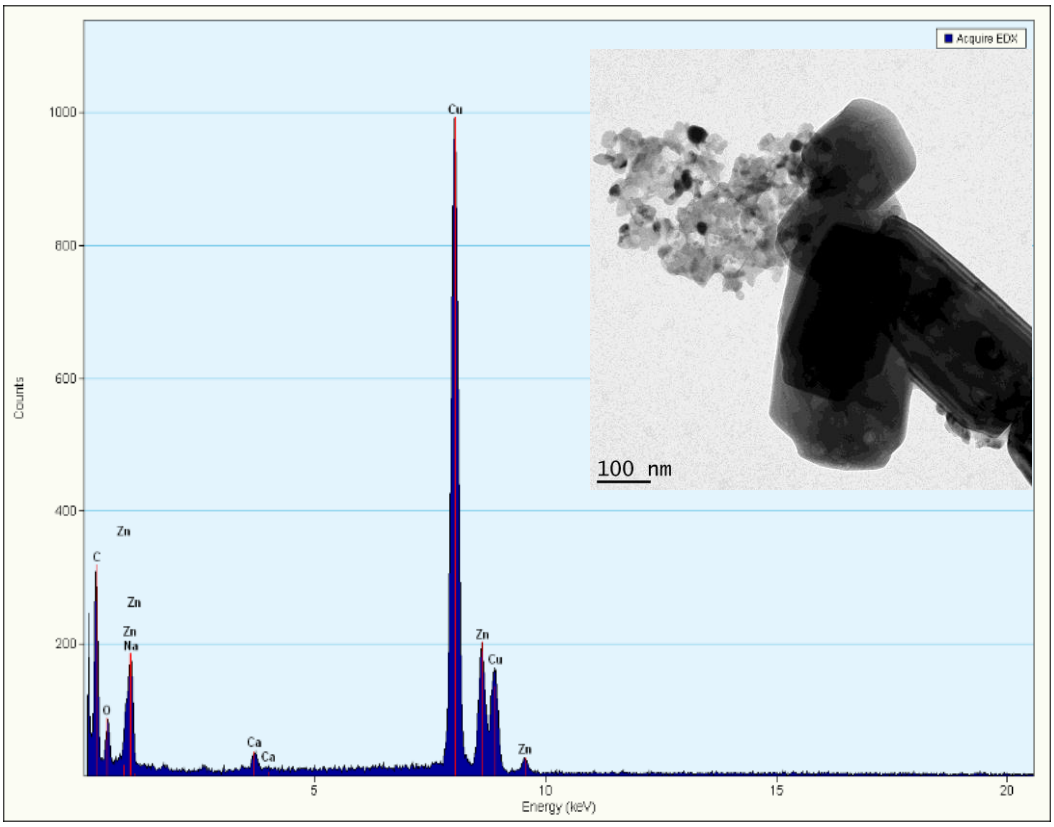

Figure 4.2.1: EDS and TEM of undoped ZnO 400 ℃.

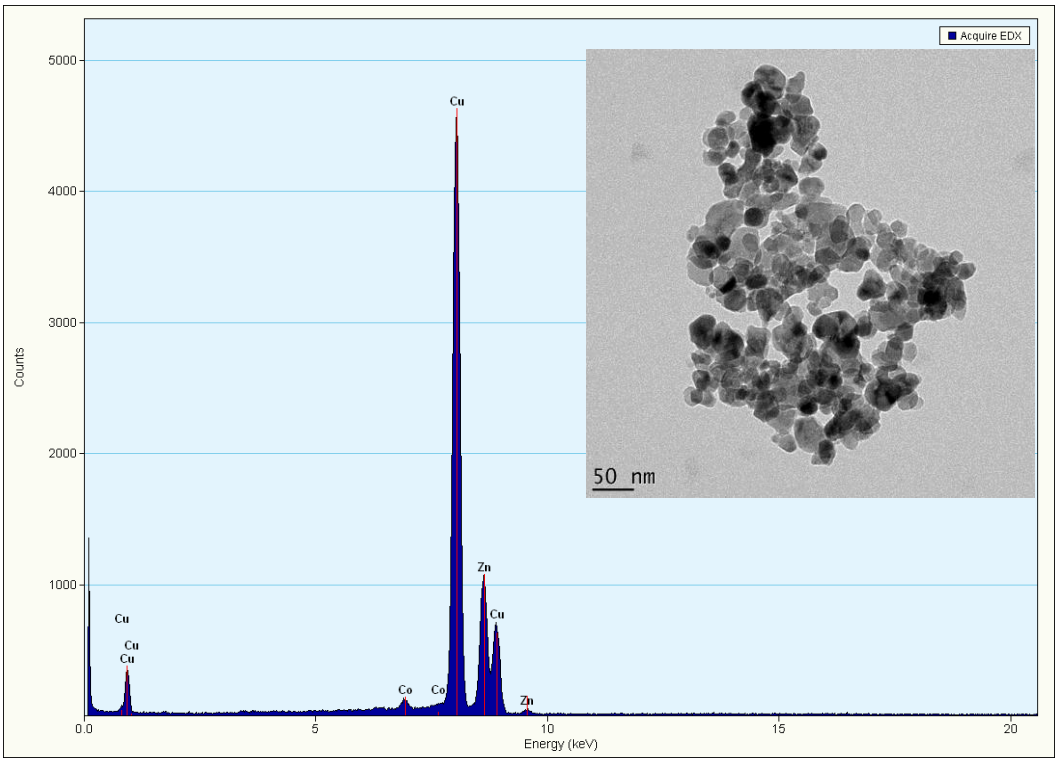

Figure 4.2.2: EDS and TEM of Co-ZnO 400 ℃.

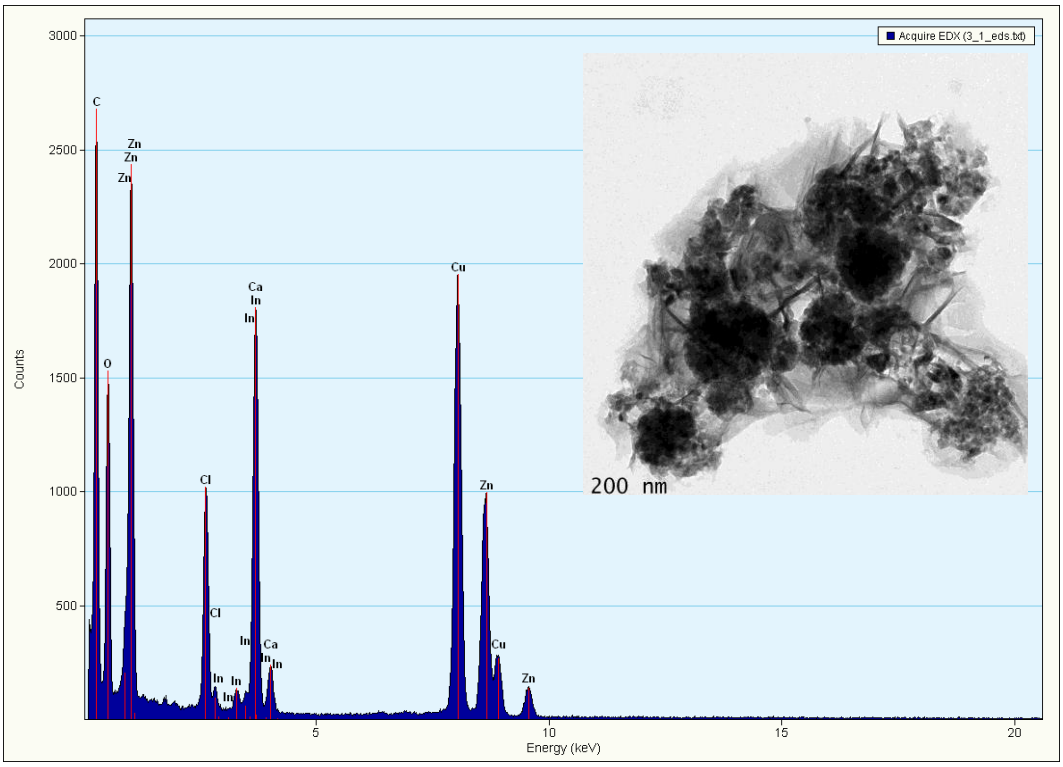

Figure 4.2.3: EDS and TEM of In-doped ZnO 400 ℃.

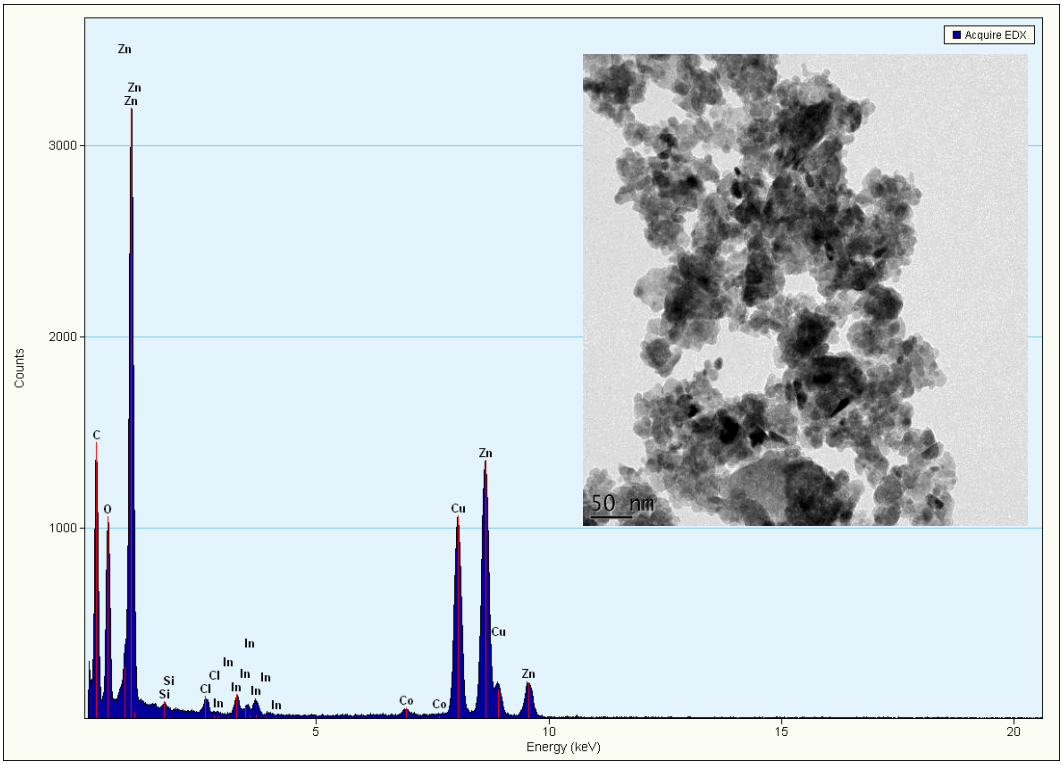

Figure 4.2.4: EDS and TEM of In-Co-doped ZnO 400 ℃.

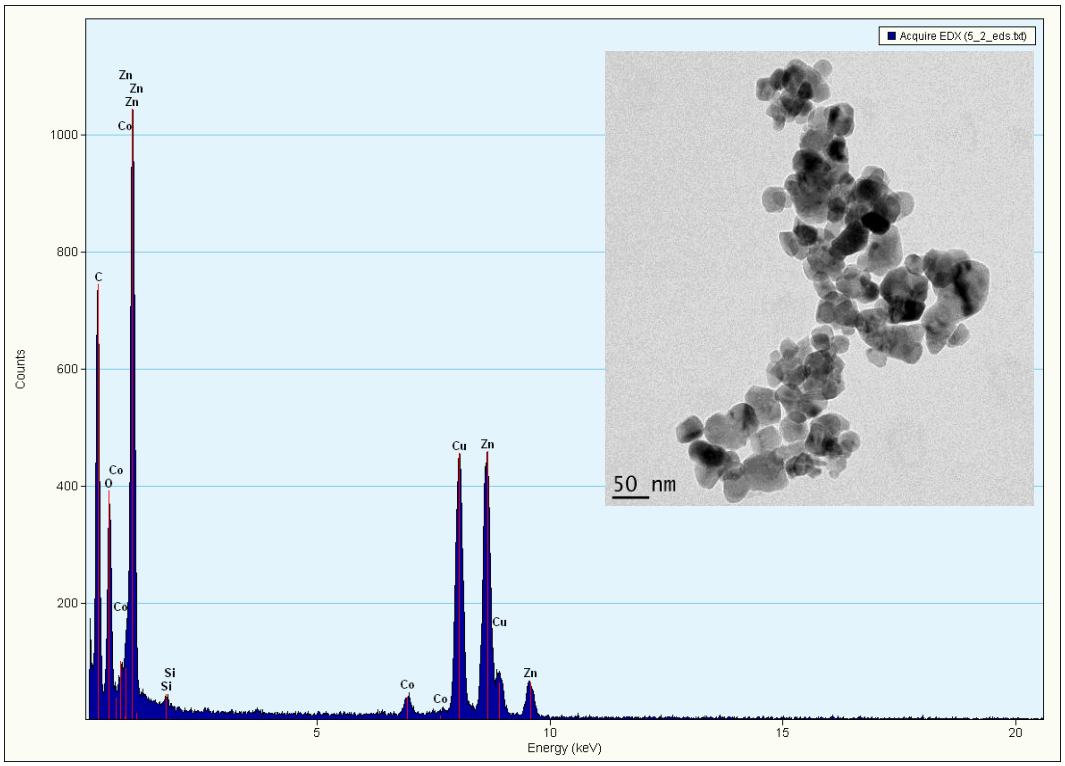

Figure 4.2.5: EDS and TEM of Co-doped ZnO 500℃.

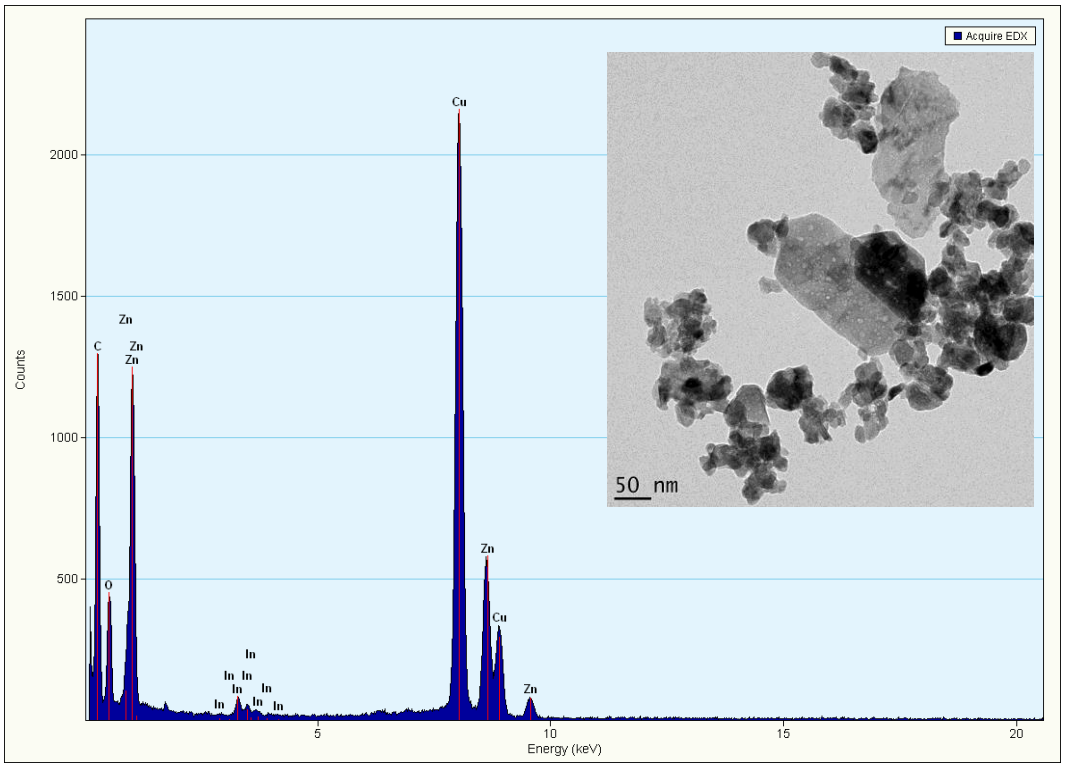

Figure 4.2.6: EDS and TEM of In-doped ZnO 500 ℃.

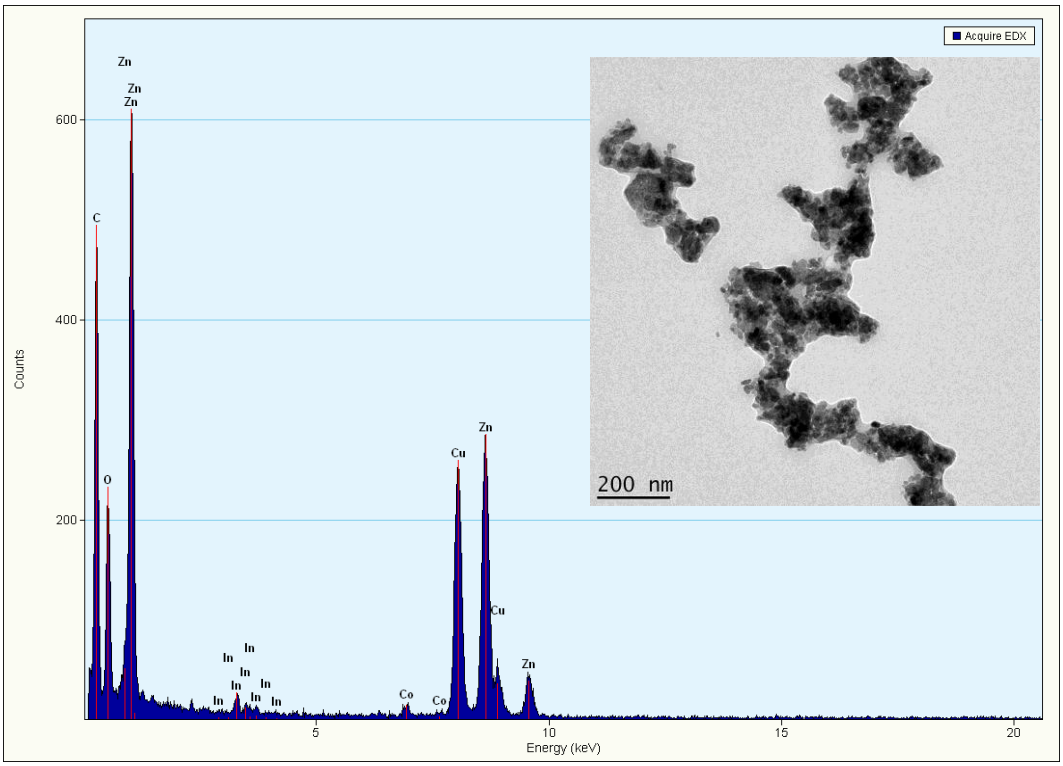

Figure 4.2.7: EDS and TEM of In-Co-doped ZnO 500 ℃.

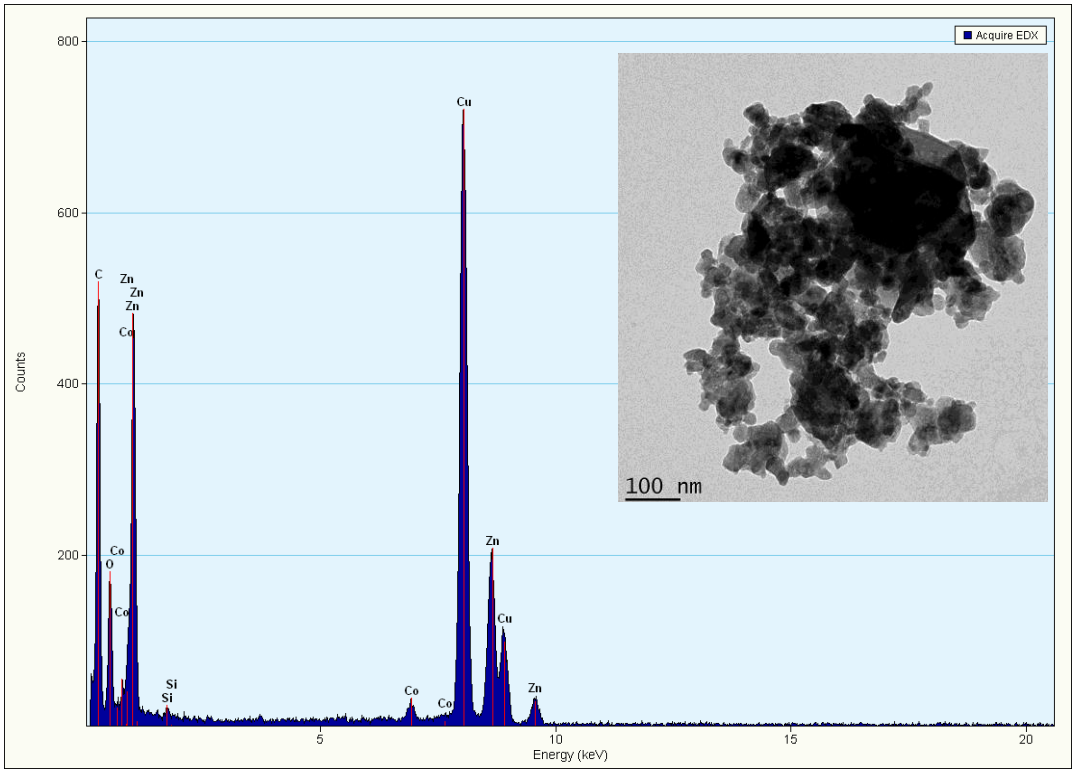

Figure 4.2.8: EDS and TEM of Co-doped ZnO 600 ℃.

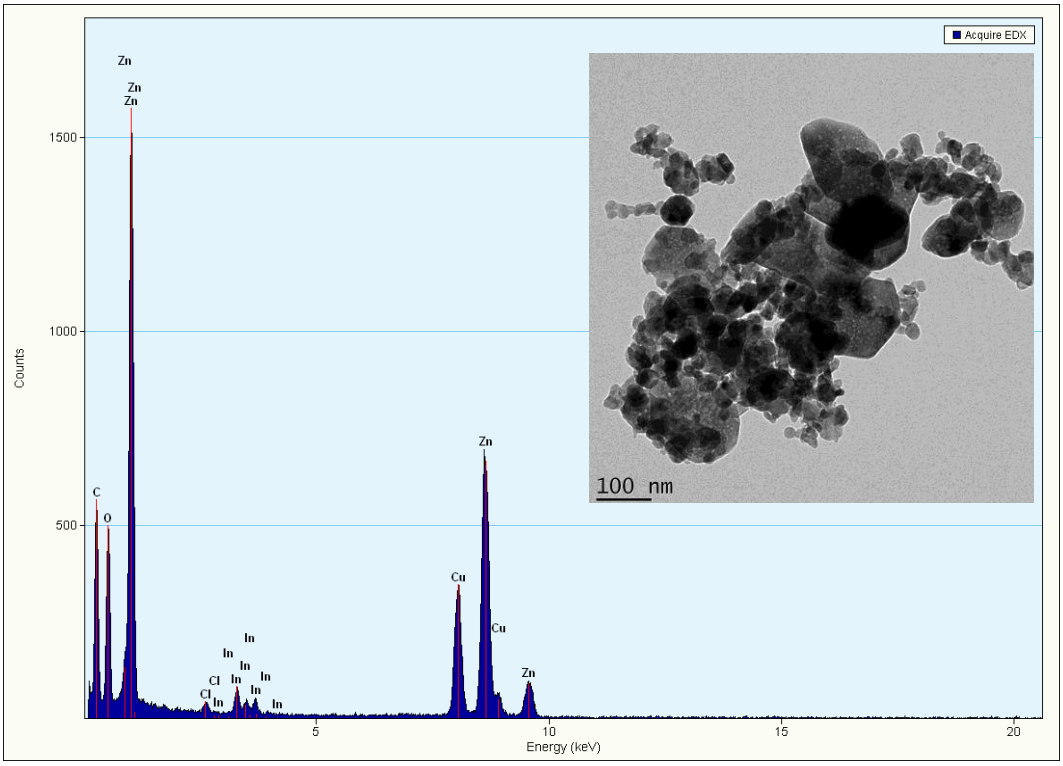

Figure 4.2.9: EDS and TEM of In-doped ZnO 600 ℃.

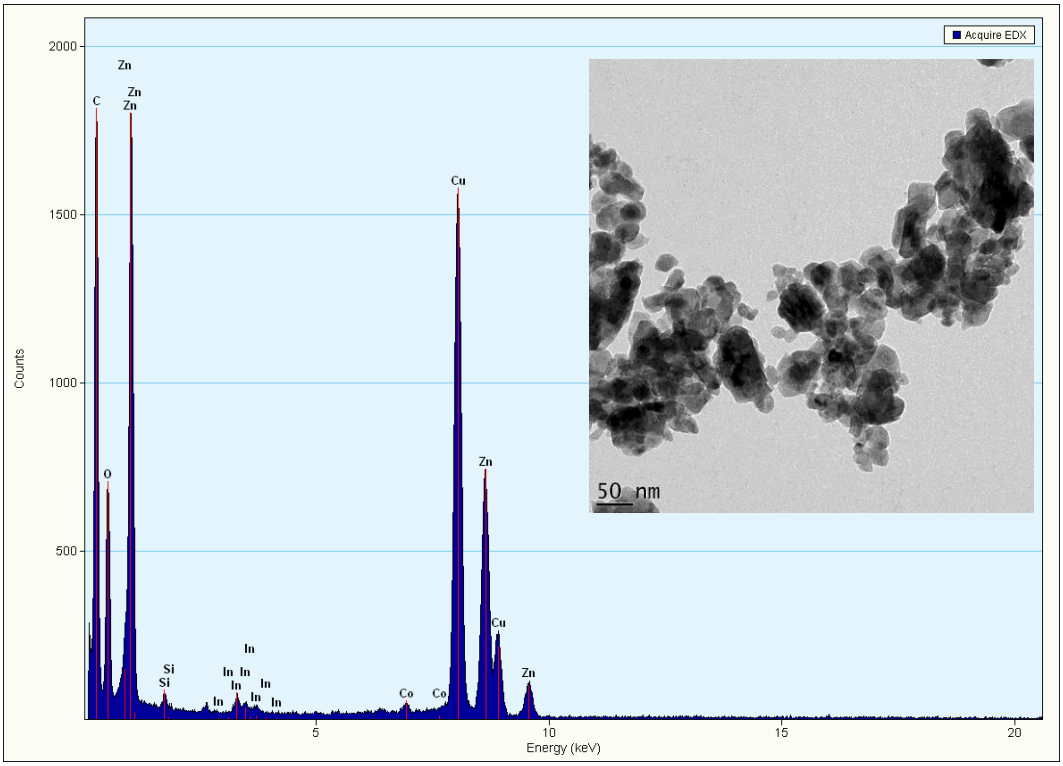

Figure 4.2.10*:* EDS and TEM of In-Co-doped ZnO 600 ℃.

4.3. Conclusion

The undoped ZnO nanoparticles, In and Co single doped ZnO nanoparticles and the In and Co co-doped ZnO nanoparticles were successfully synthesised using the sol-gel method. The XRD results showed that the samples prepared were of the ZnO wurtzite crystal structure. The lattice parameters of the prepared samples were calculated and found to be similar to the reported values of the bulk ZnO. The bond length of the undoped and doped ZnO nanoparticle samples were calculated and found to be different indicating the presence of In and Co dopants. The average particle sizes were estimated and it was found that single doping ZnO nanoparticles with In and Co reduced the average particle size while co-doping reduced them even further. It was also observed that the average particle size increase with an increase in temperature. The strains of the prepared samples were also determined using the XRD results and it was observed to be inversely proportional to the average particle size. The TEM images showed that the prepared samples were spherically shaped while the EDS results confirmed that the In and Co was successfully doped into the ZnO nanoparticle structure.

Chapter 5

Optical Studies

5.1. UV-Vis Results

In order to understand the optical properties of the prepared samples, the absorbance of all the undoped and doped ZnO nanoparticle samples were measured using UV-vis spectroscopy. The absorbance spectra's are presented in figures 5.1.1 - 5.5.4. From all the UV-vis spectra it can be seen that below a wavelength of 500 nm, the spectrum gets noisy. In all the samples doped with Co three additional absorption peaks can be observed between 550-700 nm and these peaks were assigned to $^4A_2(F) \rightarrow {}^2A_1(G)$, $^4A_2(F) \rightarrow {}^4T_1(P)$ and $^4A_2(F) \rightarrow {}^2E(G)$ transitions [111, 117, 118]. This may be suggesting that the Zn^{2+} ions in the ZnO hexagonal wurtzite structure have been replaced by the tetrahedrally coordinated Co^{2+} ions [117]. The results are corroborated by Mesaros *et al*. [111] who used wet-chemical synthesis route, Bouloudenine *et al*. [119] using hydrothermal methods, and Nam *et al*. [120] who used sol-gel spin coated films.

Table 5.1.1 Energy band gap of undoped ZnO, Co doped ZnO, In doped ZnO, and In-Co co-doped ZnO in comparison with bulk ZnO of reference [26].

Sample Name	Temperature (^oC)	E_g (eV)
Bulk ZnO [26]	-	3.37
Undoped-ZnO	400	3.10
	500	2.91
	600	2.69
Co-doped ZnO	400	2.53
	500	2.48
	600	2.46
In-doped ZnO	400	2.74
	500	2.70
	600	2.65
In-Co doped	400	2.43
	500	2.22
	600	2.17

From the absorbance spectra the band energy gaps of the undoped and doped ZnO nanoparticles samples were determined and tabulated in table 5.1.1. The energy band gaps of the undoped ZnO nanoparticles were found to be smaller than the reported values for the bulk ZnO (3.37 eV) [26], similar results were previously obtained for the ZnO nanoparticles [47, 110]. The energy band gaps of the doped samples reduced even further compared to the undoped ZnO nanoparticles when the dopants were introduced in the ZnO nanoparticles and this reduction or redshift is due to the introduction of dopants into the structural properties of ZnO nanoparticles. P. Li *et al*., [47], A. Mesaros *et al*., [111], N.F. Djaja *et al*., [121] and C. Tsay *et al*., [122] also reported a reduction in energy band gap with an introduction of dopants in the ZnO nanoparticles. The energy band gaps of all the prepared samples were also found to decrease with increase in the annealing temperature and this was due to the increase in the particle size since there is an agglomeration of nanoparticles [123]. Similar results were reported by J. El Ghoul *et al*. [124].

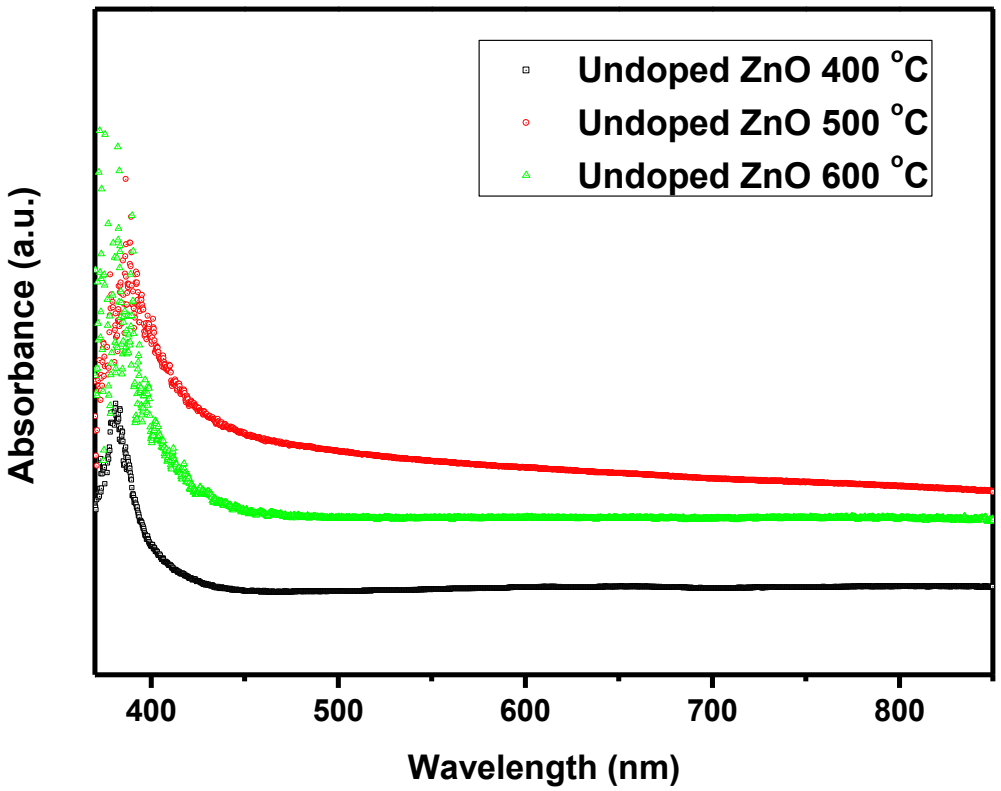

Figure 5.1.1: Absorbance spectra of undoped ZnO at 400, 500 and 600 °C.

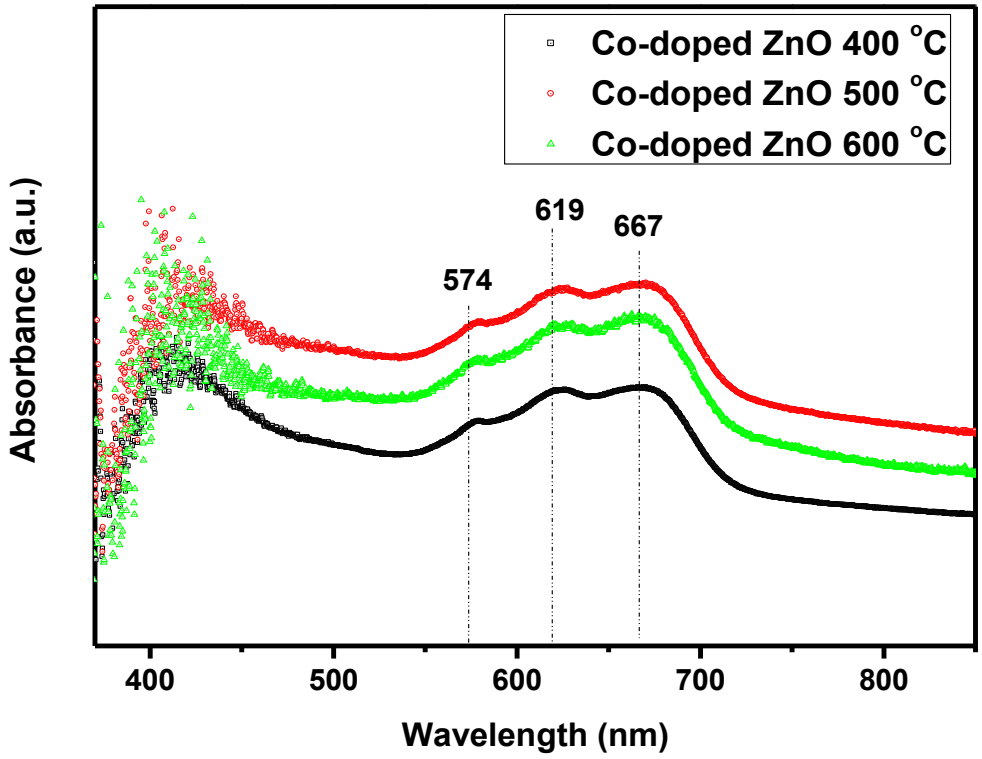

Figure 5.1.2: Absorbance spectra of Co-doped ZnO at 400, 500 and 600 °C.

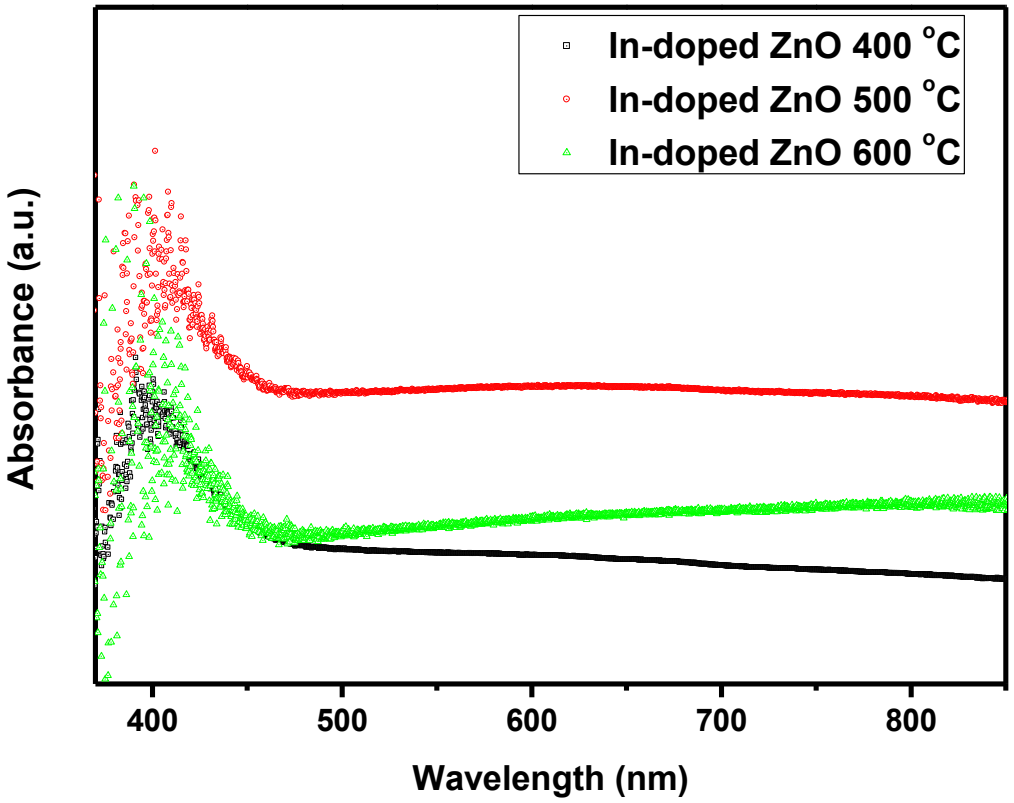

Figure 5.1.3: Absorbance spectra of In-doped ZnO at 400, 500 and 600 °C.

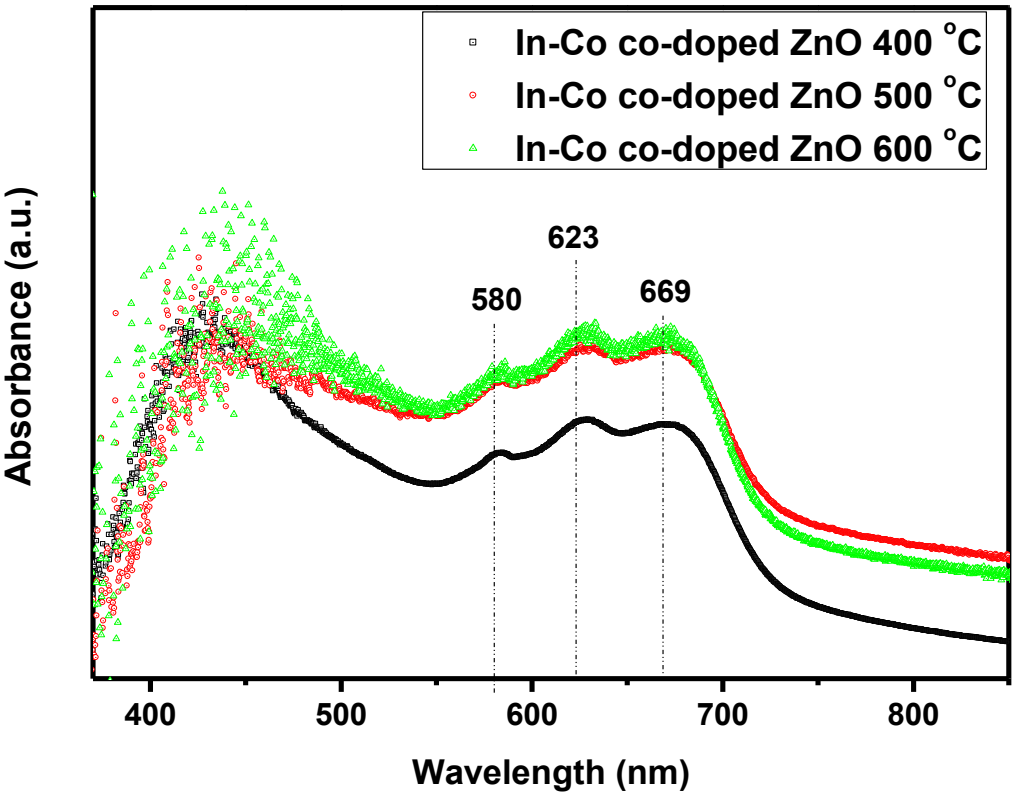

Figure 5.1.4: Absorbance spectra of In-Co co-doped ZnO at 400, 500 and 600 °C.

5.2. FTIR Results

In order to investigate and identify organic and inorganic materials in the prepared samples the FTIR studies were also performed. The FTIR spectra's are presented in Figures 5.2.1 - 5.2.4. All the figures indicate four main bands that can be observed between 1507-1524 cm^{-1}, 1351-1398 cm^{-1}, 853-869 cm^{-1} and 510-598 cm^{-1}. FTIR bands located between 1507-1524 cm^{-1} can be assigned to the $C = O$ vibrations according to T. Gfroerer *et al*. [125]. The bands near 1351-1398 cm^{-1} are assigned to the $H - O - H$ bending vibration from the zinc acetate dehydrate that was used as the precursor [126]. C. Reber [127] together with P. A. Rodnyi *et al*. [128] findings ascribe the bands located at 510-598 cm^{-1} and 853-869 cm^{-1} to Zn-O vibrations. In addition S. Suwanboona *et al*. [129] and P. P. Sharmila *et al*. [130] reported that the modes between 510-598 cm^{-1} and 853-869 cm^{-1} confirm that the prepared samples are of ZnO nature. The results are consistent with the XRD results discussed in the previous chapter. The findings further confirm that the prepared samples are of the ZnO hexagonal wurtzite structure, similar results were obtained by K. Raja *et al*. [126].

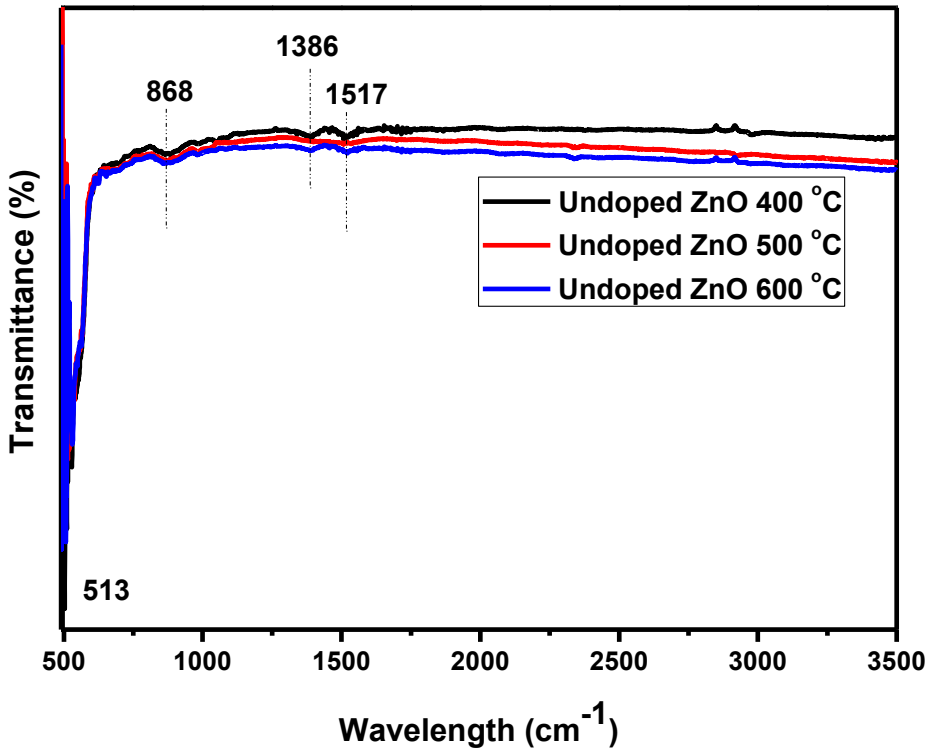

Figure 5.2.1: FTIR spectra of undoped doped ZnO nanoparticles annealed at 400 ℃, 500 ℃ and 600 ℃

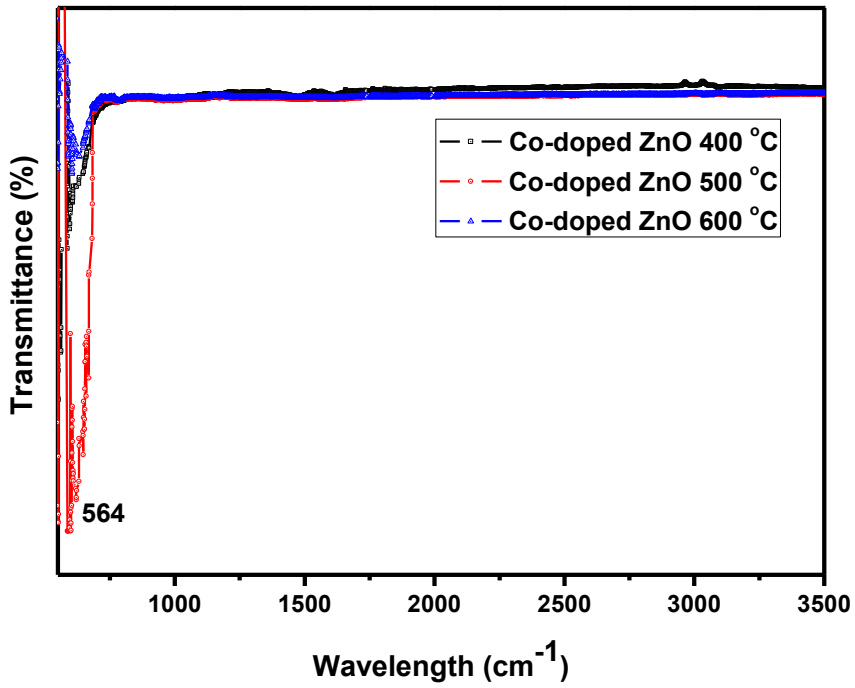

Figure 5.2.2: FTIR spectra of Co-doped ZnO nanoparticles annealed at 400 ℃, 500 ℃ and 600 ℃.

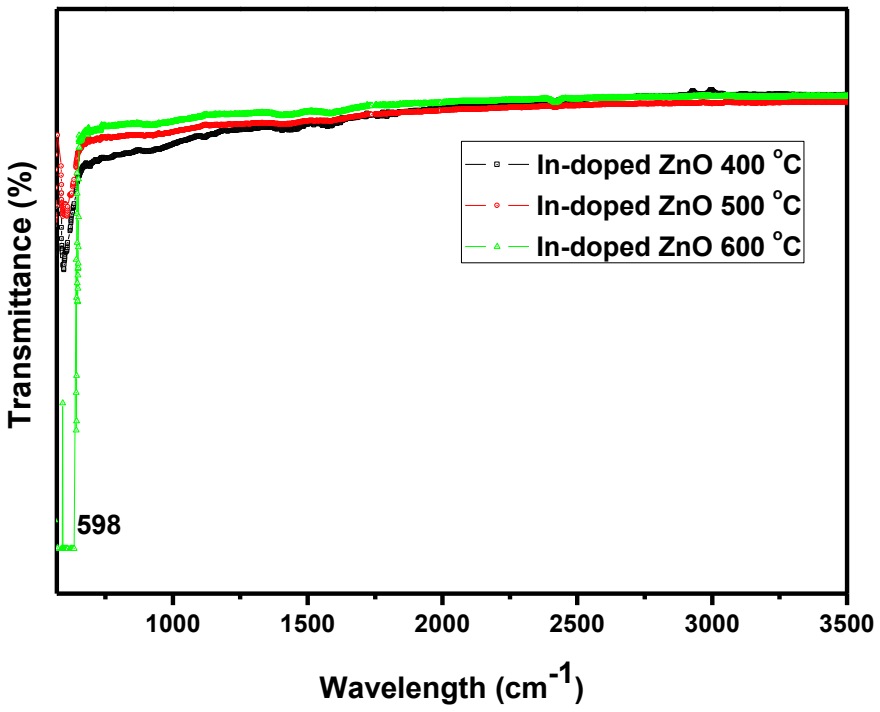

Figure 5.2.3: FTIR spectra of In-doped ZnO nanoparticles annealed at 400 ℃, 500 ℃ and 600 ℃

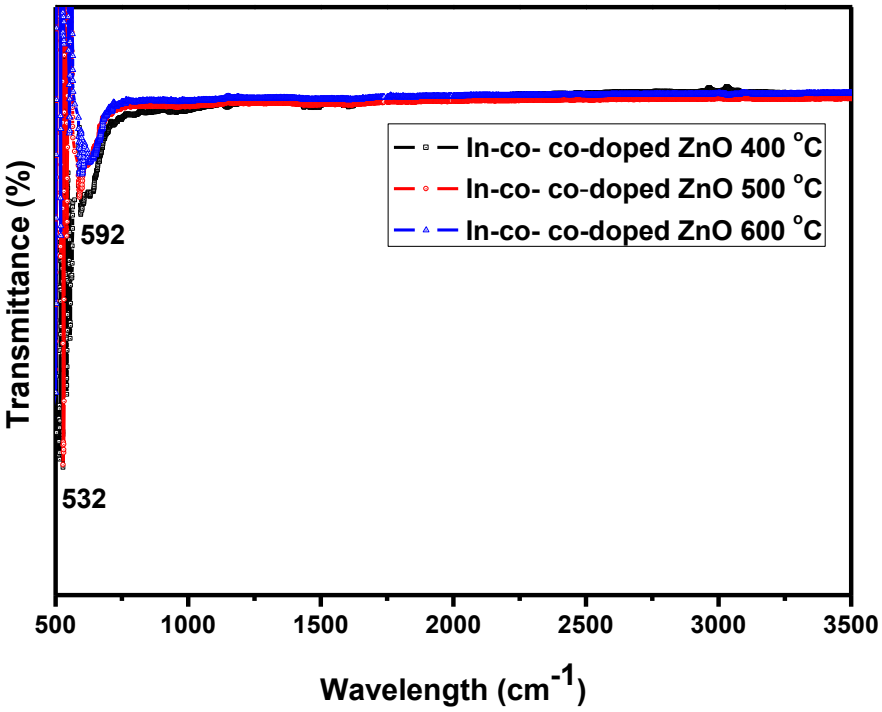

Figure 5.2.4: FTIR spectra of In-Co co-doped ZnO nanoparticles annealed at 400 ℃, 500 ℃ and 600 ℃.

5.3. Raman Results

The vibrational properties of the undoped and doped ZnO nanoparticle samples were investigated using an excitation wavelength of 514 nm. The group theory predicts that the ZnO wurtzite hexagonal structure has a space group of C_{6v}^4 [131]. This can be described by the phonon modes near the centre of the Brillouin zone given by the equation: $\Gamma = A_1 + 2B_1 + E_1 + 2E_2$, where A_1, E_1 and $2E_2$ are Raman active modes and $2B_1$ is the forbidden mode of ZnO [131, 132]. A_1 and E_1 are polar and they split into two modes namely; transverse optical (TO) and longitudinal optical (LO) phonons and E_2 is divided into E_2^{low} and E_2^{high}, the E_2^{low} mode is associated with the vibration of the heavy Zn sublattice, while E_2^{high} is coupled to the vibration of oxygen atoms in the ZnO [131].

For all the prepared samples the vibration modes are presented in table 5.3.1. The peaks near 325.1-329.6 cm^{-1} are assigned to the $E_2^{high} - E_2^{low}$ phonon modes, similar results were obtained for the undoped and metal doped ZnO nanoparticles reported by R. Y. Sato-Berru *et al*. [133]. The peaks at 374.8 - 376.0 cm^{-1} belong to the A_1(TO) modes [134]. The peaks near 430.0 - 434.3 cm^{-1} can be attributed to the ZnO E_2^{high} phonons, whilst the peaks around 562.5 - 581.2 cm^{-1} and the peak at 406.5 cm^{-1} belong to the E_1(LO) mode and E_1(TO) respectively. The peaks at 687.5 - 696.5 cm^{-1} can be assigned to the TO+ LO phonons.

N. Romcevic *et al*. [135] and S. Kumar *et al*. [109] reported that the modes between 430.0 - 435.4 cm^{-1} confirms that the samples prepared are of ZnO wurtzite hexagonal crystal structure. A decrease in Raman intensity with an increase in temperature, also a redshift with an introduction of dopants were observed for the peaks around 430.0 - 435.4 cm^{-1}. S. Kumar *et al*. [109] reported similar results where a decrease in Raman

intensity and a redshift for the Co and N co-doped ZnO nanopowders were obtained. M. Schumm *et al*. [136] and L. Yang *et al*. [137] also reported that the peaks around 562.5 - 581.2 cm^{-1} were due to the defects such as oxygen vacancies (V_O), zinc interstitials (Zn_i) and/or free carriers in some papers.

In the sample Co doped ZnO annealed at 600 ℃ the peaks 479.7 and 701.4 cm^{-1} are associated with Co_3O_4 [109], while the peak at 518.6 cm^{-1} is attributed to the Si substrate [134].

Table 5.3.1: Raman vibration modes (cm^{-1}) along with their assigned symmetry in undoped ZnO, 5% Co doped ZnO, 5% In doped ZnO, and 5% In-Co doped ZnO.

Sample Name	Symmetry (cm^{-1})						
	$E_2^{high} - E_2^{low}$	A_1 (TO)	E_1 (TO)	E_2^{high}	A_1 (LO)	E_1 (LO)	TO+ LO
Undoped ZnO 400 ℃, 500 ℃ & 600 ℃	329.6	376.0	406.5	434.3	-	581.2	-
5% Co doped ZnO 400 ℃, 500 ℃ & 600 ℃	325.3	-	-	430.6	-	562.8	-
5% In doped ZnO 400 ℃, 500 ℃ & 600 ℃	327.5	374.8	-	433.2	-	578.9	696.5
5% In-Co doped ZnO 400 ℃, 500 ℃ & 600 ℃	325.1	-	-	430.0	-	562.5	-

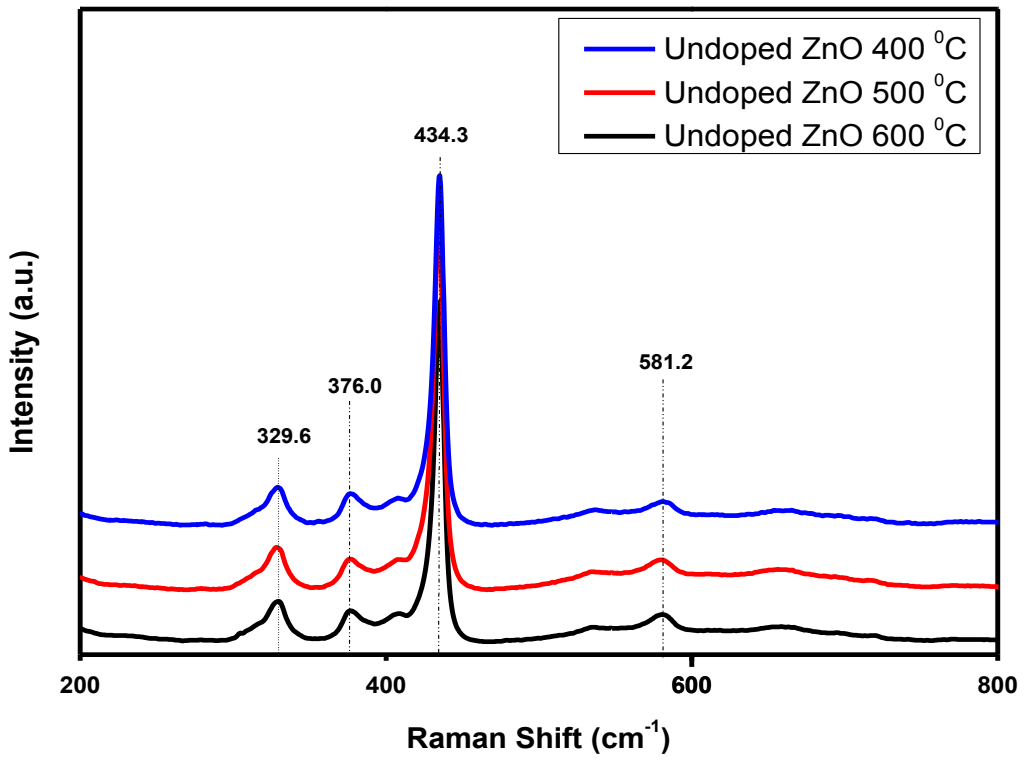

Figure 5.3.1: Raman spectroscopy of undoped doped ZnO nanoparticles annealed at 400 ℃, 500 ℃ and 600 ℃

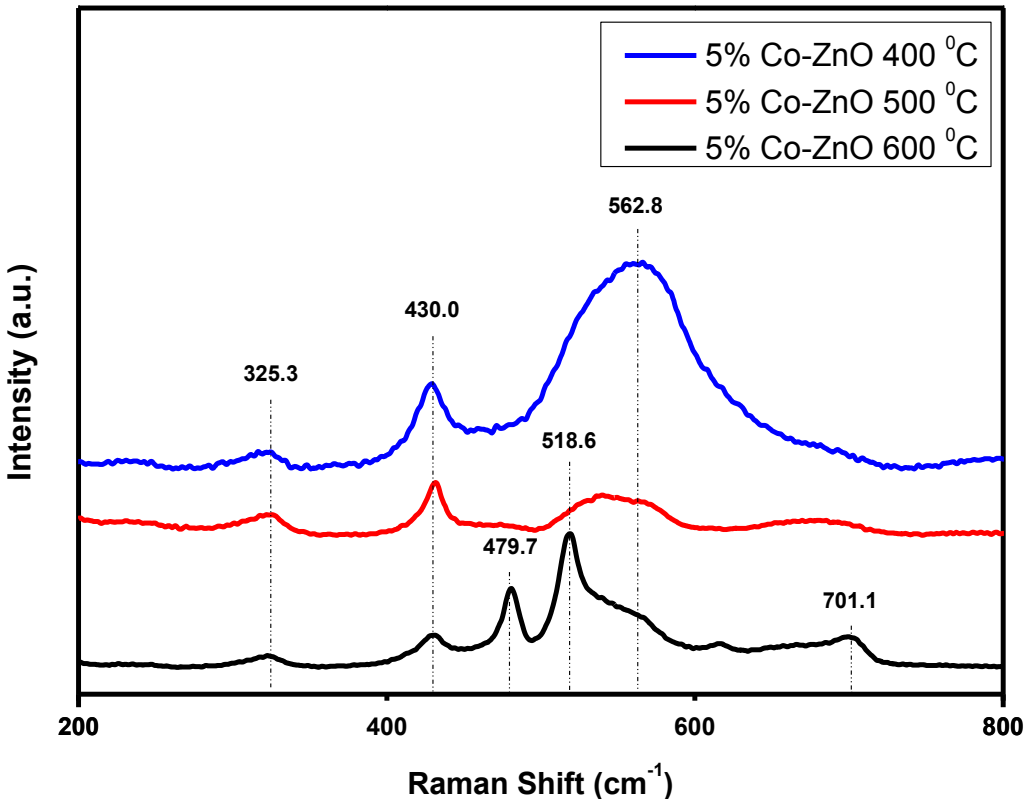

Figure 5.3.2: Raman spectroscopy of 5% Co-doped doped ZnO nanoparticles annealed at 400 ℃, 500 ℃ and 600 ℃

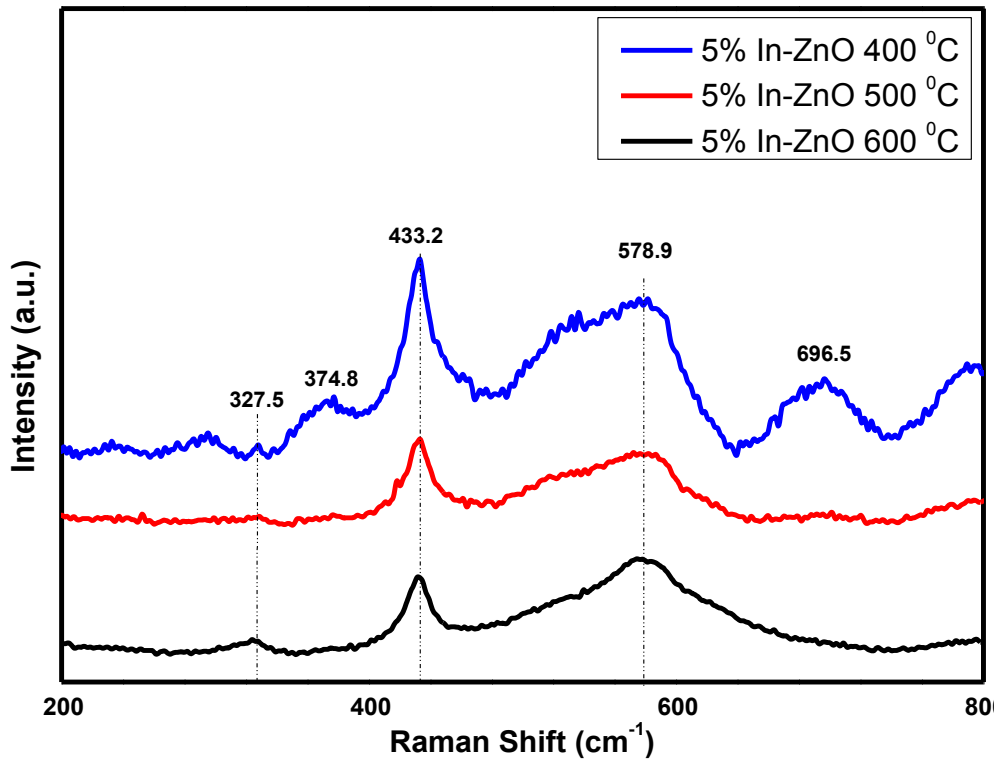

Figure 5.3.3: Raman spectroscopy of 5% Co-doped doped ZnO nanoparticles annealed at 400 ℃, 500 ℃ and 600 ℃

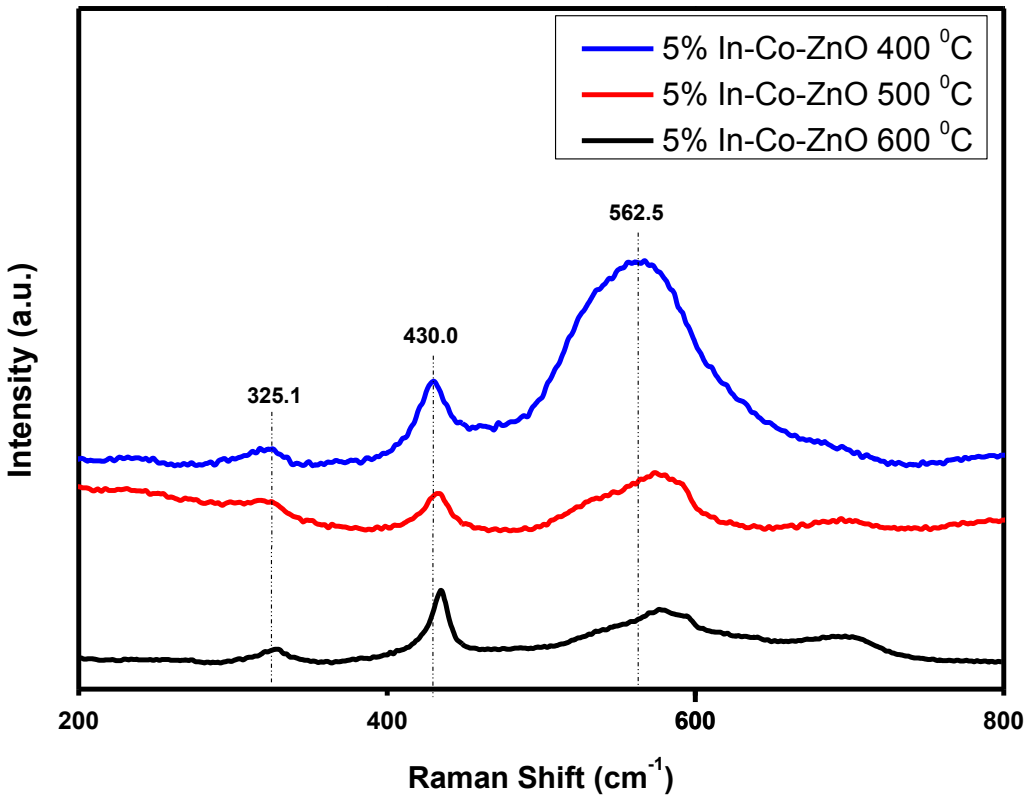

Figure 5.3.4: Raman spectroscopy of 5% In-Co co-doped doped ZnO nanoparticles annealed at 400 ℃, 500 ℃ and 600 ℃.

5.4. Photoluminescence (PL) Results

In order to study defects and optical properties of the prepared ZnO nanoparticles, PL measurements were performed using the excitation wavelength of 325 nm and the results are represented in figures 5.4.1 - 5.4.4. Two mean emission peaks of ZnO identified as UV emission peak and the visible emission peak (also known as the deep level emission) are observed in the undoped ZnO nanoparticles (see figure 5.4.1), similar results were reported by L. Yang *et al*. [61], S.K. Gupta *et al*. [81] and D. Fang *et al*. [110]. A red shift can be seen from the UV emission of the undoped ZnO nanoparticles with an increase in annealing temperature while for the In doped ZnO nanoparticles a blue shift is observed with an increase in annealing temperature. The UV emission of the Co doped ZnO is at low wavelength for the sample annealed at 400 ℃ and at higher wavelength for the sample annealed at 600 ℃, similar results were observed for the In-Co co-doped ZnO nanoparticles and this could be due to the presence of Co into the ZnO nanoparticles. These results are similar to the results obtained in the UV-vis measurements of sub-section 5.1.

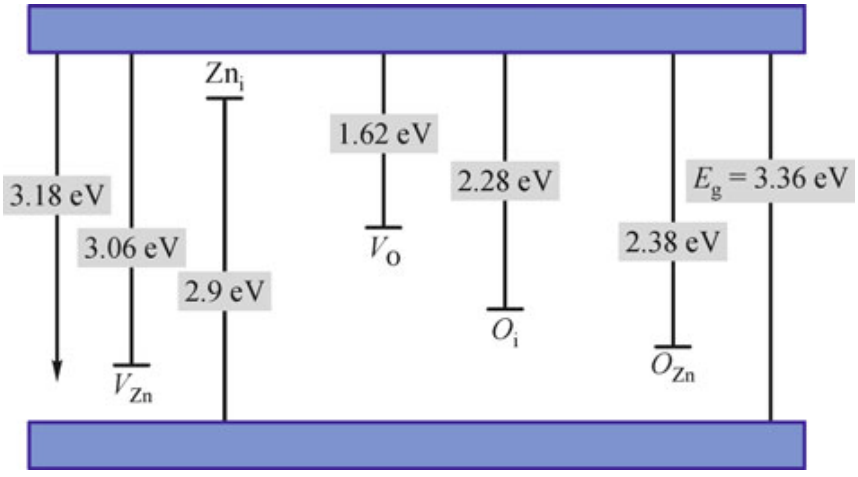

Figure 5.4.1: Energy levels of different defect states of Zinc Oxide *[138]*.

Not much evidence is known about the deep level emission peak and its formation, but S. Suwanboon *et al*. [129] and S. Chang *et al*. [139] reported that the deep level emission is related to the singly ionized oxygen vacancy in ZnO, while P.S. Xu *et al*. [138] suggested that these deep level emissions can be attributed to the oxygen interstitials.

M. Wilande *et al*. [140], reported that the deep level emission could be a combination of different deep levels mainly being the intrinsic and the extrinsic emissions. In the present study the deep level emission peaks are found to be between 2.08 and 2.29 eV and with reference to figure 5.4.1 [138], this emissions can be attributed to oxygen interstitials, with a shift to lower wavelength observed with an increase in annealing temperature. Other peaks are observed in the doped ZnO nanoparticles samples at 1.45 – 1.80 eV. These peaks can be assigned to oxygen vacancies according to P.S. Xu *et al*. [138].

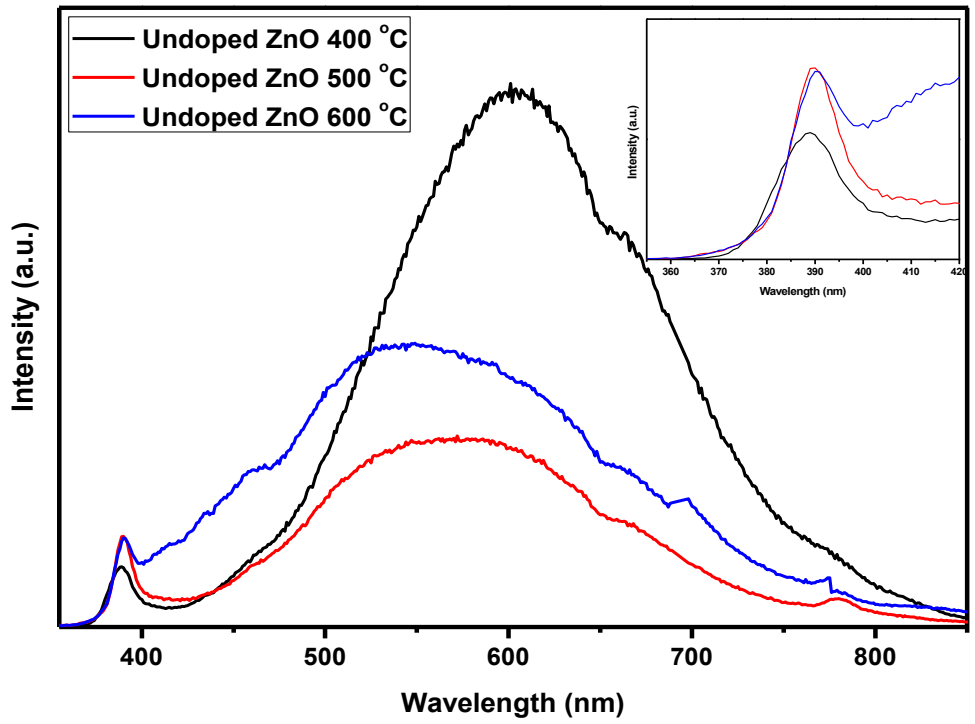

Figure 5.4.2: PL spectrum of undoped ZnO nanoparticles annealed at 400 ℃, 500 ℃ and 600 ℃.

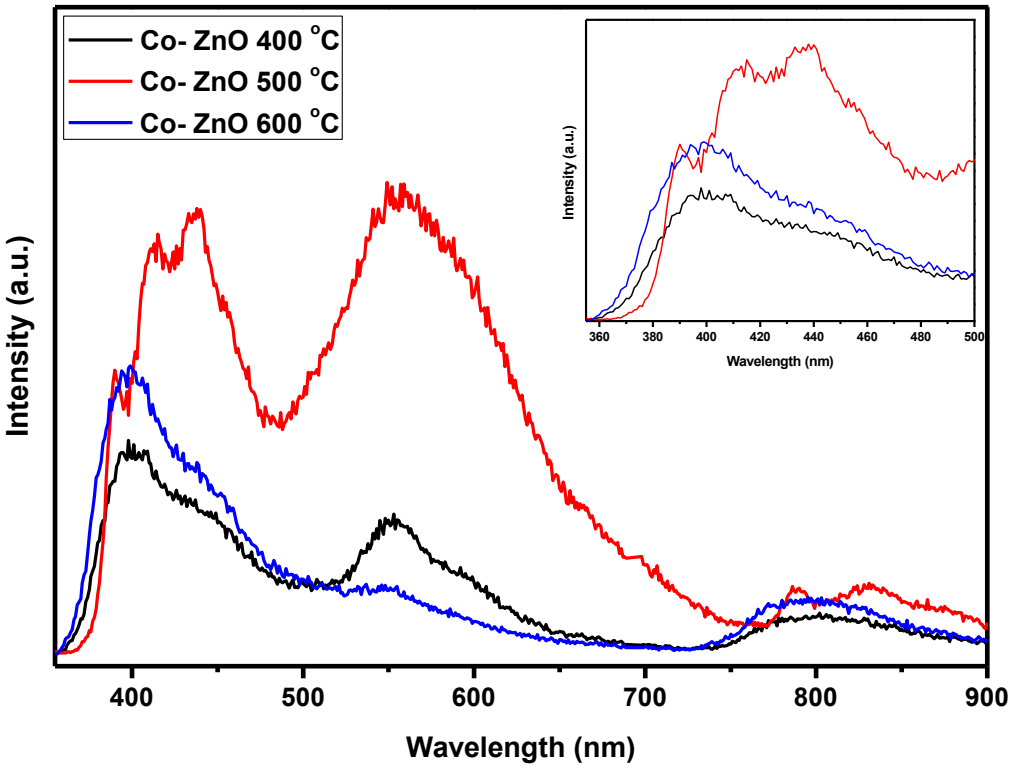

Figure 5.4.3: PL spectrum of Co-doped ZnO nanoparticles annealed at 400 ℃, 500 ℃ and 600 ℃.

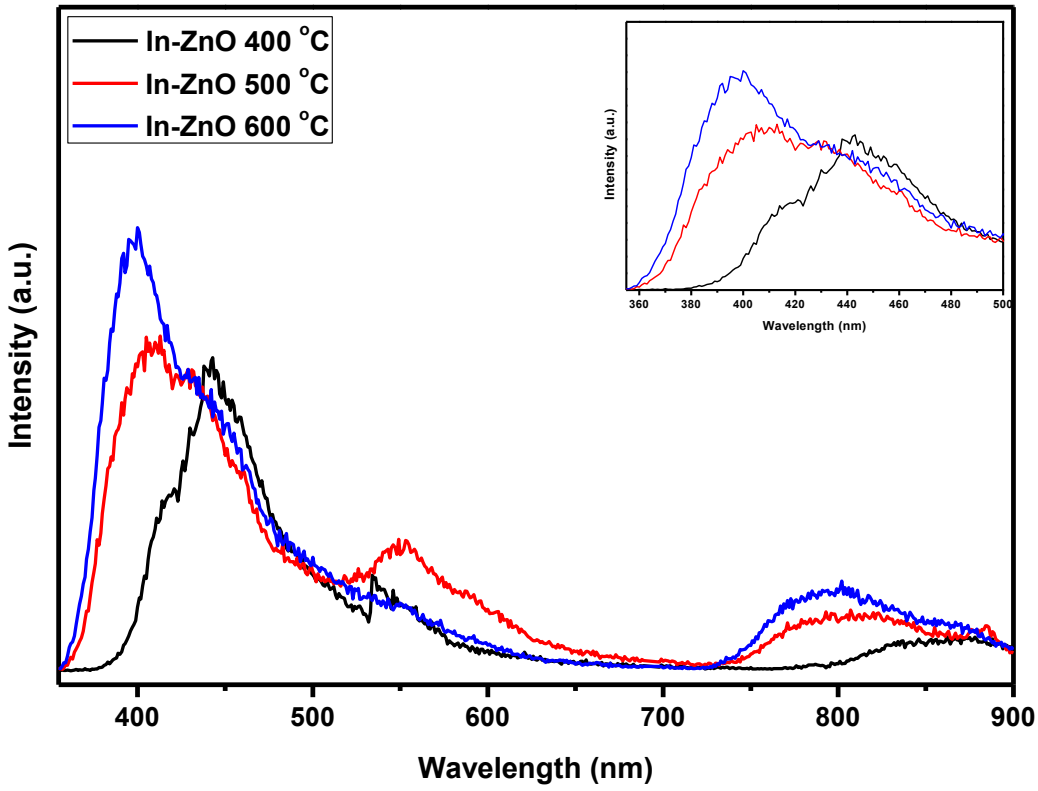

Figure 5.4.4: PL spectrum of In-doped ZnO nanoparticles annealed at 400 ℃, 500 ℃ and 600 ℃.

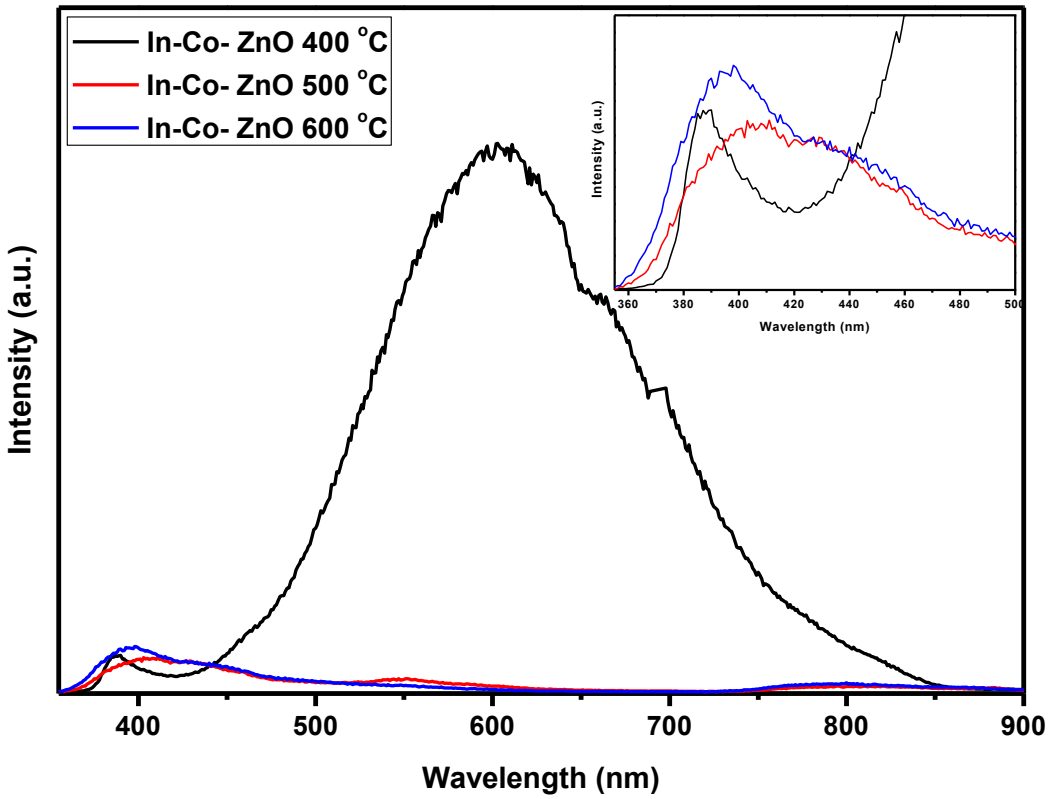

Figure 5.4.5: PL spectrum of In-Co co-doped ZnO nanoparticles annealed at 400 ℃, 500 ℃ and 600 ℃.

5.5. Conclusion

From the UV-vis results the energy band gap of all the prepared samples were determined and found to be smaller than the energy band gap of the reported bulk ZnO. The energy band gaps of the doped ZnO nanoparticles were found to decrease with an introduction of dopants as compared to the undoped ZnO nanoparticles. The energy band gaps of the undoped and doped ZnO nanoparticles were also observed to decrease with an increase in temperature. The PL measurements were performed, and found to be consistent with the UV-vis results. The Raman studies jointly with the FTIR results showed that the prepared samples were of the ZnO hexagonal wurtzite crystal structure. The two characterisations further confirmed the XRD results about the crystal phase of the ZnO nanoparticles presented here.

Chapter 6

Gas Sensing Applications

6.1. Gas sensing Results

In this chapter gas sensing applications were performed for the undoped, Co and In single doped and Co and In combinational doped ZnO nanoparticles for the humidity, carbon monoxide (CO), ammonia (NH_3), methane (CH_4) and hydrogen (H_2) gases. The humidity measurement were done for the set of Relative Humidity (RH) % as 10, 20, 30 40, 50, 60, 70, 80, 90 and 100 %, while the gas concentration of target gasses were at 5, 10, 20, 40, 60, 80, and 100 ppm. These measurements were then performed at temperatures 250, 300, 350, 400 ^{0}C in order to investigate the best suitable temperature for sensing device. The response(s) was (were) determined as

$$S = {R_a}/{R_g} \qquad (6.\ 1)$$

where R_a is the resistance of the sensor in synthetic air and R_g is the resistance of the sensor in the presence of targeted gas diluted in synthetic air. The stimuli (gas or humidity) ON and OFF time periods were set at 5 minutes each respectively and the biasing voltage was kept constant at 0.5 V. The response time was defined as the time required obtaining 90% of the steady response value while the recovery time was defined as the time attaining 10% of the initial response value.

Figure 6. 1 represents the response of the humidity measurements performed for the undoped, In, Co single doped and In, Co co-doped ZnO nanoparticles samples. It can clearly be seen that the response of the undoped ZnO nanoparticle sample is very low as compared to any of the doped ZnO nanoparticle samples where the inset of Figure 6. 1 shows the response of the undoped and In-doped ZnO nanoparticle. The

maximum response of the undoped and the In-doped ZnO reached the RH of 50 % while the maximum of the Co-doped and the Co-In co-doped ZnO reached the RH of 100 %. The response/recovery time were determined for the prepared samples at the RH of 100 %; the values for the response/recovery time were found to be 267.13910/29.63917, 271.29510/25.54768, 270.42520/25.21477 and 263.65970/27.40549 for the undoped, Co-doped, In-doped and Co-In co-doped ZnO nanoparticle samples respectively. The response/recovery of the Co-In co-doped ZnO nanoparticles are observed to be smaller as compared to the undoped and the In, Co single doped ZnO nanoparticle samples.

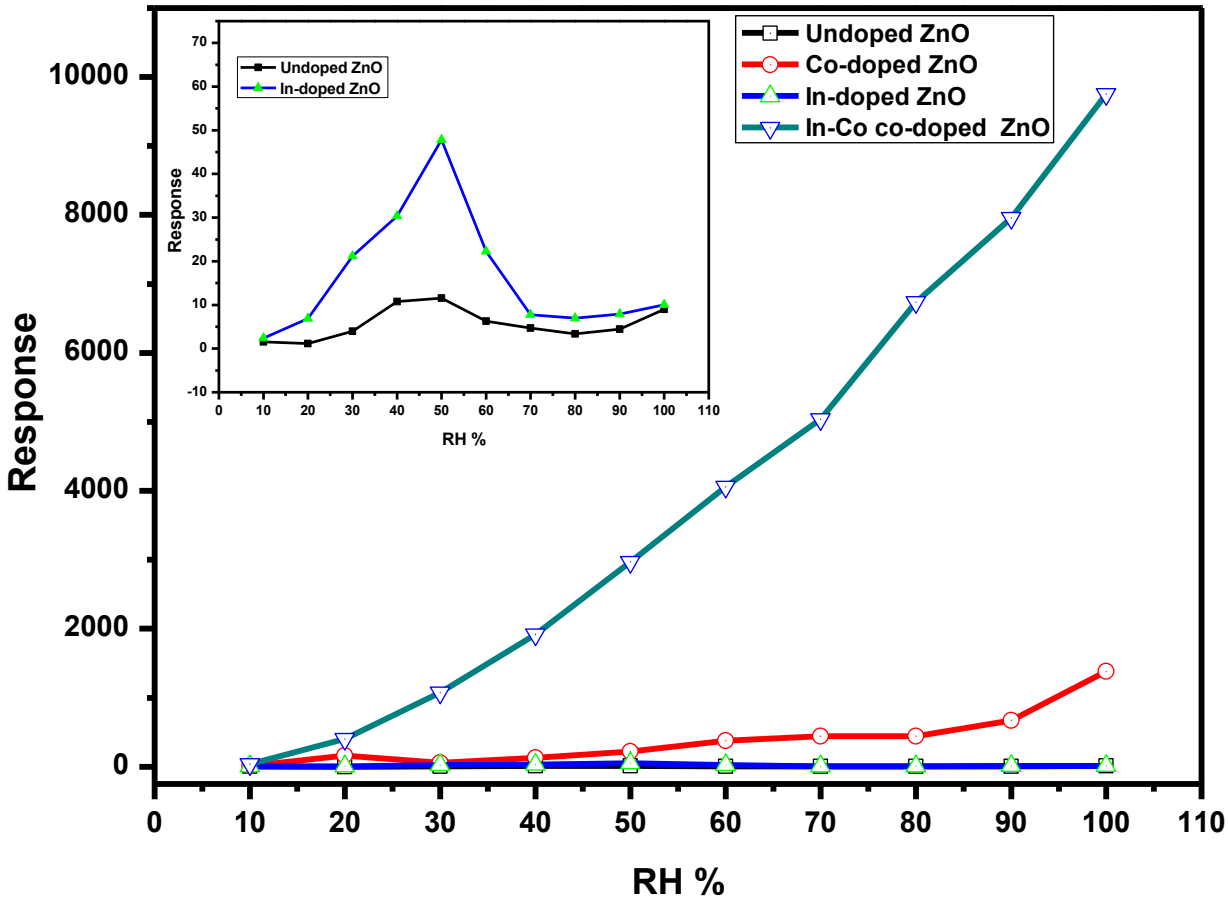

Figure 6. 1: Response of the undoped ZnO, In doped, Co doped and In-Co co-doped ZnO nanoparticle sensors to Relative Humidity (RH).

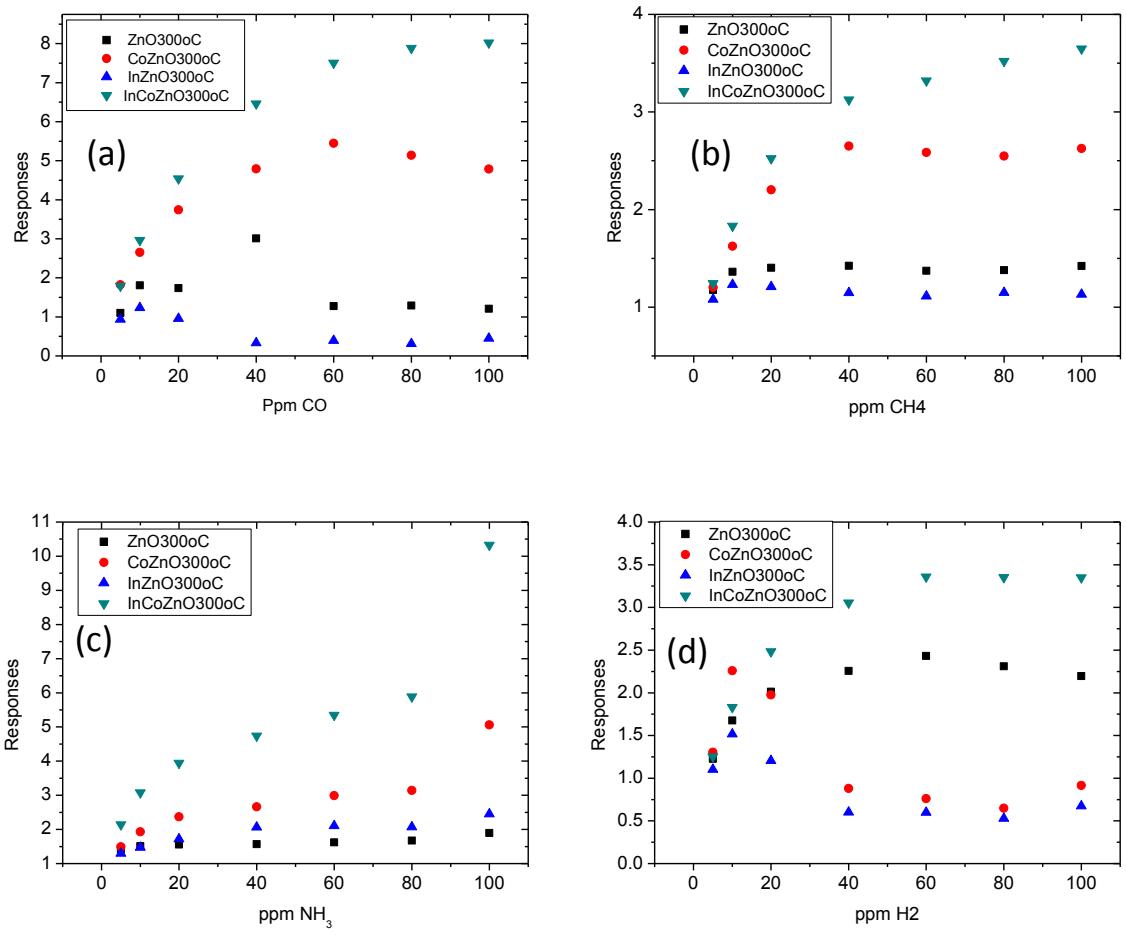

Figure 6. 2: Responses of each sensor plotted against concentration of gases (a) CO (b) CH_4 (c) NH_3 and (d) H_2.

The sensing behaviours of these nano-powders are presented in Figure 6. 2 and 6. 3. Looking at Figure 6. 2 (a, b, c, and d), responses to CO, CH_4, NH_3 and H_2 respectively are plotted against concentrations of the respective gases (in ppm) as diluted in synthetic air. These results suggest that pure ZnO and In-ZnO behave quite similarly when exposed to CO and CH_4 as they saturate below 20 ppm of each of the gases whereas Co-doped ZnO and In-Co co-doped ZnO also behave similarly in these environments as shown in Figure 6. 2 (a) and (b). However when exposed to NH_3 gas all sensors behave similarly as all of them show no signs of saturation except that they have different levels of response at all concentrations. When exposed to H_2 gas, both

Co-doped and In-doped ZnO sensors saturate below 20 ppm but the pure ZnO and the In-Co-doped ZnO both respond favourably to high concentrations of H_2 up to 60 ppm where the pure ZnO sensor gives in to the In-Co-ZnO sensor which start to show signs of saturation at higher H_2 concentrations than 80 ppm. In all gas environments considered here, the In-Co-doped ZnO shows the highest response to each gas considered showing that co-doping of In and Co in ZnO has the better advantage than singly doped samples as well as pure ZnO.

Further on Figure 6. 3 give a picture of responses of the same sensors against the temperature when these sensors are exposed to (a) CO (b) CH_4 (c) NH_3 and (d) H_2. One immediately observed peaks in such plots which have commonly been observed in temperature programmed sensing experiments and have here-in been fitted with the response-temperature equation based on the convolution of adsorption-temperature and the semiconductor resistance-temperature equations given by [141, 142]

$$\Re = \Re_0 + A.Exp\left(-\frac{E_{ad}}{k_B T} - \alpha T\right) \qquad (6.\ 2)$$

where $\Re_0$ is the response at absolute zero temperature, A is the response at optimum temperature $T_{opt} = {E_{ad}}/{k_B}$, E_{ad} is the adsorption energy and α is the rate per K of resistance decrease as temperature is raised in a semiconductor.

Equation 6. 2 can be fitted to the experimental data and the parameters $\Re_0$, A, E_{ad} and α can be extracted from the fitting or the equation can be re-written as:

$$T\ln(\Re - \Re_0) = T\ln A - \frac{E_{ad}}{k_B} - \alpha T^2 \qquad (6.\ 3)$$

This process reduces the task from a complicated fitting of Equation 6. 2 to the one of fitting a simple quadratic equation. Here an easily modified response-temperature data can be analysed.

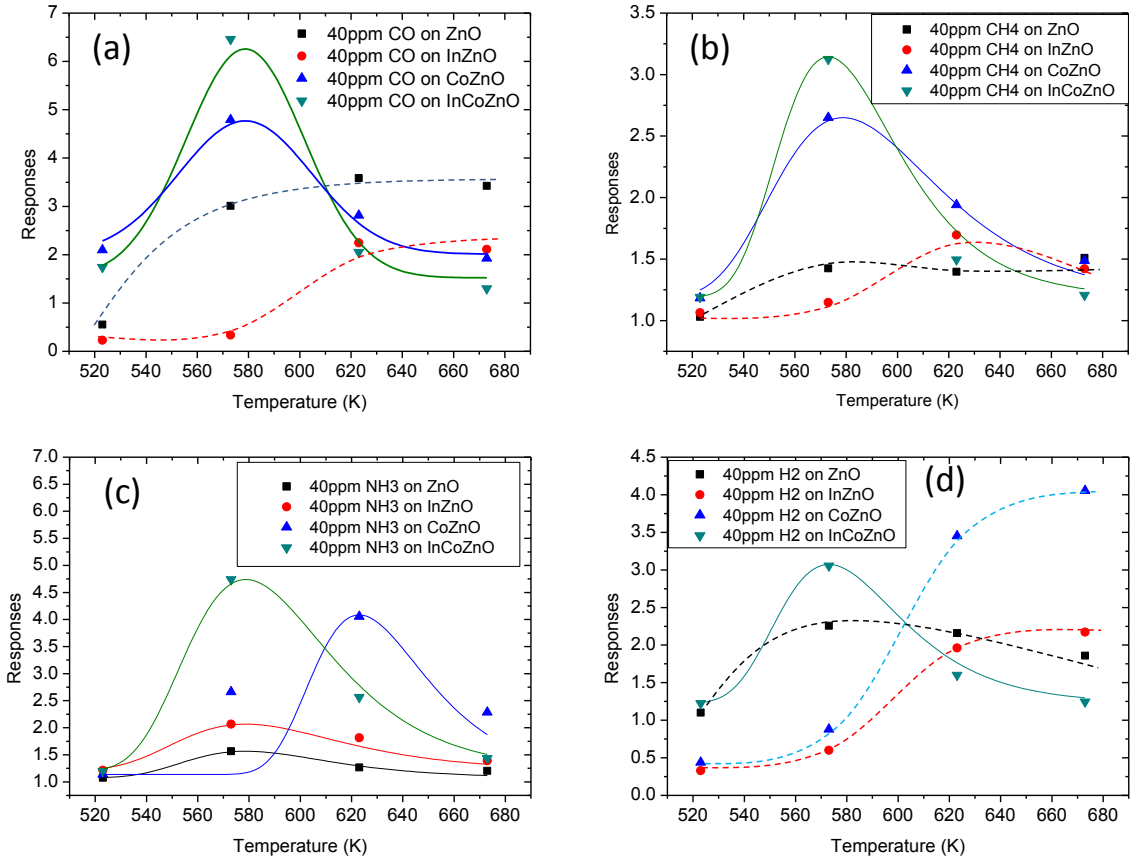

Figure 6. 3: Response of the undoped ZnO, In doped, Co doped, and In-Co co-doped ZnO samples plotted against temperature when exposed to 40 ppm of (a) CO (b) CH_4 (c) NH_3 and (d) H_2 gases.

Pure ZnO and In-doped ZnO shows no hump in the temperature range considered when they are exposed to CO and CH_4 suggesting that the optimum responses in these sensors is above 620 K. Due to Co single doping as well as In-Co co-doping of ZnO, the optimum response temperature is reduced down to about 570 K (about 300 °C) as one can see in both Figure 6. 3 (a) and (b). When exposed to NH_3, all sensors show a hump at the same 570 K except the Co-ZnO sensor which shows its distinct

peak at 620 K. This suggests that In rather than Co is responsible for the reduction of the optimum temperature to 570 K although Co-ZnO sensor suggest that there is a shoulder at around 570 K. In the presence of H_2 both single doped ZnO sensor show that their optimum temperature are higher than 640 K. The pure ZnO sensor shows a very little hump around the same temperature where In-Co-ZnO shows its distinctly high response to H_2 at 570 K.

All these results show that doping the ZnO with either Co or In can reduce or increase the optimum temperature but co-doping will consistently reduce this optimum temperature from higher than 620 K to about 570 K. Also this study shows that co-doping of Co and In in ZnO presents the highest responses regardless of gas environments.

A summary of the fitting parameters obtained using Equation 6. 2 and 6. 3 as well as the response and recovery times for all the sensors are given in Table 6. 1. One notes that the recovery time is almost 10 times shorter than the response time in all sensors and in all gas environments considered. It is also observed that there is a degree of proportionality between response times and recovery times; generally the trend is the observation that the longer the recovery time the longer is the response time.

Also both recovery times and response time have a positive bearing especially on E_{ad} and α respectively. E_{ad}, being the energy of adsorption, is expected to affect the response time whereas the parameter, α, being related to desorption when the semiconductor becomes hotter than T_{opt}, should affect recovery time of the sensor. In addition, A, being the response at the optimum temperature is greatly related to response time but with a supposedly negative correlation as large responses are related to large doses which lead fast responses and hence shorter response time.

However the question is; can co-doping of In and Co in ZnO make the ZnO any better sensor in terms of selectivity? In order to answer this question, one needs to define selectivity, σ, as the fractional response, $\Re^{gas}_{i,}$ to a particular i^{th} gas with respect to the sum of responses to all gases considered, $\sum_{i=1}^{N}\Re_i^{gas}$ as follows:

$$\sigma = \frac{\Re_i^{gas}}{\Re_1^{gas} + \Re_2^{gas} + \Re_3^{gas} + \cdots + \Re_N^{gas}} = \frac{\Re_i^{gas}}{\sum_{i=1}^{N}\Re_i^{gas}} \qquad (6.\ 4)$$

An ideal sensor should have a selectivity value of 100% to one particular gas and have 0% to any other gases. The values of σ for all sensors exposed to CO, CH_4, NH_3 and H_2 at a gas concentration of 40 ppm at 570 K are listed in the last column of Table 6. 1. It can be observed that pure ZnO, Co-ZnO and In-Co-ZnO sensors have their highest selectivity to CO gas at about 38%. However, In doped ZnO has a remarkable 48% selectivity to NH_3 gas.

Table 6. 1: List of response and recovery times alongside the fitting parameters of Equation 6. 2 and 6. 3.

Sample Name	Gas	Response time (s)	Recovery time (s)	alpha	A	E_{ad}	σ
Undoped ZnO	CO	273.71130	30.79897	0.0907	3.00	3.101119	37.50000
	CH_4	271.10180	30.64433	0.0119	1.30	0.428973	16.25000
	NH_3	263.61980	31.53598	0.0242	1.50	0.743604	18.75000
	H_2	274.29120	31.52921	0.0479	2.20	1.547929	27.50000
Co-doped ZnO	CO	265.93980	30.16112	0.0001	4.70	0.004431	38.55619
	CH_4	266.94590	30.11168	0.0002	2.62	0.004646	21.49303
	NH_3	276.38020	31.21375	0.0003	4.12	0.010349	33.79820
	H_2	276.03090	31.33591	0.00002	0.75	0.000696	6.152584
In-doped ZnO	CO	269.96130	30.21907	0.0002	0.45	0.004881	10.84337
	CH_4	267.00320	29.91407	0.00004	1.20	0.001153	28.91566

	NH_3	273.77010	30.99893	0.0001	2.00	0.003789	48.19277
	H_2	274.61980	31.21993	0.000006	0.50	0.000785	12.04819
In-Co co-doped ZnO	CO	266.3265	30.02148	0.0009	6.50	0.02722	37.14286
	CH_4	279.203	29.11708	0.0002	3.13	0.006484	17.85714
	NH_3	271.6821	31.55317	0.0005	4.75	0.013923	27.14286
	H_2	273.1314	30.189	0.0002	3.125	0.006383	17.85714

6.2. Conclusion

Pure ZnO, singly Co and In doped ZnO as well as co-doped In-Co ZnO materials were synthesised by the sol-gel process. It has been shown that the grain sizes decrease considerably with doping. Co-doping tends to increase homogeneity and mono-dispersity whereas In tends to lead to coagulation. The co-doping of In and Co in ZnO leads to a superposition of the two effects where colloids are observed. Grain sizes increase with annealing temperature where lattice parameters decrease and increase showing that there is competition between substitutional and interstitial doping. Co-doped In-Co ZnO shows the highest responses to all stimuli considered here: humidity, CO, CH_4, NH_3 and H_2 when compared to pure ZnO, Co-ZnO, In-ZnO. However selectivity seems to be better in singly doped materials, notably In-doped ZnO which has a remarkable 48% selectivity to NH_3 where the rest of the sensors respond more to CO at about 38% selectivity.

Chapter 7

Summary

In the present work the undoped, In and Co single doped and the In and Co co-doped ZnO nanoparticles were successfully synthesised using the sol-gel method. The XRD results showed that all the prepared samples were of the ZnO wurtzite crystal structure. The lattice parameters of the undoped and doped ZnO nanoparticles were calculated and found to be similar to the reported values of the bulk ZnO. The bond length of the synthesised samples were calculated and found to be different for the doped ZnO nanoparticles samples indicating the presence of In and Co dopants. The average particle sizes were determined and found to decrease with an introduction of dopants into the ZnO nanoparticles. It was also observed that the average particle size increase with an increase in temperature. The strains of the prepared samples were also determined using the XRD results and found to be inversely proportional to the average particle size. The TEM images showed that the prepared samples were spherically shaped which corroborated the XRD results that the prepared ZnO samples were of a wurtzite crystal structure. The EDS results confirmed that In and Co were successfully doped into the ZnO nanoparticle structure. The UV-vis studies were also performed to study the optical properties. The energy band gap of all the prepared samples were determined and found to be smaller compared to the energy band gap of the bulk ZnO. The energy band gaps were found to decrease with an introduction of dopants and also found to decrease with an increase of the annealing temperature. PL measurements were performed; the UV and the deep level emissions were observed for the undoped and the doped ZnO nanoparticles. The PL results were found to be consistent with the UV-vis results. The Raman and FTIR studies were

performed and confirmed that all the prepared nanoparticle samples were of the ZnO wurtzite crystal, this confirmed the XRD results. The gas sensing measurements performed for the gases CO, CH_4, NH_3, H_2 and humidity showed that co-doping of In and Co into the ZnO nanoparticles increased the gas response of the ZnO nanoparticles as compared to the response of the undoped and the singly doped ZnO particles, while the selectivity was found to be better in singly doped ZnO nanoparticles notably In-doped ZnO which had a remarkable 48% selectivity to NH_3 where the rest of the sensors responded more to CO at about 38% selectivity.

8. References

[1] C. Klingshirn, J.Fallert,H.Zhou,J.Sartor,C.Thiele,F.Maier-Flaig, D.Schneider, H.Kalt,, “65years of ZnO research—old and very recent results,” Physica Status SolidiB, vol. 247, p. 1424, 2010.

[2] H. Kim, J.S. Horwitz, W.H. Kim, A.J. Makinen, Z.H. Kafafi, D.B. Chrisey , “Doped ZnO thin films as anode materials for organic light-emitting diodes,” Thin Solid Films , vol. 420/421, p. 539, 2002.

[3] D.S. Bohle,C.J.Spina,, “Controlled Co(II) doping of zinc oxide Nanocrystals,” Journal of Physical Chemistry C, vol. 114, p. 18139–18145, 2010.

[4] A. Al-Kahlout, “ZnO nanoparticles and porous coatings for dye-sensitized solar cell application: photoelectrochemical characterization,” Thin Solid Films, vol. 520, p. 1814–1820, 2012.

[5] L.M. Cele, S. Ray, N.J. Coville, “Nanoscience and Nanotechnology in South Africa,” South African Journal of Science, vol. 105, no. 7/8, p. 242, 2009.

[6] Y. Caglar, “Sol–gel derived nanostructure undoped and cobalt doped ZnO: Structural,optical and electrical studies,” Journal of Alloys and Compounds, vol. 560, p. 181–188, 2013.

[7] H.M Yang, S. Nie, “Preparation and Characterization of Co-Doped ZnO Nanomaterials,” Materials Chemistry and Physics, vol. 114, pp. 279-282, 2009.

[8] M. Yang, Z.X. Guo, K.H. Qiu, J.P. Long, G.F. Yin, D.G. Guan, S.T. Liu, S.J. Zhou, “Synthesis and characterization of Mn-doped ZnO column arrays,” Applied Surface Science, vol. 256, pp. 4201-4205, 2010.

[9] H. Saal, T. Bredow, M. Binnewies, “Band gap engineering of ZnO via doping with manganese: effect of Mn clustering,” Physical Chemistry Chemical Physics, vol. 11, pp. 3201-3209, 2009.

[10] G.M. Kumar, P. llanchezhiyzn, J. Kawakita, M. Subramanian, R. Jayavel, crystal engineering communications, vol. 12, p. 1887, 2010.

[11] A.M. Fox, M.T. Dulay, “ Heterogeneous photocatalysis,,” Journal of Chemica lReviews , vol. 93, p. 341–357, 1993.

[12] Y. W. B. Tan, “Dye-sensitized solar cells based on anatase TiO2 nanoparticle/nanowire composites,” Journal of Physical Chemistry B, vol. 110 32, p. 15932–15938, 2006.

[13] J. Preclikova, P. Galar, Fr. Trojanek, B. Rezek, Y. Nemcova, P. Maly, “Photoluminescence of nanocrystalline titanium dioxide films loaded with silver nanoparticles,” Journal of Applied Physics, vol. 109, p. 083528, 2011.

[14] S.C. Yeow, W.L. Ong, A.S.W. Wong, G.W. Ho, Sens. Actuators B, vol. 143, p. 295–301, 2009.

[15] A. Mills, N. Elliott, G. Hill, D. Fallis, J.R. Durrant, R.L. Willis,, “Preparation and characterization of novel thick sol–gel titania film photocatalysts,” Photochemical & Photobiological Sciences, vol. 5, p. 591–596, 2003.

[16] V. Krishna, N. Noguchi, B. Koopman, B. Moudgil, “Enhancement of titaniumide photocatalysis by water-soluble fullerenes,” Journal of Colloid and Interface Science, vol. 304, p. 166–171, 2006.

[17] Y.-J. Xu, Y. Zhuang, X. Fu,, “New insight for enhanced photocatalytic activity of TiO2 by doping carbon nanotubes: a case study on degradation of benzene andmethyl orange,” Journal of Physical Chemistry C , vol. 114, p. 2669–2676, 2010.

[18] N.L.V. Carreno, H.V. Fajardo, A.P. Maciel, A. Valentini, F.M. Pontes, L.F.D. Probst,E.R. Leite, E. Longo, J. Mol., Journal of Molecular Catalysis A: Chemical, vol. 207, p. 91–96, 2004.

[19] Y.S. He, J.C. Campbell, R.C. Murphy, M.F. Arendt, J.S. Swinnea, Journal of Materials Research, vol. 8, p. 3131–3134, 1993.

[20] F. Li, J. Xu, X. Yu, L. Chen, J. Zhu, Z. Yang, X. Xin, “one-step solid state reaction synthesis and gas sensing property of Tin oxide nanoparticles,” Sensors and Actuators B, vol. 81, p. 165–169, 2002.

[21] Z. Peng, Z. Shi, M. Liu, “Mesoporous Sn–TiO2 composite electrodes for lithium batteries,” Chemical Communications, no. 21, p. 2125, 2000.

[22] J. Kong, H. Deng, P. Yanga, J. Chu., “Synthesis and properties of pure and antimony-doped tin dioxide thin films fabricated by sol–gel technique on silicon wafer,” Materials Chemistry and Physics, vol. 114, p. 854–859, 2009.

[23] T. Krishnakumar, R. Jayaprakash, M. Parthibavarman, A.R. Phani, V.N. Singh, B.R. Mehta, “Microwave-assisted synthesis and investigation of SnO2 nanoparticles,” Materials Letters, vol. 63, p. 896–898, 2009.

[24] S. Thanasanvorakun, P. Mangkorntong, S. Choopun, N. Mangkorntong., “Characterization of SnO2 nanowires synthesized from SnO by carbothermal reduction process,” Ceramics International, vol. 34, p. 1127–1130, 2008.

[25] M.A. Gondala, Q.A. Drmosh,T.A. Saleh., “Preparation and characterization of SnO2 nanoparticles using high power pulsed laser,” Applied Surface Science, vol. 256, p. 7067–7070, 2010.

[26] A.N. Mallika, A. Ramachandra Reddy, K. Sowri Babu, Ch. Sujatha, K. Venugopal Reddy, “Structural and photoluminescence properties of Mg substituted ZnO nanoparticles,” Optical Materials, vol. 36, p. 879–884, 2014.

[27] M. Liu, A.H. Kitai, P. Mascher, “Point defects and luminescence centers in zinc oxide and zinc oxide doped with manganese,” Journal of Luminescence, vol. 54, p. 35– 42, 1992.

[28] C. Jayachandraiah, A. Divya, K. Siva Kumar, G. Krishnaiah, “Effect of Nd on structural and optical properties of Nd doped ZnO nanoparticles,” in International Conference on Advanced Nanomaterials and Emerging Engineering Technologies, India, 2013.

[29] A. Sivagamasundari, R. Pugaze, S. Chandraekar, S. Rajagopan, R. Kannan, “Absence of carrier and paramagnetism in cobalt-doped ZnO nanoparticles

synthesized at low temperature using citrate sol-gel route," Applied Nanoscience, vol. 3, pp. 383-388, 2013.

[30] S.J. Pearton, D.P. Norton, K. Ip, Y.W. Heo, T. Steiner, "Recent advances in Processing of ZnO," Journal of Vacuum Science & Technology B , vol. 22, p. 932–948, 2004.

[31] S.J. Pearton, D.P. Norton, K. Ip, Y.W. Heo, T. Steiner , " Recent advances in processing of ZnO," Journal of Vacuum Science and Technology B, vol. 22, p. 932–948, 2004.

[32] K. Omri, J. El Ghoul, O.M. Lemine, M. Bououdina, B. Zhang, L. El Mira, , "Magnetic and optical properties of manganese doped ZnO nanoparticles synthesized by sol–gel technique," Superlattices and Microstructures , vol. 60, p. 139–147, 2013.

[33] T. Dietl, H. Ohno, F. Matsukura, J. Cibert and D. Ferrand , "Zener model description of ferromagnetism in zinc-blende magnetic semiconductors," Science , vol. 287, pp. 1019-1022, 2000.

[34] J. M. Kikkawa and D. D. Awschalom, " Lateral drag of spin coherence in gallium arsenide," Nature, vol. 397, pp. 139-141 , 1999.

[35] I. Zutic, J. Fabian and S. Das Sarma, "Spin injection through the depletion layer: a theory of spin-polarized p-n junctions and solar cells," Physical Review B , vol. 64, p. 121201, 2001.

[36] S.Y. Kim, I.S. Lee, Y.S. Yeon, S.M. Park, J.K. Song, Bull,, “ZnO Nanoparticles with Hexagonal Cone, Hexagonal Plate, and Rod Shapes: Synthesis and Characterization,” Korean Chemical Society, vol. 29, p. 1960–1964, 2008.

[37] B.K. Woo, W. Chen, A.G. Joly, R. Sammynaiken, “The Effects of Aging on the Luminescence of PEG-Coated Water-Soluble ZnO Nanoparticle Solutions,” Journal of Physical Chemistry C, vol. 112, p. 14292–14296, 2008.

[38] R.K. Dutta, P.K. Sharma, R. Bhargava, N. Kumar, A.C. Pandey,, “Differential susceptibility of Escherichia coli cells toward transition metal-doped and matrix- embedded ZnO nanoparticles,” Journal of Physical Chemistry B, vol. 114, p. 5594–5599, 2010.

[39] M. Poloju, M.V. R. Reddy, “structural and morphological features of sol-gel processed pure and Indium doped ZnO nanoparticles,” in proceedings of the International Conference on Advanced Nanomaterials and Emerging Engineering Technologies, India, 2013.

[40] J. Nishino, T. Kawarada, S. Ohshio,, “Conductive indium-doped zinc oxide films prepared by atmospheric pressure chemical vapour deposition,” journal of materials science letters, vol. 16, pp. 629-631, 1997.

[41] M sathyal, A.Claude, , “Growth of pure and doped ZnO thin films for solar cell applications,” advanced in applied science research, vol. 3, pp. 2591-2598, 2010.

[42] M. RezaeeRokn-Abadi, M. Behdani, H. Arabshahi and N. Hosseini, , “Indium-doped zinc oxide thin films by sol-gel method,” international review of physics, vol. 12, pp. 103-106, 2009.

[43] Y. Liu, J. Dong, P.J. Hesketh, M. Liu , “Synthesis and gas sensing properties of ZnO singlecrystal flakes.,” Journal of Materials Chemistry, vol. 15, pp. 2316-2320, 2005.

[44] C. Wang, L. Yin, L. Zhang, D. Xiang, R. Gao, , “Metal Oxide Gas Sensors: Sensitivity and Influencing Factors,” Sensors, vol. 10 , pp. 2088-2106, 2010.

[45] J. Xu, Q. Pan, Y.Shun, Z.Tian, “Grain size control and gas sensing properties of ZnO gas sensor,” Sensors and Actuators B: Chemical, vol. 66, p. 277–279, 2000.

[46] R. Bhargava, P.K. Sharma, R.K. Dutta, S. Kumar, A.C. Pandey, N. Kumar, “Influence of Co-doping on the the thermal, structural, and optical properties of sol-gel derived ZnO nanoparticles,” materials chemistry and physics , vol. 120, pp. 393-398, 2010.

[47] P. Li, S. Wang, J. Li, Y. Wei , “Structural and optical properties of Co-doped ZnO nanocrystallites prepared by a one-step solution route,” Journal of Luminescence., vol. 132, p. 220–225, 2012.

[48] M. Arshada, A. Azama, A. S. Ahmeda, S. Mollahc, A. H. Naqvia, “Effect of Co substitution on the structural and optical properties of ZnO nanoparticles

synthesized by sol–gel route," Journal of Alloys and Compounds, vol. 509, p. 8378– 8381, 2011.

[49] M. Rezaee Rokn-Abadi, M. Behdani, H. Arabshahi, N. Hosseini, "Indium-doped Zinc Oxide Thin Films by Sol–Gel Method," International Review of Physics, vol. 12, pp. 103-106, 2009.

[50] F. Paraguay D, M. Miki-Yoshida, J. Morales, J. Solis, W. Estrada L, "Influence of Al, In, Cu, Fe and Sn dopants on the response of thin film ZnO gas sensor to ethanol vapour," Thin Solid Films , vol. 373, pp. 137-140, 2000.

[51] J. Song, J. Zheng, Z. Zhao, B. Zhou, J. Lian, "Synthesis and photoluminescence of Y and Cd co-doped ZnO nanopowder," Transactions of Nonferrous Metals Society of China, vol. 23, p. 2336−2340, 2013.

[52] Z. Pan , J. Luo, X. Tian, S. Wu, C. Chen, J. Deng, C. Xiao, G. Hu, Z. Wei, "Highly transparent and conductive Sn/F and Al co-doped ZnO thin films prepared by sol–gel method," Journal of Alloys and Compounds , vol. 583 , p. 32–38, 2014.

[53] N. B. S. G.-L. L. M. J.E. Ghoul, "Structural and optical properties of nanoparticles (V, Al) co-doped ZnO synthesized by sol–gel processes," Superlattices and Microstructures , vol. 64, p. 451–459, 2013.

[54] H. Gu, Y. Jiang, Y. Xu, M. Yan, "Effect of defects on room-temperature ferromagnetism in Co and Na co-doped ZnO," Applied Physics A, vol. 107, p. 919–923, 2012.

[55] K. Vignesh, M. Rajarajan, A. Suganthi, “Visible light assisted photocatalytic performance of Ni and Th co-doped ZnO nanoparticles for the degradation of methylene blue dye,” Journal of Industrial and Engineering Chemistry, vol. 20, p. 3826–3833, 2014.

[56] John E. Jaffe, James A. Snyder, Zijing Lin, and Anthony C. Hess, “LDA and GGA calculations for high-pressure phase transitions in ZnO and MgO,” Physical Review B, vol. 62, pp. 1660-1665, 2000.

[57] G. Amin, “White LEDs Printed on Paper,” 2012.

[58] D.I. Rusu, G.G. Rusu, D.Luca, “structural charateristics and optical properties of thermally oxidized zinc films,” Acta Physica Polonica, vol. 119, pp. 850-856, 2011.

[59] A.J. Hashim, M.S. Jaafar, Alaa, J.Ghazai, N.m. Ahmed, “fabrication and characterization of tetraleg zinc oxide nanostructure using evaporation methode,” Digest journal of nanomaterials and Biostructures, vol. 7, no. 2, pp. 487 - 491, 2012.

[60] P. Barnes, T. Csoka, S. Jacques, “Advanced Certificate in Powder Diffraction on the Web,” Birkbeck College, University of London., [Online]. Available: http://pd.chem.ucl.ac.uk/pdnn/powintro/braggs.htm.

[61] L. Yang, “Synthesis and Optical Properties of ZnO Nanostructures,” Liu-Tryck, Sweden, 2008.

[62] J. pankove, optical processes in semiconductors, new york: dover, 1976.

[63] A. Hamrouni, N. Moussa, A. Di Paolab, F. Parrino, A. Houasa, L. Palmisano, “Characterization and photoactivity of coupled ZnO–ZnWO4 catalystsprepared by a sol–gel method,” Applied Catalysis B: Environmental, vol. 154–155, p. 379–385, 2014.

[64] Surabhi Siva Kumar, Putcha Venkateswarlu,Vanka Ranga Raoand Gollapalli Nagewsara Rao, “Synthesis, characterization and optical properties,” Kumar et al. International Nano Letters, vol. 30, 2013.

[65] D. Sridevi, K.V. Rajendran, “Synthesis and optical characteristics of ZnO nanocrystals,” Bulletin of Materials Science, vol. 32, p. 165–168, 2009.

[66] O. Behera, S. Paul, “Synthesis and Characterization of ZnO nanoparticles of various sizes and Applications in Biological systems,” Orissa, India.

[67] P. H. Kasai, “Electron Spin Resonance Studies of Donors and Acceptors in ZnO,” Physical Review, vol. 130, pp. 989-995, 1963.

[68] K. Vanheusden, W. L. Warren, C. H. Seager, D. R. Tallant, J. A. Voigt, and B. E. Gnade, “Mechanisms behind green photoluminescence in ZnO phosphor powders,” Applied Physics, vol. 79, pp. 7983-7990, 1996.

[69] S. Yamauchi, Y. Goto, T. Hariu,, “Photoluminescence Studies of Undoped and Nitrogen-Doped ZnO Layers Grown by Plasma-Assisted Epitaxt,” Journal of Crystal Growth, vol. 260, no. 1-2, pp. 1-6, 2004.

[70] M. Liu, A. H. Kitai, and P. Mascher,, “Point defects and luminescence centers in ZnO and ZnO doped,” Journal of Luminescence , vol. 54, pp. 35-42, 1992.

[71] E. G. Bylander, “Surface effects on the low-energy cathodoluminescence of zinc oxide,” Journal of Applied Physics, vol. 49, no. 3, p. 1188, 1978.

[72] X. Yang, G. Du, X. Wang, J. Wang, B. Liu, Y. Zhang, D. Liu, D. Liu,H. C. Ong, S. Yang, “Effect of post-thermal annealingon properties of ZnO thin film grown on c-Al2O3 by metal-organic chemical vapor deposition,” Journal of Crystal Growth, vol. 252, p. 275, 2003.

[73] J. Zhong, A. H. Kitai, P. Mascher, and W. Puff, “The Influence of Processing Conditions on Point Defects and Luminescence Centers in ZnO,” Journal of The Electrochemical Society, vol. 140, pp. 3644-3649, 1993.

[74] K. Johnston, M. O. Henry, D. M. Cabe, T. Agne, and T. Wichert, in Proceedings of Second Workshop on “SOXESS European Network on ZnO", Caernarfon, Wales, UK, 2004..

[75] Q. X. Zhao, P. Klason, M. Willander, et al, “Deep Level Emissions Influenced by O and Zn Implantations in ZnO,” Applied Physics Letters, vol. 87, p. 211912, 2005.

[76] T. Moe Børseth, B. G. Svensson, A. Yu. Kuznetsov, P. Klason, Q. X. Zhao, and M. Willander, “Identification of oxygen and zinc vacancy optical signals in ZnO,” Applied Physics Letters, vol. 89, p. 262112, 2006.

[77] P. Klason, T. M. Børseth, Q. X. Zhao, et al., “Temperature dependence and decay times of zinc and oxygen vacancy related photoluminescence bands in zinc oxide,” Solid State Communication, vol. 145, pp. 321-326, 2008.

[78] Y. Gong, T.Andelman, G.F. Neumark,S. O'Brien , I.L. Kuskovsky, "Origin of defect-related green emission from ZnO nanoparticles:effect of surface modification," Nanoscale Research Letters, vol. 2, p. 297–302, 2007.

[79] P. Qi, O. Vermesh, M. Grecu, A. Javey, Q. Wang, H. Dai, S. Peng , K. J. Cho, "Toward large arrays of multiplex functionalized carbon nanotube sensors for highly sensitive and selective molecular detection," Nano Letter , vol. 3, pp. 347-35, 2003.

[80] Y.N. mazoe, G. Sakai, K. Shimanoe, "Oxide semiconductor gas sensor," Catalysis Surveys from Asia, vol. 7, pp. 63-75, 2003.

[81] S.K. Gupta, A. Joshi, M. Kaur , "Development of gas sensors using ZnO nanostructures," Journal of Chemical Sciences, vol. 122, p. 57–62, 2010.

[82] J. Xu, Y. Chen, Y. Li, J. Shen, "Gas sensing properties of ZnO nanorods prepared by hydrothermal method," Journal of Materials Science, vol. 40, pp. 2919-2921, 2005.

[83] M. M. Arafat, B. Dinan, S.A. Akbar and A. S. M. A. Haseeb, "Gas Sensors Based on One Dimensional Nanostructured Metal-Oxides: A Review," Sensors, vol. 12, pp. 7207-7258, 2012.

[84] O. Lupan, G. Chai, L. Chow, "Novel hydrogen gas sensor based on single ZnO nanorod," Microelectronic Engineering, vol. 85, p. 2220–2225, 2008.

[85] B.L. Zhua, C.S. Xie, D.W. Zeng, W.L. Song, A.H. Wang, “Investigation of gas sensitivity of Sb-doped ZnO nanoparticles,” Materials Chemistry and Physics , vol. 89, p. 148–153, 2005.

[86] M. Liu, “Synthesis of ZnO Nanowires and Applications as Gas Sensors,” Canada, 2010.

[87] Z.L.S. Seow, A.S.W. Wong, V. Thavasi, R. Jose, S. Ramakrishna, G.W. Ho, “Controlled synthesis and application of ZnO nanoparticles, nanorods and nanospheres in dye-sensitized solar cells,” Nanotechnology , vol. 20, pp. 1-6, 2009.

[88] J. Yang, X. Liu, L. Yang, Y. Wang, Y. Zhang, J. Lang, M. Gao, B. Feng, “Effect of annealing temperature on the structure,” Journal of Alloys and Compounds, vol. 477, p. 632–635, 2009.

[89] DoITPoMS, T.D. Skinner, M Vickers, “www.doitpoms.ac.uk,” DoITPoMS - TLP Library X-ray Diffraction, 01 April 2004. [Online]. Available: http://www.doitpoms.ac.uk/tlplib/xray-diffraction/printall.php. [Accessed 05 March 2010].

[90] W. M. H. Oo, “infrared spectroscopy of Zinc Oxide and magnesium nanostructures,” 2007.

[91] “DST/CSIR National Centre for Nano-structured Materials,” 06 November 2015. [Online]. Available: http://ls-

ncnsm.csir.co.za/gup/grafx/Opti_ram_spctmtr.jpg. [Accessed 04 November 2015].

[92] A. Schulte, Y. Guo, Handbook of Applied Solid State Spectroscopy, New York: 2006, Springer.

[93] princetoninstruments, 06 November 2015. [Online]. Available: http://www.princetoninstruments.com/spectroscopy/raman.aspx#raman_anchor4. [Accessed 04 November 2015].

[94] K. Molhave, “Tools for In-situ Manipulation and Characterization of Nanostructures,” MIC - Department of Micro and Nanotechnology Technical University of Denmark Orsteds Plads, Lyngby, 2004.

[95] S. Akhtar, “Trasmission Electron Microscopy of graphene and hydrated biomaterial nanostructures: Novel and analysis,” Acta Universitatis Upsaliensis, Sweden, 2012.

[96] R. Groningen, “Transmission electron microscopy studies of interfaces in multicomponent component systems,” Groningen University Press, 2004.

[97] S. Selladurai, “Engineering Physics part 1,” PHI learning private limited, New Delhi, 2010.

[98] “Tecnai Transmission Electron Microscopy,” FEI Tecnai™, [Online]. Available: http://www.fei.com/uploadedImages/FEISite/Pages/Products/TEM/Tecnai/Tecnai%20G2%20tool.png. [Accessed 31 October 2014].

[99] T. Spectric, “Basic UV-Vis Theory, Concepts and Applications,” [Online]. Available: Bttp://www.plant.uoguelph.ca/research/homepages/raizada/Equipment/RaizadaWeb%20Equipment%20PDFs/5B.%20UV%20VIS%20theory%20ThermoSpectric.pdf. [Accessed 28 February 2013].

[100] J.-C.G. Bunzli and S.V. Eliseeva, Basics of Lanthanide Photophysics in Lanthanide Luminescence: Photophysical, Analyticaland Biological Aspects, Springer-Verlag Berlin Heidelberg : Springer SerFluoresc, 2010.

[101] “Thermo Nicolet,” Thermo Nicolet Co. 2001, [Online]. Available: http://mmrc.caltech.edu/FTIR/FTIRintro.pdf. [Accessed 23 November 2014].

[102] W. Thomas, “Use of Fourier transform infrared (FTIR) spectroscopy to determine the health-promoting index (HPI) of cow's milk,” Digital Repository @ Iowa State University, Ames, Iowa , 2008.

[103] “Thermo Scientific,” [Online]. Available: http://www.thermoscientific.com/content/dam/tfs/ATG/CAD/CAD%20Product%20Images/Molecular%20Spectroscopy/FTIR/FTIR%20Spectrometers/F71298~p.eps/jcr:content/renditions/cq5dam.thumbnail.450.450.png. [Accessed 03 November 2015].

[104] T. Gfroerer, “Photoluminescence in Analysis of Surfaces and Interfaces,” in Encyclopedia of Analytical Chemistry, Chichester, John Wiley & Sons Ltd,, 2000, p. 9209–9231.

[105] A.R. Barron, S. Gullapalli, Optical Characterization of Group 12-16 (II-VI) Semiconductor Nanoparticles by Fluorescence Spectroscopy, Openstax-CNX.

[106] C. Reber, “Absorption and luminescence spectroscopy of transition metal compounds: from coordination geometries to excited-state properties,” Canadian Journal of Analytical Sciences and Spectroscopy, vol. 53, pp. 91-101, 2008.

[107] P. A. Rodnyi, I. V. Khodyuk, “Optical and Luminescence Properties of Zinc Oxide,” Optics and Spectroscopy , vol. 111, pp. 776-785 , 2011.

[108] M. Thambidurai, J.Y. Kim, C. Kang, N. Muthukumarasamy, H. Song, J. Song, Y. Ko, D. Velauthapillai, C. Lee, “Enhanced photovoltaic performance of inverted organic solar cells with In-doped ZnO as an electron extraction layer,” Renewable Energy, vol. 66 , pp. 433-442, 2014.

[109] S. Kumar, C. L. Chen, C. L. Dong, Y. K. Ho, J. F. Lee, T. S. Chan, R. Thangavel, T. K. Chen, B. H. Mok, S. M. Rao, M. K. Wu, “Structural, optical, and magnetic characterization,” Journal of Materials Science, vol. 48, p. 2618–2623, 2013.

[110] D. Fang, P.Yao, H. Li, “Influence of annealing temperature on the structural and optical properties of Mg–Al co-doped ZnO thin films prepared via sol–gel method,” Ceramics International, vol. 40, p. 5873–5880, 2014.

[111] A. Mesaros, C.D. Ghitulica, M. Popa, R. Mereu, A. Popa, T. Petrisor Jr, M.Gabor, A.I. Cadis, B.S. Vasile, “Synthesis, structural and morphological

characteristics, magnetic and optical properties of Co doped ZnO nanoparticles," Ceramics International , vol. 40, p. 2835–2846, 2014.

[112] J. Gubicza, S. Naoyoks, L. Balogh, J. Labar, T.W. Zerda, T. Ungar, "Influence of sintering temperature and pressure on crystallite size and lattice defect structure in nanocrystalline SiC," Journal of Materials Research, vol. 22, pp. 1314-1321, 2007.

[113] X.-Y. Li, H.-J. Li, Z.-J. Wang, H.X. Z.-Y. Xiong, J.-X. Wang, B.-C. Yang, "Effect of substrate temperature on the structural and optical properties of ZnO and Al-doped ZnO thin films prepared by dc magnetron sputtering," Optics Communications, vol. 282, p. 247–252, 2009.

[114] R.W. Kelsall, I.W. Hamley, M. Geoghegan,, Nanoscale Science and Technology, West Sussex: John Wiley and Sons, 2005.

[115] A.K. Zak, M.E. Abrishami, W.H.A. Majid, R. Yousefi, S.M. Hosseini, "Effects of annealing temperature on some structural and optical properties of ZnO nanoparticles prepared by a modified sol–gel combustion method," Ceramics International, vol. 37, p. 393–398, 2011.

[116] L. Xu, H. Zhang, K. Shen, M. Xu, Q. Xu, "Room-Temperature Ferromagnetism in Co-doped ZnO prepared by microemulsion," Journal of Superconductivity and Novel Magnetism, vol. 25, pp. 1951-1956, 2012.

[117] H. weakliem, "Optical Spectra of Ni2+, Co2+, and Cu2+ in Tetrahedral Sites in Crystals," Journal of Physical Chemistry, vol. 36, p. 2117, 1962.

[118] P. Li, S. Wang, J. Li, Y. Wei, “Structural and optical properties of Co-doped ZnO nanocrystallites prepared by a one-step solution route,” Journal of Luminescence, vol. 132, p. 220–225, 2012 .

[119] M. Bouloudenine, N. Viart, S. Colis, A. Dinia, “Zn1-xCoxO diluted magnetic semiconductors synthesizedunder hydrothermal conditions,” Catalysis Today , vol. 113, p. 240–244, 2006.

[120] G. Nam, H. Yoon, J. Leem, J.S. Kim, J.S. Kim, “structural properties and optical constants of Co-doped ZnO thin films deoposited using sol-gel spin-coating,” Journal of the Korean physical society, vol. 63, no. 10, pp. 1962-1967, 2013.

[121] N.F. Djaja, D.A. Montja, R. Saleh, “The effect of Co incorporation into ZnO nanoparticles,” advances in materials physics and chemistry, vol. 3, pp. 33-41, 2013.

[122] C. Tsay, W. Lee, “Effect of dopants on the structural, optical and electrical properties of sol-gel derived ZnO semiconductor thin films,” current applied physics, vol. 13, pp. 60-65, 2013.

[123] R. Rusdi, A.A. Rahman, N.S. Mohamed, N. Kamarudin, N. Kamarulzaman, “Preparation and band gap energies of ZnO nanotubes, nanorods and spherical nanostructures,” powder technology , vol. 210, p. 18–22, 2011.

[124] J. El Ghoul, C. Barthou, L. El Mir, “Synthesis, structural and optical properties of nanocrystalline vanadium doped zinc oxide aerogel,” Physica E , vol. 44, p. 1910–1915, 2012.

[125] T. Gfroerer, “Photoluminescence in Analysis of Surfaces and Interfaces,” in Encyclopedia of Analytical Chemistry, Chichester, John Wiley & Sons Ltd, 2000, p. 9209–9231.

[126] K. Raja, P.S. Ramesh, D. Geetha, “Structural, FTIR and photoluminescence studies of Fe doped ZnO nanopowder by co-precipitation method,” spectrochimica acta part A: molecular and biomolecular spectroscopy , vol. 131, p. 183–188, 2014.

[127] C. Reber, “Absorption and luminescence spectroscopy of transition metal compounds: from coordination geometries to excited-state properties,” Canadian Journal of Analytical Sciences and Spectroscopy, vol. 53, pp. 91-101, 2008.

[128] P. A. Rodnyi, I. V. Khodyuk, “Optical and Luminescence Properties of Zinc Oxide,” Optics and Spectroscopy, vol. 111, pp. 776-785, 2011.

[129] S. Suwanboon, P. Amornpitoksuk,S. Muensit, “Enhancement of optical bandgap and luminescent characteristics of one-dimensional ZnO nanoparticles,” Journal of ceramic processing research, vol. 11, p. 419~424, 2010.

[130] P. P. Sharmila, J. T. Nisha , “DNA Assisted Synthesis, Characterization and Optical Properties of Zinc Oxide Nanoparticles,” international journal of materials science and engineering , vol. 2, pp. 147-151, 2014.

[131] H. Morkoç, Ü. Özgür, Front Matter, in Zinc Oxide: Fundamentals, Materials and Device Technology, KGaA, Weinheim, Germany: Wiley-VCH Verlag GmbH & Co, 2009.

[132] R.S. Zeferino, M. B. Flores, U. Pal, “Photoluminescence and Raman Scattering in Ag-doped ZnO Nanoparticles,” journal of applied physics , vol. 109, p. 014308, 2011.

[133] R. Y. Sato-Berru, A. Vazquez-Olmos, A. L. Fernandez-Osorio, S. Sotres-Martınez, “Micro-Raman investigation of transition-metal-doped ZnO nanoparticles,” Journal of Raman sepctroscopy, vol. 38, p. 1073–1076, 2007.

[134] Y. Yang, J. Qi, Q. Liao, Y. Zhang, L. Tang, Z. Qin, “Synthesis and Characterization of Sb-Doped ZnO Nanobelts with Single-Side Zigzag Boundaries,” journal of physical chemistry C, vol. 112, p. 17916–17919, 2008.

[135] N. Romcevic, R. Kostic, M. Romcevic, B. Hadzic, I. Kuryliszyn-Kudelska, W. Dobrowolski, U. Narkiewicz, D. Sibera, “Raman Scattering from ZnO(Fe) Nanoparticles,” Acta Physica Polonica A, vol. 114, pp. 1323-1326, 2008.

[136] M. Schumm, “ZnO-based semiconductors studied by Raman spectroscopy: semimagnetic alloying, doping, and nanostructures, PhD Thesis,” Julius–Maximilians–Universitat Wurzburg, 2008.

[137] L. Yang, Y. Tang, A. Hu, X. Chen, K. Liang, L. Zhang,, “Raman scattering and luminescence study on arrays of ZnO doped with Tb3+,” Physica B, vol. 403, pp. 2230 - 2234, 2008.

[138] P.S. Xu, Y.M. Sun, C.S. Shi, F.Q. Xu, H.B. Pan, “The electronic structure and spec-tral properties of ZnO and its defects.,” Nuclear instruments and methods in physics reseach section B, vol. 199, pp. 286-290, 2003.

[139] S. Chang, K. Chen, “UV illumination room-temperature ZnO nanoparticle Eethanol gas sensors,” International scholarly research network, vol. 2012, pp. 1-5, 2012.

[140] M. Willander, O. Nur, J.R. Sadaf, M.I. Qadir, S. Zaman, Ahmed Zainelabdin, N. Bano, I. Hussain, “Luminescence from Zinc Oxide nanostructures and polymers and their hybrid devices,” Materials , vol. 3, pp. 2643-2667, 2010.

[141] BW Mwakikunga, S Motshekga, L Sikhwivhilu, M Moodley, M Scriba, “A classification and ranking system on the H 2 gas sensing capabilities of nanomaterials based on proposed coefficients of sensor performance and sensor efficiency equations,” Sensors and Actuators B: Chemical, vol. 184, pp. 170-178 , 2013.

[142] BW Mwakikunga, T Malwela, KT Hillie, G Ndlovu, “Towards an electronic nose based on nano-structured transition metal oxides activated by a tuneable UV light source,” Sensors, 2011 IEEE, pp. 1109-1112 , 2011.

9. Publications and Conference Presentations

9.1 Publications

9.1.1 MW Maswanganye, KE Rammutla, TE Mosuang, BW Mwakikunga, TS Bertrand and M Maaza, Synthesis, structural and optical characterisation of cobalt and indium co-doped ZnO nanoparticles, Proceedings of the SAIP2015, the 60th Annual Conference of the South African Institute of Physics, pp. 61-66, **ISBN: 978-0-620-70714-5**, (2016).

9.1.2 Maswanganye MW, Mosuang TE, Mwakikunga BW, The Influence of incorporating cobalt (Co) and indium (In) co dopants on the structural and optical properties of ZnO nanoparticles, Advanced Materials Letters, 8 (1), pp. 37 - 41, **DOI: 10.5185/amlett.2017.6876**, (2017).

9.1.3 Maswanganye MW, Rammutla KE, Mosuang TE, Mwakikunga BW, The effect of Co and In combinational or individual doping on the structural, optical and selective sensing properties of ZnO nanoparticles, Sensors and Actuators B, 247, pp. 228–237, **DOI: 10.1016/j.snb.2017.02.039**, (2017).

9.2 Conference Presentations

9.2.1 Maswanganye MW, Rammutla KE, Mosuang TE, Mwakikunga BW Bertrand TS and Maaza M, Synthesis, structural and optical characterisation of cobalt (Co) and indium (In) co-doped ZnO nanoparticles. South African Institute of Physics (SAIP) 60th annual conference, Boardwalk convention centre, Port Elizabeth, South Africa, 2015.

9.2.2 Maswanganye MW, Rammutla KE, Mosuang TE, Mwakikunga BW Bertrand TS and Maaza M, The Influence of incorporating cobalt (Co) and indium (In) co dopants on the structural and optical properties of ZnO nanoparticles. International Conference on Recent Advances in Nano Science and Technology (RAINSAT-2015), Sathyabama University, Chennai in association with Central Leather Research Institute, Council of Scientific and Industrial Research, Chennai, India, 2015.

9.2.3 Maswanganye MW, Mosuang TE, Mwakikunga BW, Bertrand TS and Maaza M "The effect of incorporating cobalt (Co) and indium (In) combinational dopants on the structural and optical properties of ZnO nanoparticles" Faculty of Science and Agriculture Research Day (FSA-RD), Bolivia Lodge, Polokwane, South Africa 2015.

9.2.4 Maswanganye MW, Mosuang TE and Mwakikunga, Gas sensing applications of Cobalt and Indium double-doped ZnO nanoparticles prepared by sol-gel method. 61st annual conference of the South African Institute of Physics (SAIP2016), University of Cape Town, Cape Town, South Africa, 2016

9.2.5 Maswanganye MW, Mosuang TE, Mwakikunga BW "Undoped versus (Co and In) single and double doped ZnO nanoparticles for gas sensing applications" Faculty of Science and Agriculture Research Day (FSA-RD), Bolivia Lodge, Polokwane, South Africa 2016.